NOTICE

The quality of this microform is heavily dependent upon the quality of the original thesis submitted for microfilming. Every effort has been made to ensure the highest quality of reproduction possible.

If pages are missing, contact the university which granted the degree.

Some pages may have indistinct print especially if the original pages were typed with a poor typewriter ribbon or if the university sent us an inferior photocopy.

Previously copyrighted materials (journal articles; published tests, etc.) are not filmed.

Reproduction in full or in part of this microform is governed by the Canadian Copyright Act, R.S.C. 1970, c C-30.

AVIS

La qualité de cette microforme dépend grandement de la qualité de la thèse soumise au microfilmage. Nous avons tout fait pour assurer une qualité supérieure de reproduction.

S'il manque des pages, veuillez communiquer avec l'université qui a conféré le grade.

La qualité d'impression de certaines pages peut laisser à désirer; surtout si les pages originales ont été dactylographiées à l'aide d'un ruban usé ou si l'université nous a fait parvenir une photocopie de qualité inférieure.

Les documents qui font déjà l'objet d'un droit d'auteur (articles de revue, tests publiés, etc.) ne sont pas microfilmés.

La reproduction, même partielle, de cette microforme est soumise à la Loi canadienne sur le droit d'auteur, SRC 1970, c. C-30

Canada

A Submodel-Component Reanalysis Technique for Liquid Tanker Body Design Using the Finite Element Method

Vineet Gupta

A Thesis

in

The Department

of

Mechanical Engineering

Presented in Partial Fulfillment of the Requirements
for the Degree of Master of Engineering at
Concordia University
Montreal, Quebec, Canada

April 1988

ISBN 0-315-44806-7

ABSTRACT

A Submodel Component Reanalysis Technique for Liquid Tanker Body Design Using the Finite Element Method

Vineet Gupta

The main objective of this thesis is to develop a technique for the reanalysis of components within a finite element submodel subjected to design modifications, without having to reanalyze the complete model. A problem involving the analysis of three types of liquid tankers manufactured by Remtec Inc. is chosen for the study. A parametric design study is carried out on each of the three tankers to determine the design parameters on the tankers which satisfy a specified stress criteria.

A new technique for reanalysis of a component within a submodel of interest via the Finite Element technique is presented. This technique significantly reduces the computational efforts and eliminates Finite Element analysis of complete model for design variations. In this technique, a submodel of interest is first extracted from the complete model. The components of interest are then modified according to the parametric variations required in the new design. The submodel is then analyzed using a matrix partitioning technique. The complete software is developed to demonstrate this new technique. The ability to carry out design sensitivity analyses with minimal

computational effort is incorporated into this software. Two case studies: baffle geometry and shape variation, and support component thickness variation, are studied. The results are validated using finite element analyses of the complete model with these parametric design changes.

ACKNOWLEDGEMENT

The author is greatly indebted to Prof. S. Sankar for suggesting a practical problem and providing continued support and guidance during this endeavor.

Thanks are also due to Mr. R.V. Ranganathan and other members of the faculty and staff of the Concave Research Center, Department of Mechanical Engineering, Concordia University for their assistance and time during the course of this work.

Technical assistance provided by Remtec Inc., by way of furnishing the drawings and specifications is greatly appreciated.

The Financial support provided by the NSERC, FCAR, and D'Actions Structurantes grants are gratefully acknowledged.

Finally, the author wishes to thank his wife for her encouragement and understanding during the course of this work.

TABLE OF CONTENTS

PAGE

PAGE

LIST OF FIGURES

PAGE

PAGE

PAGE

PAGE

PAGE

PAGE

PAGE

PAGE

LIST OF TABLES

NOMENCLATURE

[D]	Diagonal matrix of order n.
E	Modulus of elasticity.
[I]	Identity matrix of order n.
[K]	Global stiffness matrix of order n.
$[K]^{-1}$	Inverse of the global stiffness matrix of order n.
[Ki]	Stiffness matrix of the ith element.
k_{ij}	Stiffness coefficient of global matrix [K] corresponding to the ith column and the jth row.
[K11]	Left top section of partitioned global matrix [K].
[K12]	Right top section of partitioned global matrix [K].
[K21]	Bottom left section of partitioned global matrix [K].
[K22]	Bottom right section of partitioned global matrix [K].
{P}	Load vector of size n.
[P1]	Top part of partitioned load vector {P}.
[P2]	Bottom part of partitioned load vector {P}.
{Y}	Displacement solution vector of size n.
[Y1]	Top part of partitioned solution vector {Y}.
[Y2]	Bottom part of partitioned solution vector {Y}.
[L]	Lower triangular matrix of order n.
$[L]^{T}$	Transpose of the lower triangular matrix [L].
$[L]^{T^{-1}}$	Inverse of the transpose of the lower triangular matrix [L].
m_k	Bandwidth of global stiffness matrix [K].

CHAPTER 1

INTRODUCTION, LITERATURE SURVEY AND OBJECTIVES

CHAPTER 1

INTRODUCTION, LITERATURE SURVEY AND OBJECTIVES

1.1 General

Liquid tankers are often used to transport bulk liquids such as fuel oils and gasoline on highways. They have a circular or modified oval shaped tank welded on to the chassis of a truck. These tankers are usually designed for the type of liquid they carry. In the past two decades, the usage of these liquid tankers to transport bulk liquids across highways has been increasing constantly. Much attention is presently being given to the specific design of these tankers, because of their numerous on the road accidents, and the increased number of fatalities and property damage cases.

Modern liquid tankers are of a reinforced stressed skin design. In these tankers, the thin shell or barrel, reinforced with baffles and supports is the main load carrying member. The optimum design of these tankers has always been a difficult task due to the complexity and variation of different components. Classical analytical means normally cannot determine the best design and therefore, other techniques are often necessary for the analysis.

To investigate the best design for these tankers, a large number of parametric variation and reanalysis has to be carried out. This normally involves analysis of the full finite element model to determine the effect of the design change. However, reanalysis of only part of the model can be carried out by utilizing substructuring techniques. But often, it is not possible to know beforehand where the high stresses will occur and hence this limits the designer in determining exactly how to discretize the tanker into substructures and where to place the boundaries of these substructures. The designer may often also want to investigate the effect of a minor design change on an existing finite element model not created with substructures.

A new technique to overcome this difficulty is presented in this thesis. This technique utilizes the concept of submodelling and allows a component reanalysis using matrix partitioning. This technique can be applied to any area of interest in the full model after an initial analysis run has been examined.

1.2 Literature Survey

A discussion of the different components in liquid tankers has been given by Johannson [1]. In his paper, he discussed the selection criteria for tankers for a specific

application. He also discussed [2], the many problems involved in the design, selection and operation of tankers.

Thevendran and Thambiratnam [3] in their paper discussed minimum weight design of cylindrical water tanks. The finite element method was used for the analysis. Variations of wall thickness keeping the internal radius and height to be fixed were studied to determine an optimum design.

The modeling and analysis of tankers under consideration requires that a CAD software and a finite element program be utilized. There are several programs used in industry for CAD modeling and finite element analysis. CAD softwares such as Unigraphics [4], Euclid [5], PDGS [6], and Auto-trol [7] are used widely for CAD modeling and finite element pre-processing. Softwares such as Nastran [8] , Ansys [9], Patran-G [10], Stardine [11], and Spar [12] are used for finite element analysis. For reanalysis purposes, the element stiffness matrices have to be accessed. All these programs generate large binary files containing the element stiffness matrices of the model. A program such as Ansys [9] provides utilities to convert this data to ASCII format.

An important element of Computer Aided Design is geometric modeling [13]. This paper illustrates the use of solid modeling, advanced graphics and system geometric models used in three dimensional space layouts, interference considerations, and serviceability.

A survey on geometric modeling is presented in the paper by A. Baer, C. Eastman and M. Hension [14]. Issues and alternatives in geometric modeling are discussed with emphasis on solid modeling. The data storage and handling, languages, conceptual design, and logic structures are reviewed. Construction of geometric models using building blocks are discussed in the paper by J. Krouse [15]. Wire frame modeling, surface modeling, and solid modeling are illustrated.

The concept of automated drafting is described by J. K. Krouse [16]. The hardware, software, and the usage of automated drafting is explained. The concept of computer aided design is also explained by J. K. Krouse [17]. In this paper, the emphasis is on structural analysis using finite element programs.

Vehicle modeling techniques applied to structures using the finite element method has been outlined in several papers. The use of the finite element method in

Automotive structural analysis has been described by Kamal and Wolf [18]. A discussion of finite element vehicle models using beams, plates, and shells and the use of substructuring techniques are explained for a typical automobile.

A recent book by M. Kamal and J. Wolf [19] is totally dedicated to modern automotive structural analysis. This book describes structural analysis using the finite element method and presents examples of their applications. It discusses in detail, the criteria for structural design and finite element modelling.

A paper by K. H. Wadleigh [20] shows the minimum complexity models of complete automobile structural design evaluation. Calculations of deflection and stresses resulting from load applications are presented.

The substructuring technique in finite element models has been described in several papers. Przemieniecki [21] in his paper, describes the calculation of stresses and deflections in an aircraft structure divided into a number of substructures. Dodds and Lopez [22] examine the advantages and disadvantages of substructuring relative to computational efficiency. The program Finite is used for illustration purposes in their paper. Taig [23] in his

paper, discusses an automated stress analysis scheme with particular attention given to the implementation of substructure analysis .

Basas and D'Souza [24] describe a scheme which takes advantage of the accessibility to Ansys data. They use this scheme for the automated finite element model generation of automotive components using Ansys.

Different reanalysis techniques have been reviewed by Arora [25] for the static response of modified structures. Noor and Lowder [26] have carried out a study of two approximate techniques for structural reanalysis. These include Taylor series expansion for response variables and the reduced basis method. Fox [27] has explained some rapid reanalysis techniques including the utilization of matrix partitioning as well as iterative solution methods.

George and Liu [28] have described an algorithm based on the Cuthill-McKee scheme for the bandwidth reduction of symmetrical matrices. They have also presented a method for the storage of sparse matrices. Tewarson [29] has discussed a method for storing non-zero elements of a sparse matrix using linked lists.

Bathe and Wilson [30] have discussed Cholesky's decomposition method for solving a series of linear equations.

A methodology is given by Giles [31] for the automation of aircraft wing structural design. He also gives a description of the Dawns software which was developed as a tool utilizing structural analysis for the automation of the design of aircraft wings.

1.3 Scope of the Present Investigation

The objective of the present work is to investigate the best design for a specified class of liquid tankers using finite element analysis and to develop an improved method for the reanalysis of components within these tankers.

In the present study, Chapter 2 deals with the CAD modeling and the finite element pre-processing of three different tankers under investigation. The loading and the boundary conditions for a dead weight case and a torsion case are also considered in the finite element model.

In Chapter 3, the results of finite element analysis of the complete models are presented for the above loading. A parametric study involving the thickness variation for the tanker body as well as the shape variation for the baffles

is carried out for all three tankers. The best tanker design for the specified criteria is determined from this study.

Chapter 4 presents a detailed explanation of the new technique for component reanalysis. The software and the numerical techniques used for the reanalysis are also presented in this chapter. Validation of this technique is also presented.

In Chapter 5, two case studies are presented; variation of baffle geometry and support thickness . Baffle geometry which produces the lowest stress is determined by a parametric study and validated with finite element analysis of the complete models.

Finally, conclusions, highlights, and recommendations for future work are presented in the Chapter 6.

CHAPTER 2

CAD AND FINITE ELEMENT MODEL GENERATION OF A LIQUID TANKER BODY

CHAPTER 2

CAD AND FINITE ELEMENT MODEL GENERATION OF A LIQUID TANKER BODY

2.1 General

Shapes and sizes of liquid tankers vary greatly with their type of applications. Generally, tanker cross-sections vary from round to modified oval shapes according to its type of use.

For a given liquid load and a fixed tanker length, round tanks experience the lowest surface stress as compared to other shapes of tanks. On the other hand, tanks with round cross-section have a lesser volume for the same criteria. Hence, modified oval tanks are normally used so as to maximize the volume usage, and to minimize the stresses on the tanker body. These modified oval tanks may also have either single or double supports according to its type of usage. Double supports are provided if more baffles are used inside the tank for structural support. The double supports can thus provide support for the extra baffles.

Due to the high complexity of the shape of a liquid tanker body, it is virtually impossible to do a complete stress analysis of the tanker body by classical analytical means in order to determine the optimal shape and support.

Finite Element Analysis is one of the possible methodologies for evaluation of stresses. The first step in the finite element analysis is the model generation in terms of nodes and elements. In this chapter, the procedure used to generate the finite element model of a tanker body is described for three different types of tankers. The Auto-trol CAD package along with the Ansys Finite Element Software is used for the generation of the three models.

2.2 Description of Candidate Liquid Tankers

In this thesis three types of tankers are analyzed. These liquid tankers were proposed designs to be manufactured by Remtec Inc. for the US Air Force. They were to be utilized for carrying aircraft fuel at airports in Europe for refuelling purposes.

The tankers were to be manufactured from 5454-d Aluminum for the baffles and 5454-h32 Aluminum for the rest of the tank. The baffles and supports were to be welded to the main body. These tankers are 284 in (7.21 m) in length with either five or six baffles placed inside the tank and with two end caps. The baffles inside the tank have a large manhole in the center to allow for liquid flow, as well as to provide easy access to each section for cleaning purposes. The tanks are supported on the vehicle chassis by two identical supports. The supports can be

either single or double supports and are composed of outriggers, pads, and channels. In the case of a double support under the tank, the number of channels are doubled and they are joined together by angles. The tank rests on the pads and is welded to them.

The first tanker analysed (Tanker A) is a seven baffle tanker with two single supports. Baffles are placed at an equidistant position. Details of this tanker are shown in Figure 2.1. The second tanker (Tanker B) considered is a similar tanker with a more rounded cross section (Figure 2.2) and has the same number of baffles as Tanker A. Tanker C is similar in cross section to the Tanker A ,but has an extra baffle and the single supports are replaced by double supports. The positioning of the baffles is also different as shown in Figure 2.3.

2.3 Model Generation

CAD systems with their own general finite element pre-processors are now widely available in the market. They are generally more user friendly than most pre-processors in finite element softwares. They have the capability to utilize the CAD database for the automatic creation of the finite element model. Although some limitations such as the number of elements supported, and the lack of functions to

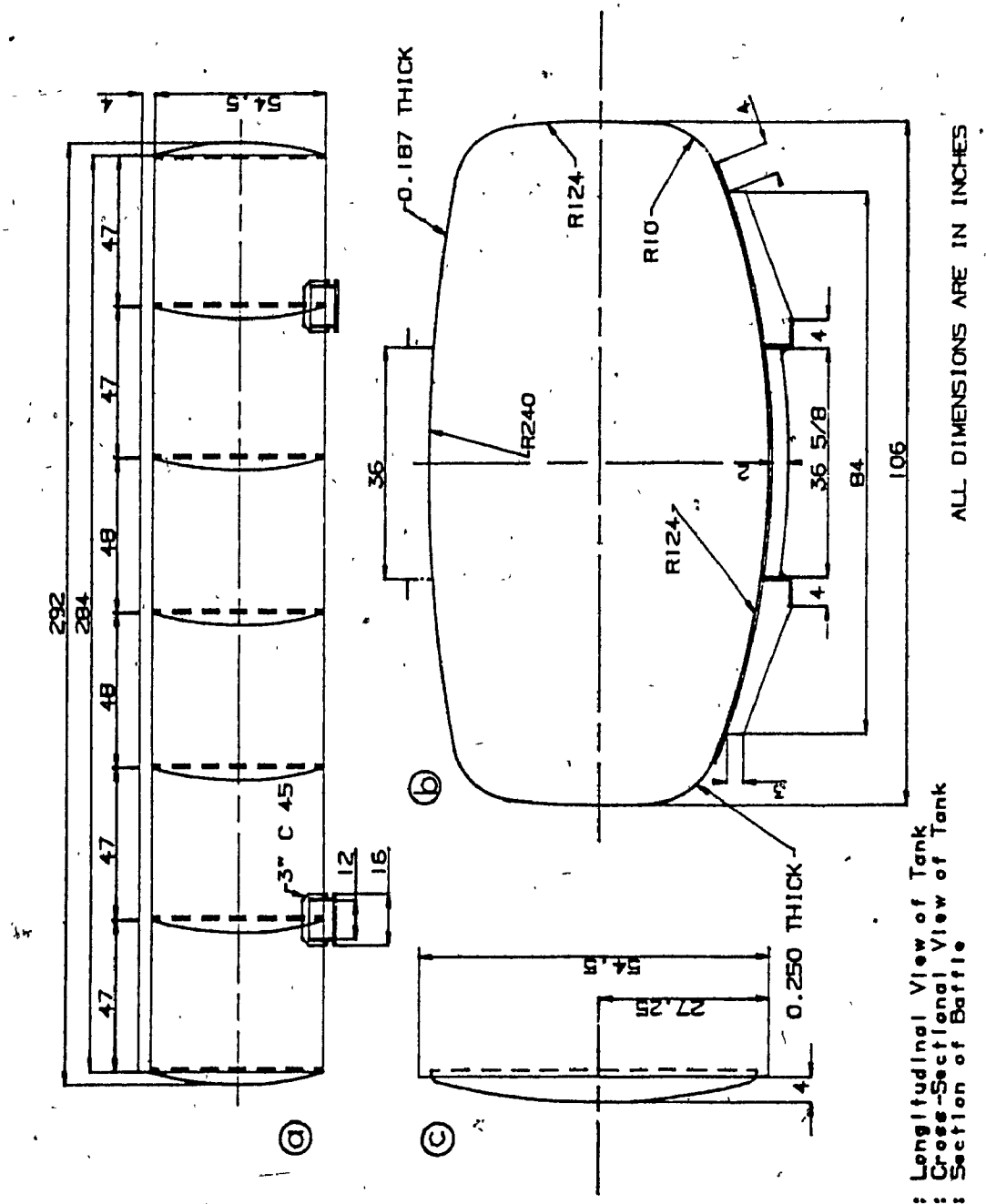

Figure 2.1: Schematic Diagram of Tanker A

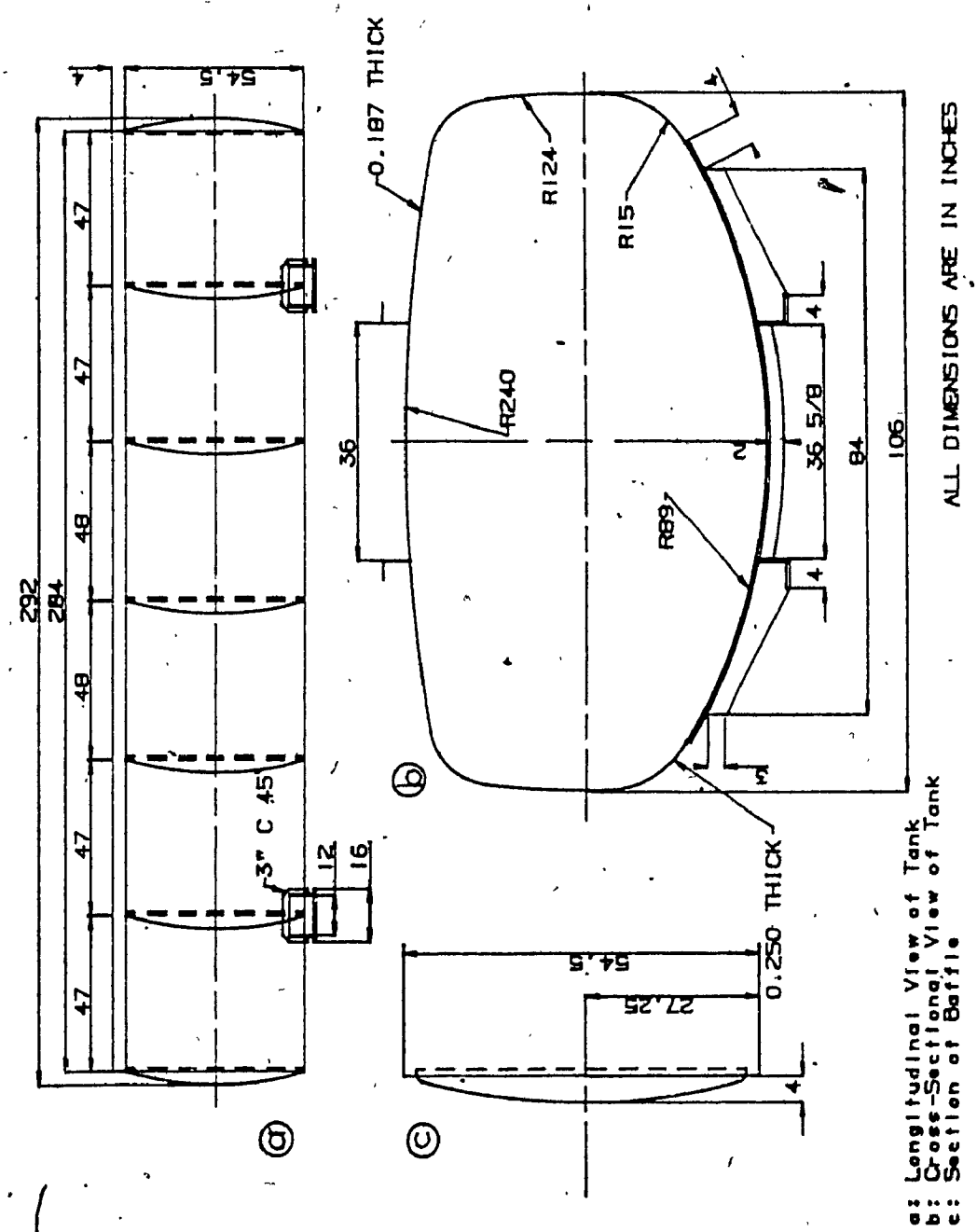

Figure 2.2: Schematic Diagram of Tanker B

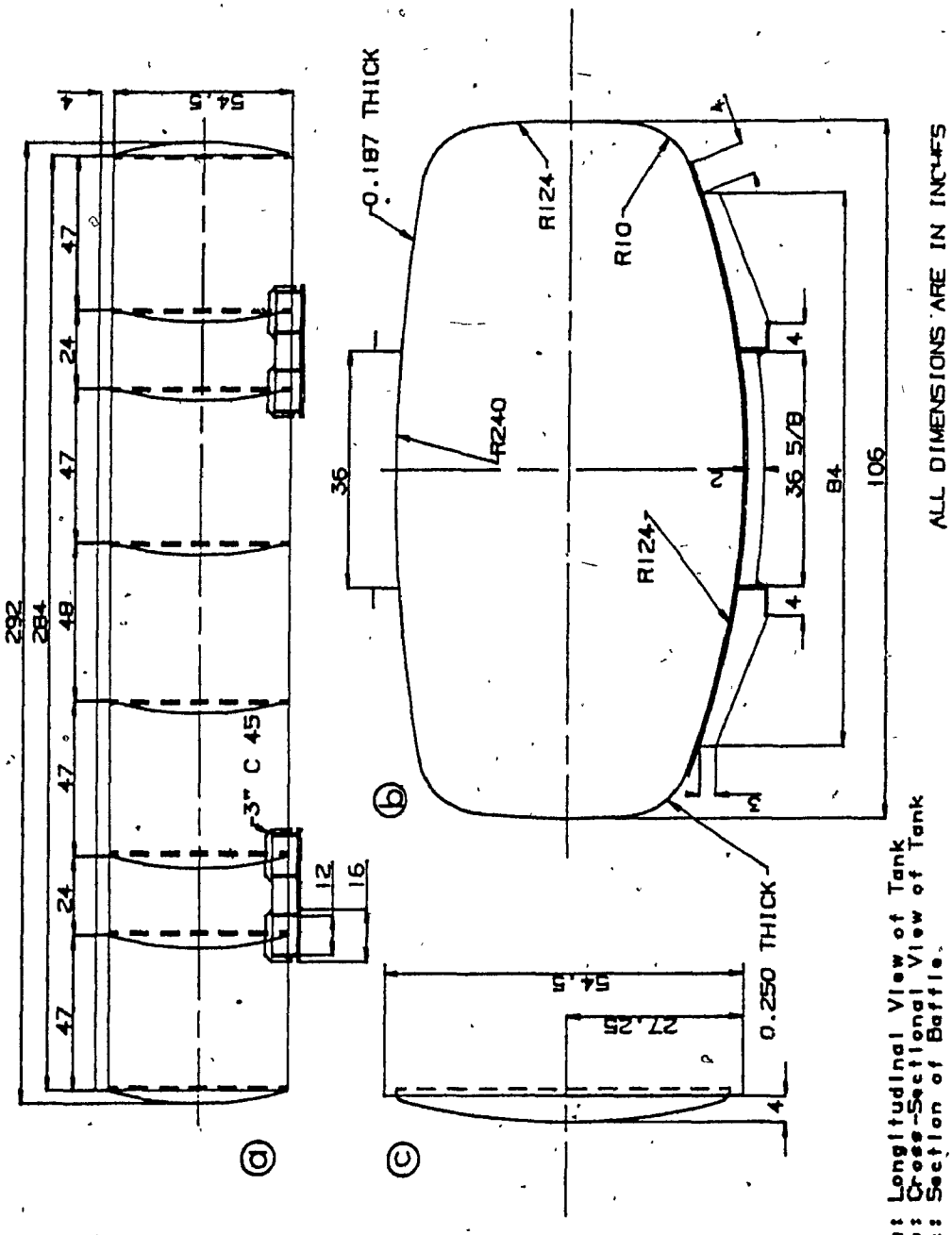

Figure 2.3: Schematic Diagram of Tanker C

input material properties and boundary conditions exist, they are still preferred over finite element software pre-processors. They are more versatile and the elimination of recreation of geometry for finite element discretization is quite significant. Auto-trol, Euclid, PDGS, and Unigraphics are some of the CAD systems with a finite element pre-processor module. All these pre-processors can output the data in a generic type of format which can then be converted to the input format of any commercially available finite element software such as Ansys or Nastran.

For the finite element analysis of the three liquid tankers, the Auto-trol CAD system with surface model capability was used. The Ansys finite element software was then used for the inputting of the material properties, boundary conditions, loads, and the type of analysis.

For the creation of the model, some assumptions can be made for those areas of tanker body which has secondary importance. The following are the assumptions made for modelling the three tankers:

1) The four wheel-wells are not modelled due to the high complexity of the well surfaces and because previous experience at Remtec had shown this not to be a highly stressed area.

2) The fuel inlet and outlet holes are not modelled because these areas are not of great concern and would not significantly affect the analysis results.

3) The manhole cover and the walkway on the top are not modelled for the same reason stated as above.

2.3.1 The Auto-trol CAD Package

The Auto-trol Series 7000 CAD/CAM software is a full 3-D wire-frame and surface modelling system. It is a menu driven software which is available on Apollo standalone workstations. It utilizes a common database (Figure 2.4) for all its modules. This saves in the recreation of the geometry when the same part is utilized for different purposes such as CAD modelling, Finite Element pre-processing, or N.C. Programming. It has modules for:

- wire-frame geometry creation
- surface creation
- drafting
- N.C. machining
- finite element pre-processing
- user application interface for fortran programs

Its graphic visualization capabilities include single- and multi-view windowing where up to 32 views can be displayed simultaneously.

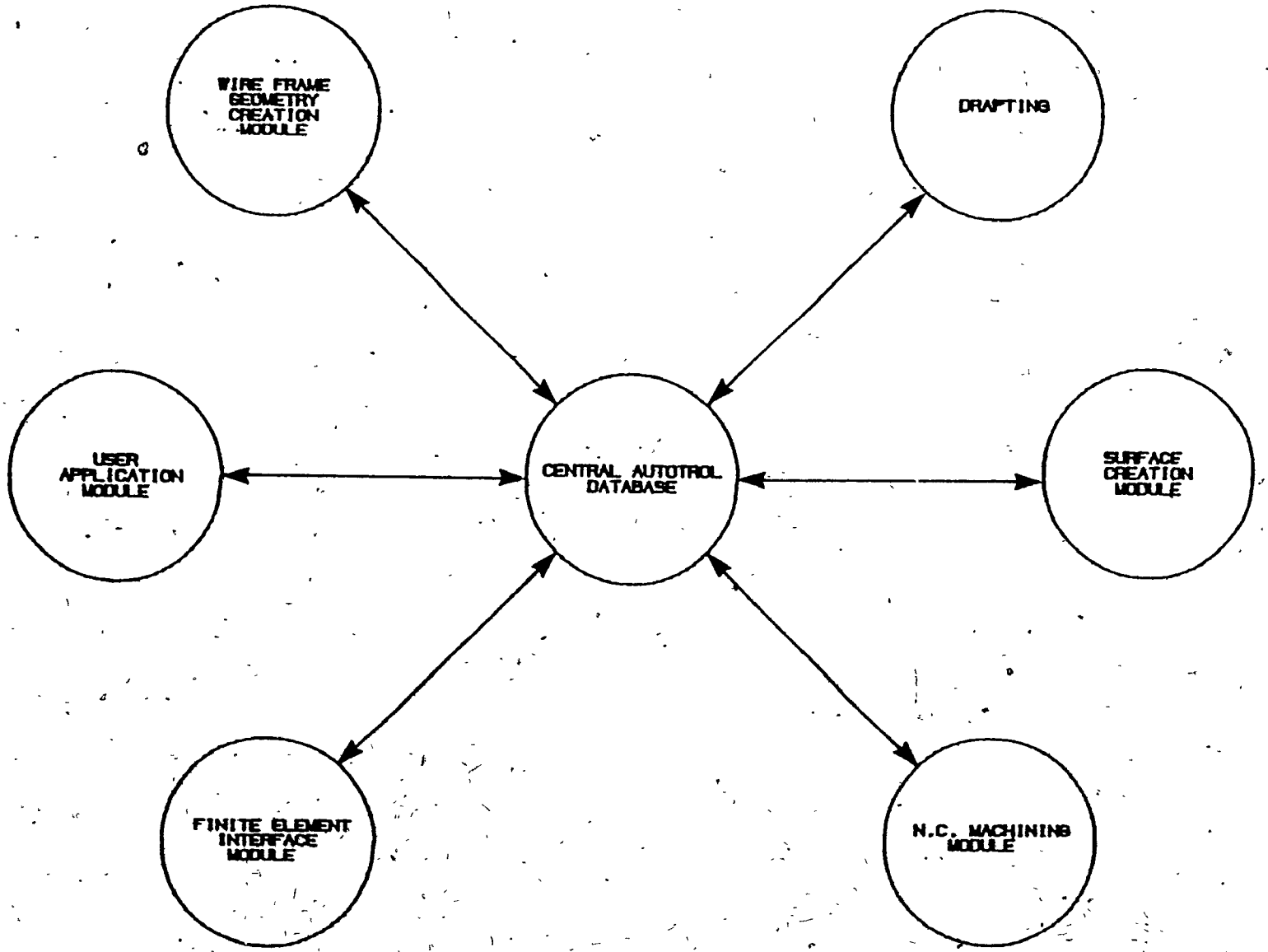

Figure 2.4: Autotrol CAD/CAM System

2.3.2 CAD Model Generation

The CAD models of the three tankers were generated utilizing the basic drawing module along with the surface creation module. The cross-section of the tank was first generated to exact dimensions and the tank surface extracted from this using the 'projected' function within the surface creation module in Auto-trol. The baffles and the support were created seperately also using the surface creation module. All three models were then combined to create full surface models of the three tankers. Figure 2.5 shows the full surface CAD model of Tanker A composed of the tank body, the baffles, and the supports.

2.3.3 Node and Element Generation

The finite element pre-processing module of Auto-trol provides the capability to work with the surfaces created by the surface creation module. Different element types including triangular and quadrilateral shell elements can be generated automatically. The user has to select the surface and specify the type of element to be placed on the surface. The software prompts for the node spacing to be specified on the surface. Figure 2.6 shows a finite element model of Tanker C as was created in Auto-trol. Figure 2.7 shows a zoomed in section of the tanker front support. As it can be seen in Figure 2.7 both triangular and quadrilateral type elements are utilized to create the

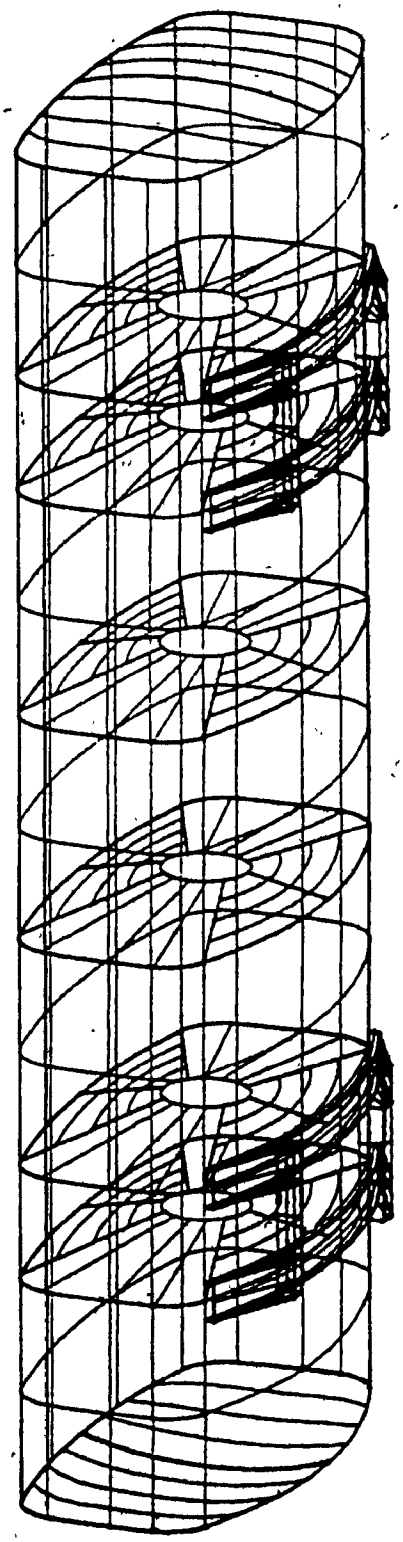

Figure 2.5: Tanker C Surface CAD Model

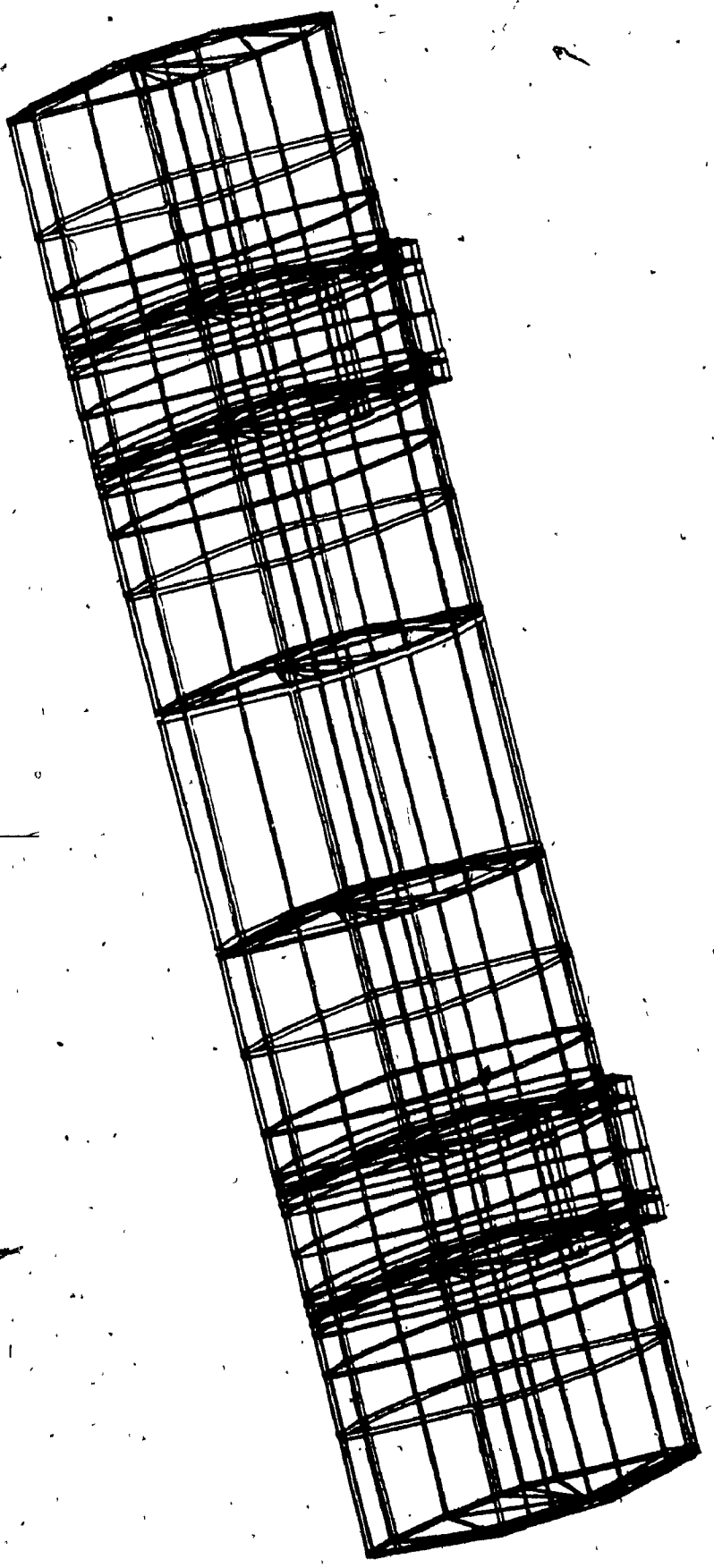

Figure 2.6: Tanker C Finite Element Model

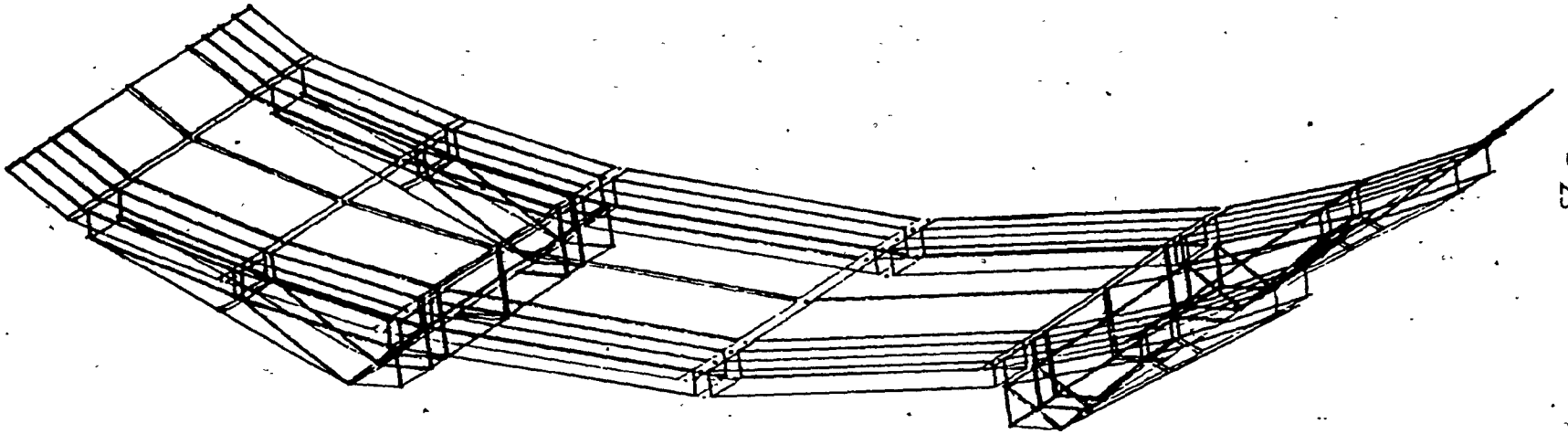

Figure 2.7: Tanker C Support Finite Element Model

finite element model. The computer model then provides output as numeric data in a readable format for Ansys.

2.3.4 The ANSYS Finite Element Package

The Ansys software is a large scale general purpose finite element program which has capabilities for linear and non-linear static and dynamic analyses. It can handle small and large displacements, as well as solve problems involving elastic, plastic creep, and swelling effects. It utilizes the matrix displacement method for the analysis and the wavefront method for matrix reduction and solution. Over a hundred linear and non-linear elements are available in its library for modelling purposes.

There are basically three phases involved in an Ansys solution. Figure 2.8 shows a flowchart of the analysis methodology for any type of problem. The pre-processing is generally carried out using the Prep7 module either interactively or by inputting the model data from CAD finite element modelling pre-processor. User interaction in this module is done by using a command language specific to this module. Any one of the different analysis options can be specified in this module before the model is sent for analysis. After the analysis stage, there are a number of post-processors available within Ansys for the plotting and sorting of the data. Post25 is the post-processor normally

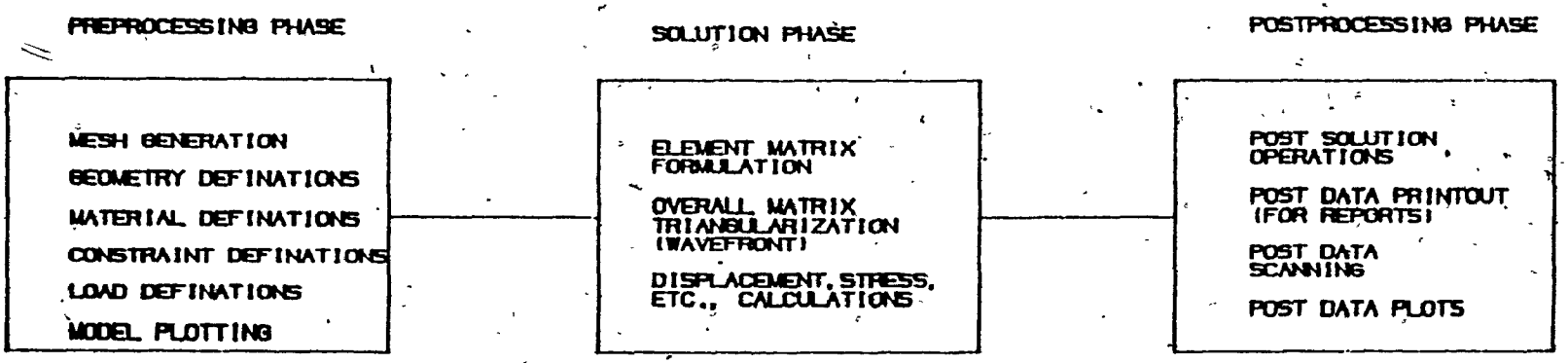

Figure 2.8: Typical Phases of an Ansys Analysis

used for shell elements. Stress contour plots as well as displaced shape plots can be generated within this post-processor.

2.3.5 Finite Element Model of the Tanker Body

Figures 2.9, 2.10, and 2.11 show the finite element models of the three tanks with the baffles and the supports as displayed using some of the commands in the Prep7 module of Ansys. Tanker A and Tanker B are each composed of 473 nodes and 657 elements. Tanker C which is the largest model has 856 nodes and 1078 elements. Tankers A and B each have 7 baffles and two single supports (Figures 2.9 and 2.10). The basic variation between the two tanks is the cross-section. Tanker C is similar in cross-section to Tanker A but has 8 baffles and two double supports (Figure 2.11). Thickness of the first two and the last two baffles in all three tanks is 0.187 in (0.00475 m). The rest of the baffles are 0.173 in (0.00440 m) thick. The pad has a thickness of 0.5 in (0.0127 m). The channels and angles of the support are all 0.375 in (0.00953 m) thick. The top two thirds of the tank body is 0.187 in (0.00475 m) thick while the bottom third is 0.25 in (0.00635 m).

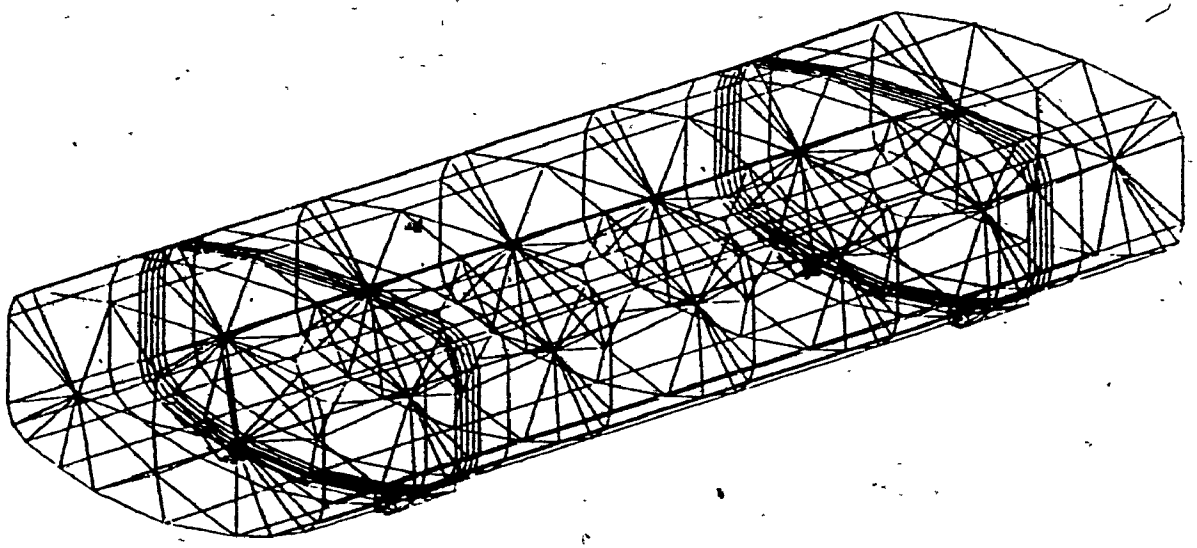

Figure 2.9: Ansys Finite Element Model of Tanker A

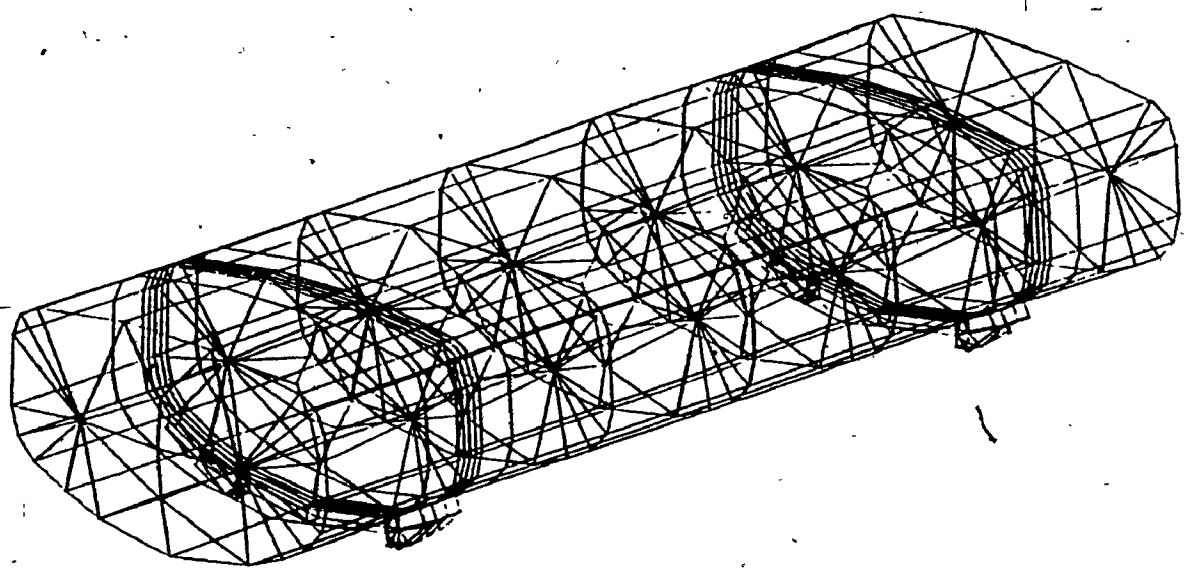

Figure 2.10: Ansys Finite Element Model of Tanker B

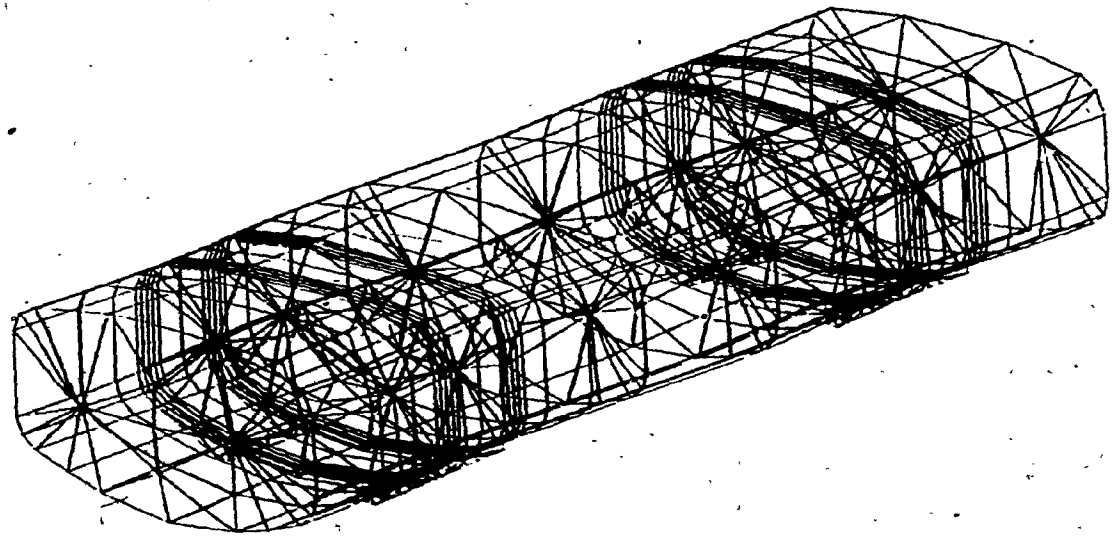

Figure 2.11: Ansys Finite Element Model of Tanker C

2.4 Material Properties, Loading, and Boundary Conditions

The tankers are manufactured from Aluminum 5454. Standard aluminum material properties were inputted into Ansys for analysis purposes. The following material properties were used for the analysis of the three tankers:

Modulus of Elasticity = 10×10^6 Lbs/in^2 (6.89×10^7 kPa)

Density = .098 Lbs/in^3 (2712.67 kg/m^3)

Poisson's ratio = 0.33

Density of liquid (aircraft fuel) = 0.24555 lbs/in^3 (6796.91 kg/m^3)

There are two load cases considered for the stress analysis. The first is a dead weight case where the tank is resting evenly on all four supports. The second case is for a torsional load, which simulates the condition of the tanker going over a large pothole. The torsional load is simulated by removing the left-end of the back support, leaving the tanker resting on only three support points.

The weight of the fuel is simulated as liquid pressure acting on the inner walls of the tank. As the pressure of the liquid varies with its height, a reasonable assumption can be made for Ansys input purposes to discretize this pressure variation into ten steps . The

tank circumference can also be thus divided into ten sections and the pressure on each section will be a constant and will be based on the height of the center of each section of the tank. These sections can thus be taken as actual elements along the bottom, sides, and top of the tank. Figure 2.12 shows the division of the tank into these ten sections.

The maximum load these tankers are designed for is the load due to the aircraft fuel when the tanker is 90% full. Thus, for the analysis, hydrostatic pressure corresponding to 90% of the tank fill (nine sections) is used in the finite element model. Figure 2.12 also shows the magnitude of the hydrostatic pressure as applied to an element face on each section for Tanker A.

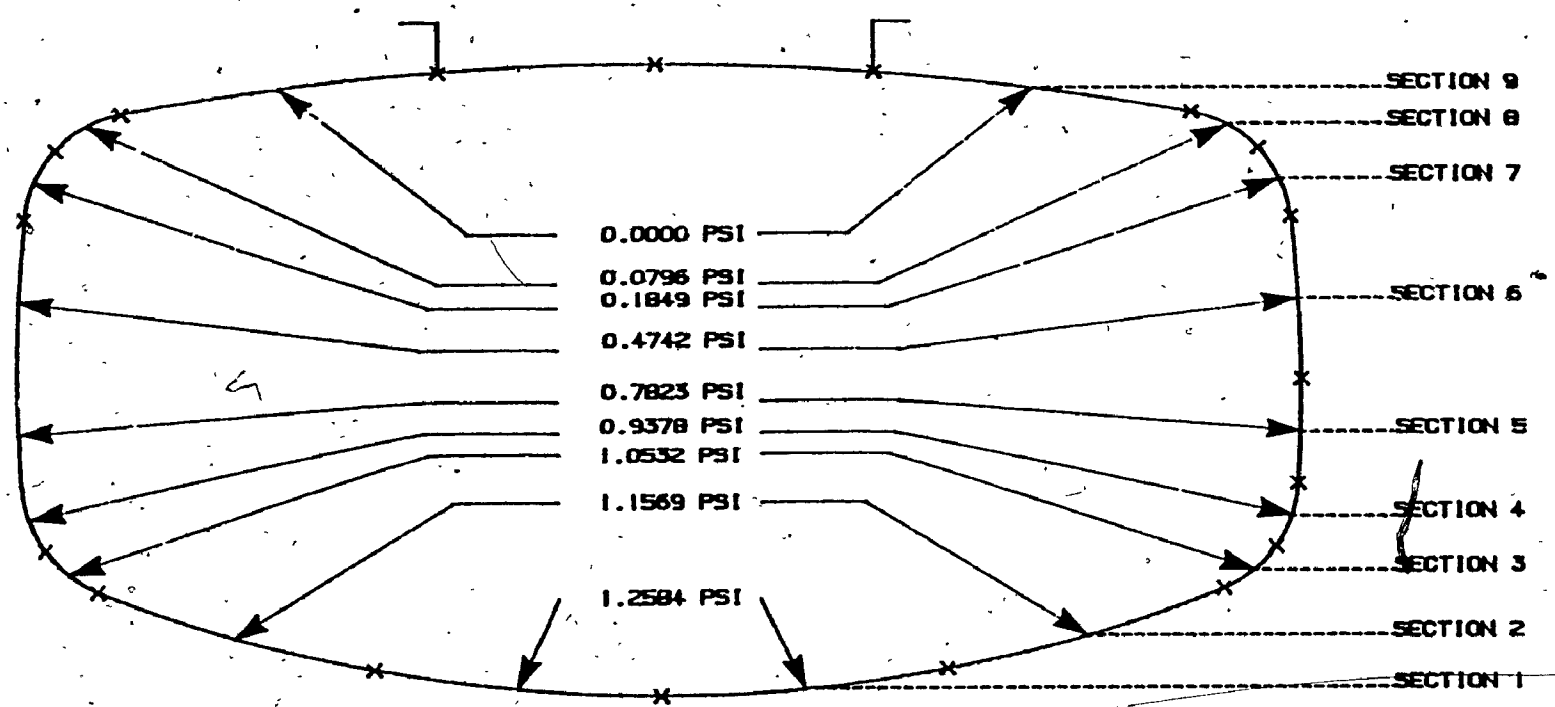

Figure 2.12: Pressure Distribution on Tanker A

2.5 Summary

Description of the three tankers to be analyzed is presented in this chapter. Softwares and techniques used for the CAD and finite element modelling are also discussed. A brief discussion on the load types considered and the procedure for inputting into the finite element model is also given.

CHAPTER 3

FINITE ELEMENT ANALYSIS OF LIQUID TANKERS

CHAPTER 3

FINITE ELEMENT ANALYSIS OF LIQUID TANKERS

3.1 General

As discussed in the previous chapter, there are three types of tankers which are analyzed in this thesis. These liquid tankers were proposed designs for tankers to be manufactured by Remtec Inc. The two criteria used in the design of liquid tankers are minimum tanker weight and structural integrity. Minimizing the maximum stress below a critical stress value for any part of the tanker under extreme loading conditions is chosen as the objective for structural integrity. The critical stress value is selected as per the recommendation of the manufacturer to be 1/3rd of the yield strength of the tanker material (Aluminum 5454). The yield strength for Aluminum 5454 is 17000 psi (117.2 MPa) and hence in the following study, the maximum acceptable stress is selected to be 5,667 psi (39.07 MPa) for any part of the tanker.

All models were analyzed on Ansys using the static analysis option. The post processing was carried out utilizing the Ansys Post25 shell post processor to plot the data in the form of stress contours. In all of the analyses, the Von Mises or the equivalent stress was plotted.

3.2 Tanker A

Tanker A has a single support and seven baffles. It was the tanker initially proposed by the manufacturer because of the fact that a single support makes it easier to manufacture.

3.2.1 Case 1: Dead Weight

The first type of loading is when the tanker is set on all four supports with the internal pressures of the liquid acting on it. The results show that the stresses are symmetrical about the center of the tanker. The highest stress of 7,890 psi (54.39 MPa) occurs on the bottom of the tanker on the two corners of both pads. This is seen in Figure 3.1 which shows the stress contours on the bottom of the tank around the rear pad area. The most highly stressed baffles are the first and last baffles which experience a maximum stress of 7,343 psi (50.63 MPa). A stress contour plot of the first baffle is shown in Figure 3.2. Figures 3.3 and 3.4 show stress contours of the most highly stressed areas on the supports (max. stress = 2,665 psi (18.37 MPa)) and the top portion of the tank (max. stress = 5,628 psi (38.80 MPa)) respectively.

3.2.2 Case 2: Torsion

The second load case to be analyzed is the torsional load case. In this case the torsional load is applied on

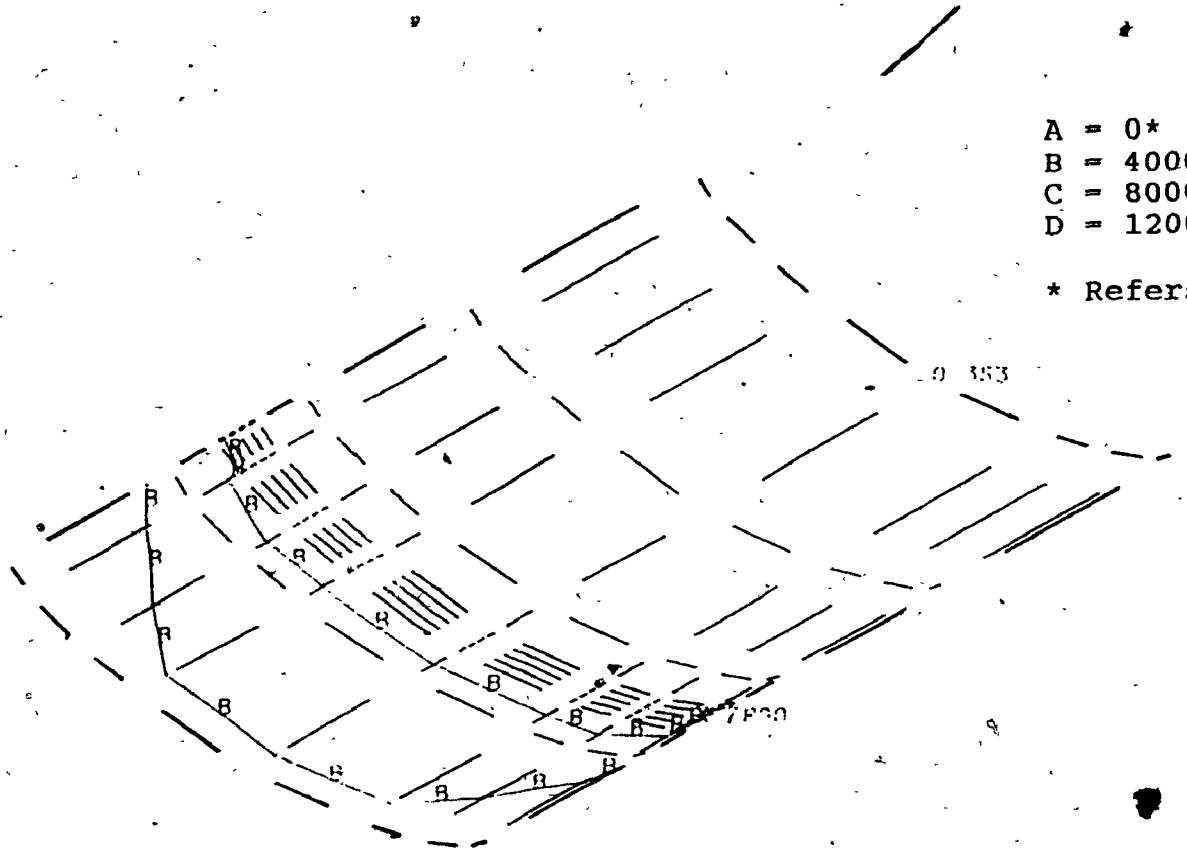

A = 0*
B = 4000
C = 8000
D = 12000

* Refers to stress value in psi.

Figure 3.1: Stress Contours for Rear Bottom Half of
Tanker A - Dead Weight Load
(Top thickness = 0.187 in., Bottom Thickness = 0.250 in.)
(For conversion to SI Units: 1 in = 0.0254 m; 1 psi = 0.00689 MPa)

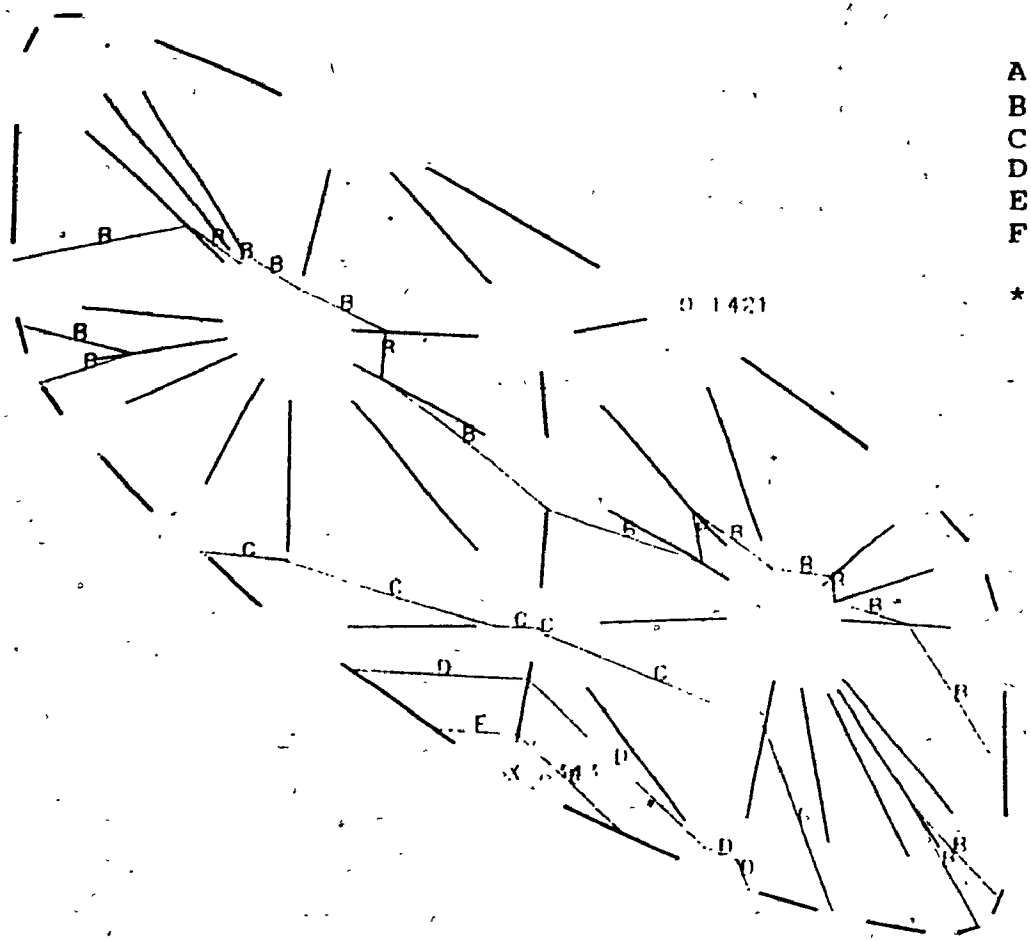

A = 1250*
B = 2500
C = 3750
D = 5000
E = 6250
F = 7500

* Refers to stress value in psi.

Figure 3.2: Stress Contours for the First Baffle of
Tanker A - Dead Weight Load
(Top thickness = 0.187 in., Bottom Thickness = 0.250 in.)
(For conversion to SI Units: 1 in = 0.0254 m; 1 psi = 0.00689 MPa)

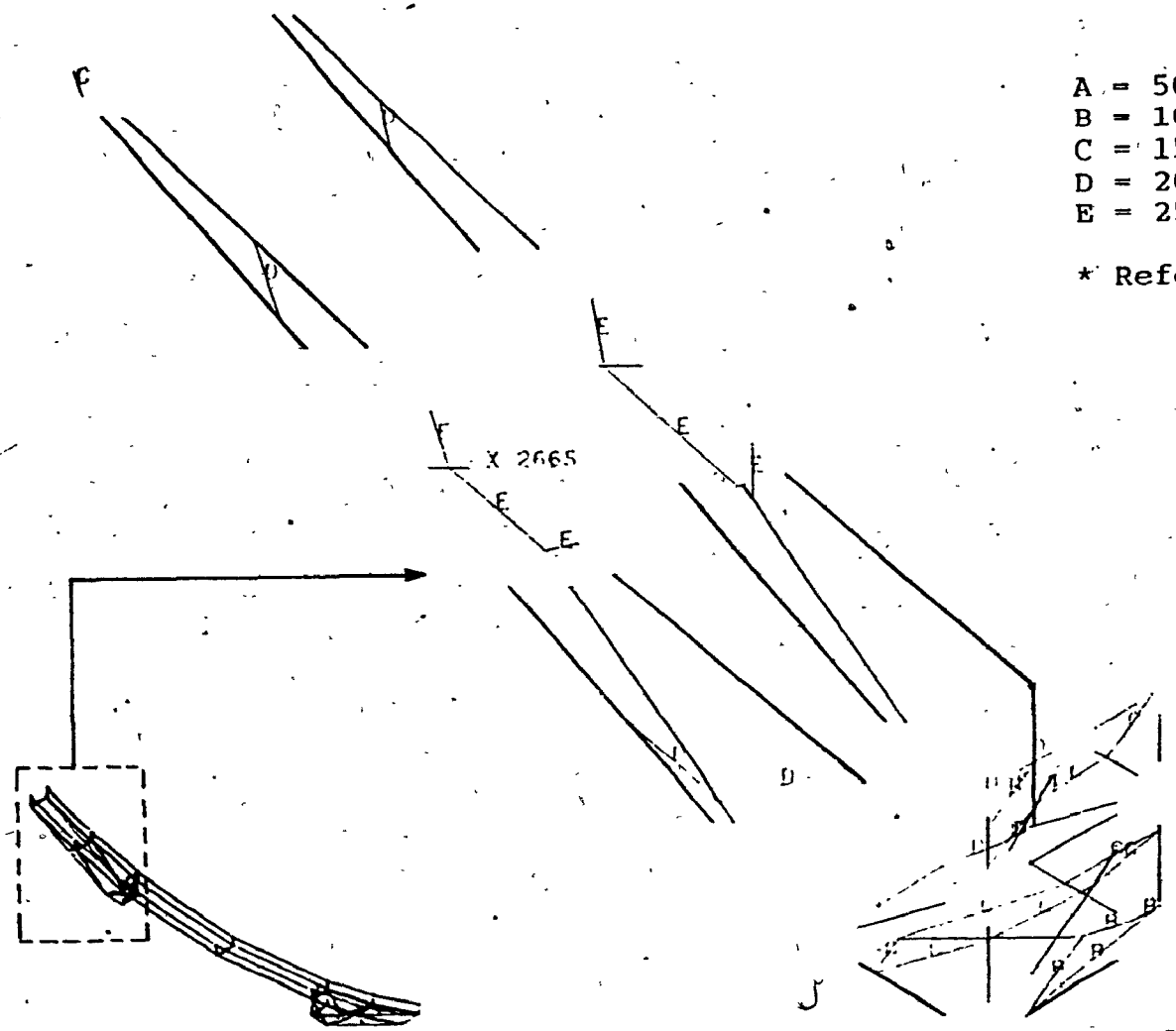

A = 500*
B = 1000
C = 1500
D = 2000
E = 2500

* Refers to stress value in psi.

Figure 3.3: Stress Contours for the Right Rear Support of Tanker A - Dead Weight Load
(Top thickness = 0.187 in., Bottom Thickness = 0.250 in.)
(For conversion to SI Units: 1 in = 0.0254 m; 1 psi = 0.00689 MPa)

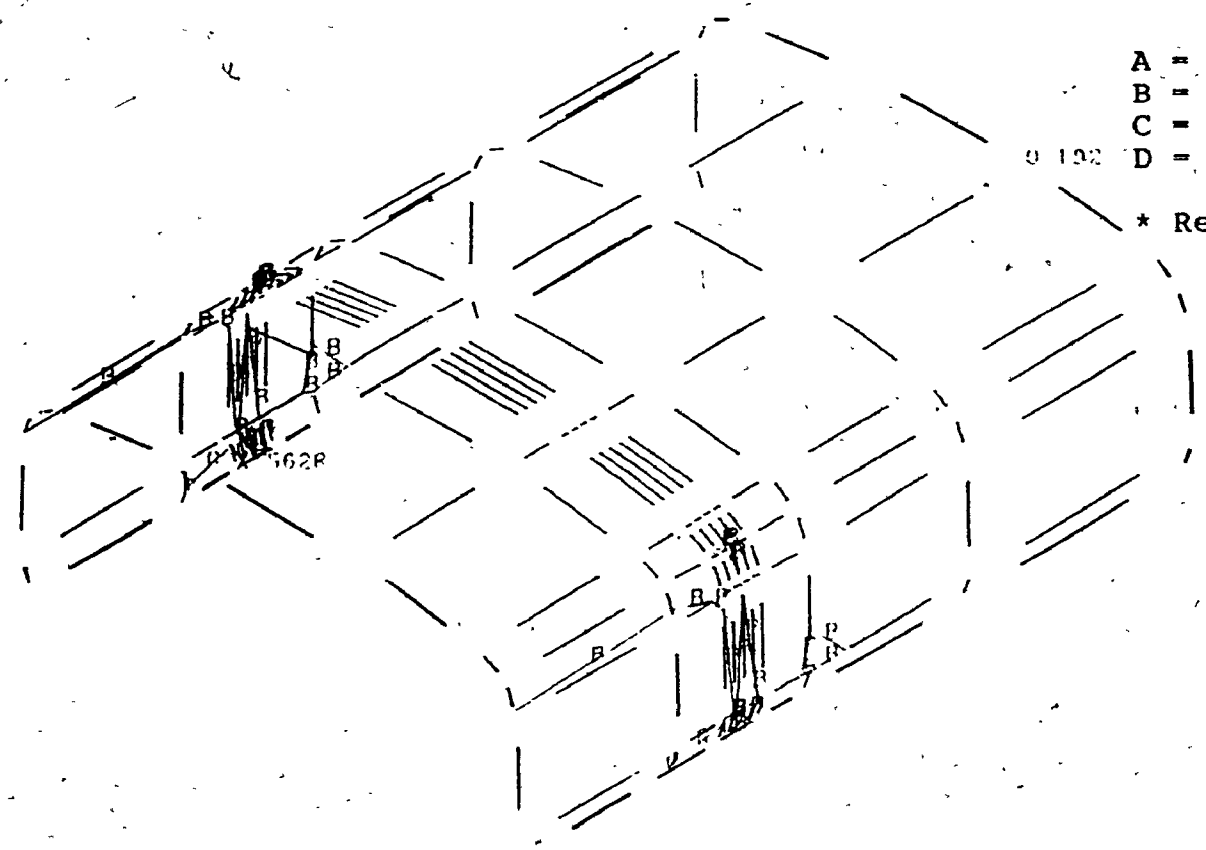

Figure 3.4: Stress Contours for Rear Top Half of
Tanker A - Dead Weight Load
(Top thickness = 0.187 in., Bottom Thickness = 0.250 in.)
(For conversion to SI Units: 1 in = 0.0254 m; 1 psi = 0.00689 MPa)

the tanker model by removing the rear left support. This is the most severe static load case which the tanker can be expected to undergo in normal operating conditions.

For this load case, the most highly stressed area on Tanker A was determined to be the rear pad area at the bottom of the tank . The maximum stress in this area is 8,132 psi (56.07 MPa). Baffle number one is the most highly stressed baffle with a maximum Von Mises stress of 7,140 psi (49.23 MPa) occurring on the bottom of the baffle. The maximum stress of 5,773 psi (39.80 MPa) on the top part of the tank occurs on the rear half of the tank. The support area is most highly stressed around the left front outrigger with the highest stress being 4,175 psi (28.78 MPa). As expected, the stresses in the torsion load case are higher than the dead weight case. In both types of loading, the stresses are found to be above the acceptable level of 5,667 psi (39.07 MPa).

3.2.3 Parametric Variation for Tank Thickness

As many parts of the tanker experienced stresses over the acceptable level, a parametric study was attempted to reduce the stresses on the tanker to an acceptable level. The initial tank thickness for the top two thirds of the tank is 0.187 in (0.00475 m) and the bottom third is 0.250 in (0.00635 m). A parametric variation as shown in Table

3.1 is applied to the bottom and top tank thicknesses for the case 2 loading. The maximum stresses on the different parts on the tanker are also shown on Table 3.1. As seen from Table 3.1, the maximum stresses on the tanker increases as the thickness of the bottom is reduced. The change in the thickness of the top of the tank does not significantly reduce the stresses. The lowest stress on the tanker is found to occur when the thickness of both the top and the bottom parts of the tank is set to 0.250 in (0.00635 m). The maximum stress occurring on the top of the tanker is 5,741 psi (39.58 MPa), while the bottom experiences a maximum stress of 6,625 psi (45.68 MPa). The first baffle has the highest stress amongst all the baffles with a value of 7,123 psi (49.11 MPa) while the support where the stress increased slightly, has a stress of 4206 psi (28.99 MPa). The stresses are still found to be above the acceptable level of 5,667 psi (39.07 MPa).

3.2.4 Parametric Variation for the Baffles

To try and further reduce the stresses , a parametric variation for baffle geometry was carried out as shown on Table 3.2. The tanker thickness used for this baffle parametric variation is the lowest stress case determined in the previous section. Table 3.2 also shows the maximum stresses which occurs on different parts of the tanker due to this variation. Although the change in stress is not

Table 3.1 Tank Thickness Variation for Tanker A - Case 2 Loading

Case No.	Top Thickness (in)	Bottom Thickness (in)	Top Max. Stress (psi)	Bottom Max. Stress (psi)	First Baffle Max. Stress (psi)	Support Max. Stress (psi)
1	0.187	0.187	7,895	9,542	11,122	4,167
2	0.187	0.250	5,773	8,132	7,140	4,175
3	0.250	0.187	7,508	9,490	11,116	4,199
4	0.250	0.250	5,741	6,625	7,123	4,206

(For conversion to SI Units: 1 in = 0.0254 m; 1 psi = 0.00689 MPa)

Table 3.2 Baffle Variation for Tanker A – Case 2 Loading

(Tanker top thickness = 0.250 in.; bottom thickness = 0.250 in.)

Case No.	Hole Diameter (in)	Shape Radius (in)	Top Max. Stress (psi)	Bottom Max. Stress (psi)	First Baffle Max. Stress (psi)	Support Max. Stress (psi)
1	18.0	3.0	5,696	6,497	7,545	4,047
2	18.0	4.0	5,741	6,625	7,123	4,206
3	20.0	3.0	5,699	6,497	7,452	4,053
4	20.0	4.0	5,771	6,660	7,109	4,270

(For conversion to SI Units: 1 in = 0.0254 m; 1 psi = 0.00689 MPa)

significant in any part of the tanker, some reduction in stresses on the baffles occurs due to the increase in the hole diameter to 20 in (0.508 m) and the reduction in the shape radius to 3 in (0.0762 m). On the other hand, the stresses on other parts of the tanker show an increase due to this baffle design parameters. Figures 3.5 , 3.6, 3.7, and 3.8 show the stress contours occurring in the bottom, the first baffle, the support, and the top corresponding to case 4 of Table 3.2. The maximum stress on the baffle, 7,109 psi (49.01 MPa), is still found to be above the acceptable level of 5,667 psi (39.07 MPa).

3.3 Tanker B

Tanker B has a single support and seven baffles with more rounded crossection compared to Tanker A. Like Tanker A, it has a single support structure.

3.3.1 Case 1: Dead Weight

In this case, as in Tanker A, Tanker B was set on all four supports with the internal pressures of the liquid acting on it. The results show that the highest stress of 6,907 psi (47.62 MPa) occurs on the bottom part of the first and last baffles. The bottom of the tanker has a maximum stress of 6,461 psi (44.54 MPa) on the two corners of the two pad areas. Figures 3.9 and 3.11 show the stress contours on the bottom of the tank around the rear pad area

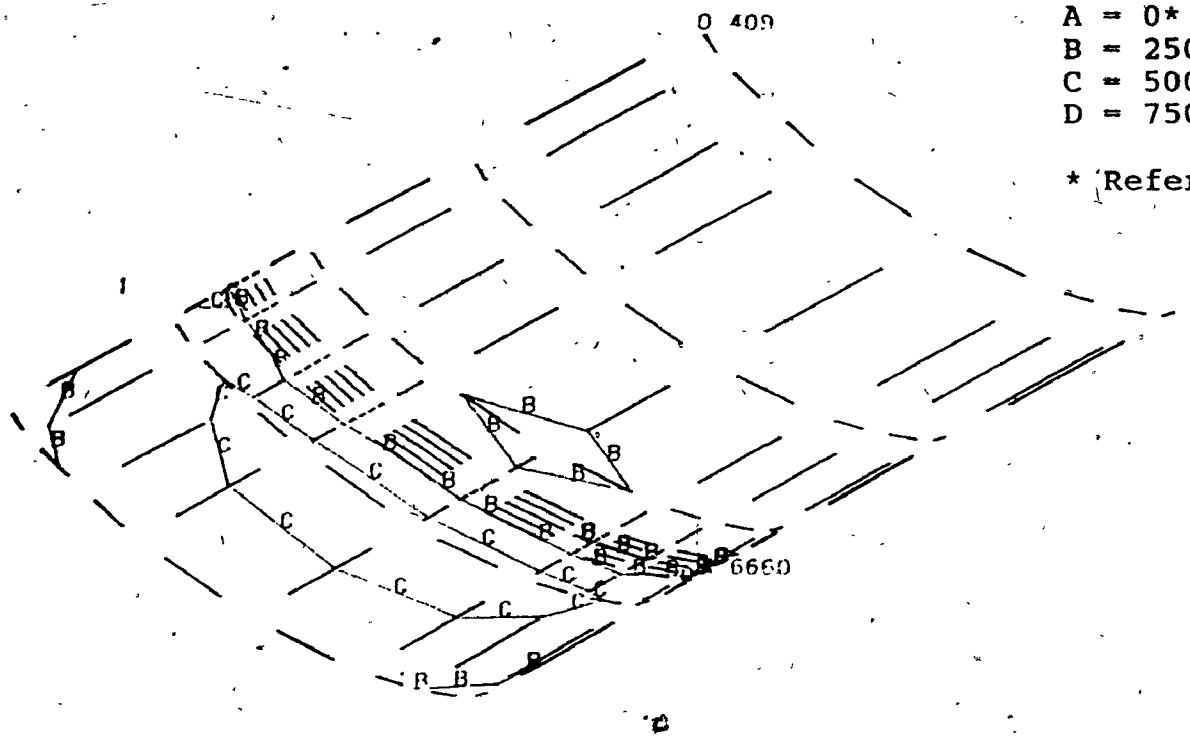

A = 0*
B = 2500
C = 5000
D = 7500

* Refers to stress value in psi.

Figure 3.5: Stress Contours for Rear Bottom Half of Tanker A - Torsion Load
(Top thickness = 0.250 in., Bottom Thickness = 0.250 in.)
(Baffle Hole Diam. = 20.0 in., Baffle Shape Rad. = 4.0 in.)
(For conversion to SI Units: 1 in = 0.0254 m; 1 psi = 0.00689 MPa)

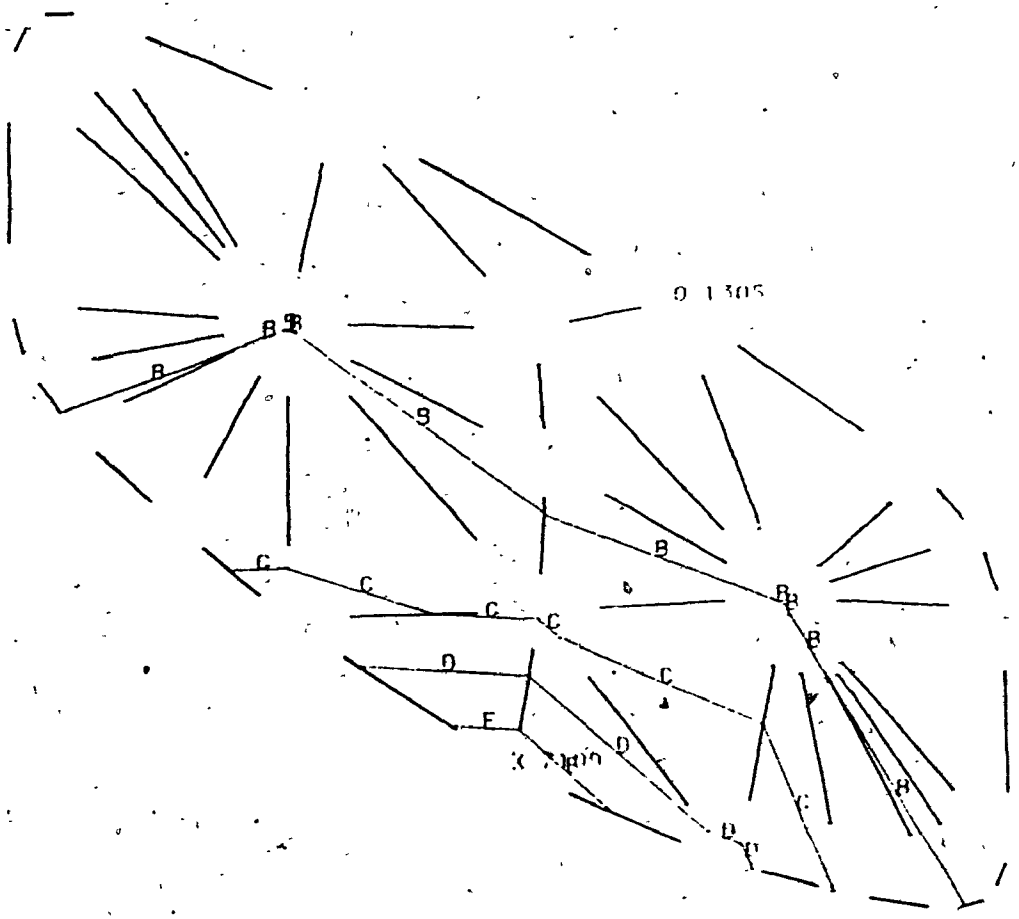

A = 1250*
B = 2500
C = 3750
D = 5000
E = 6250
F = 7500

* Refers to stress value in psi.

Figure 3.6: Stress Contours for the First Baffle of Tanker A - Torsion Load
(Top thickness = 0.250 in., Bottom Thickness = 0.250 in.)
(Baffle Hole Diam. = 20.0 in., Baffle Shape Rad. = 4.0 in.)
(For conversion to SI Units: 1 in = 0.0254 m; 1 psi = 0.00689 MPa)

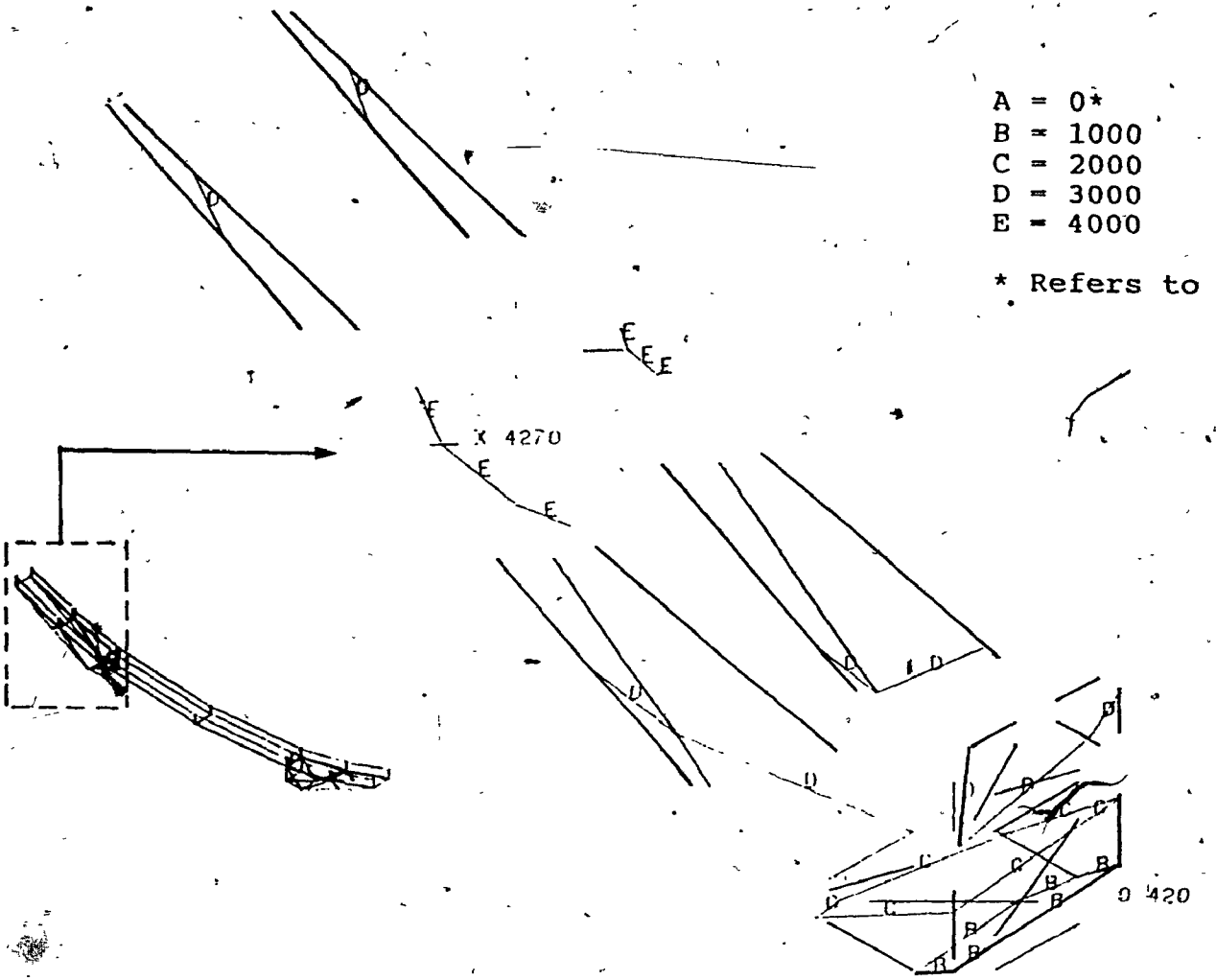

Figure 3.7: Stress Contours for the Right Rear Support of Tanker A - Torsion Load
(Top thickness = 0.250 in., Bottom Thickness = 0.250 in.)
(Baffle Hole Diam. = 20.0 in., Baffle Shape Rad. = 4.0 in.)
(For conversion to SI Units: 1 in = 0.0254 m; 1 psi = 0.00689 MPa)

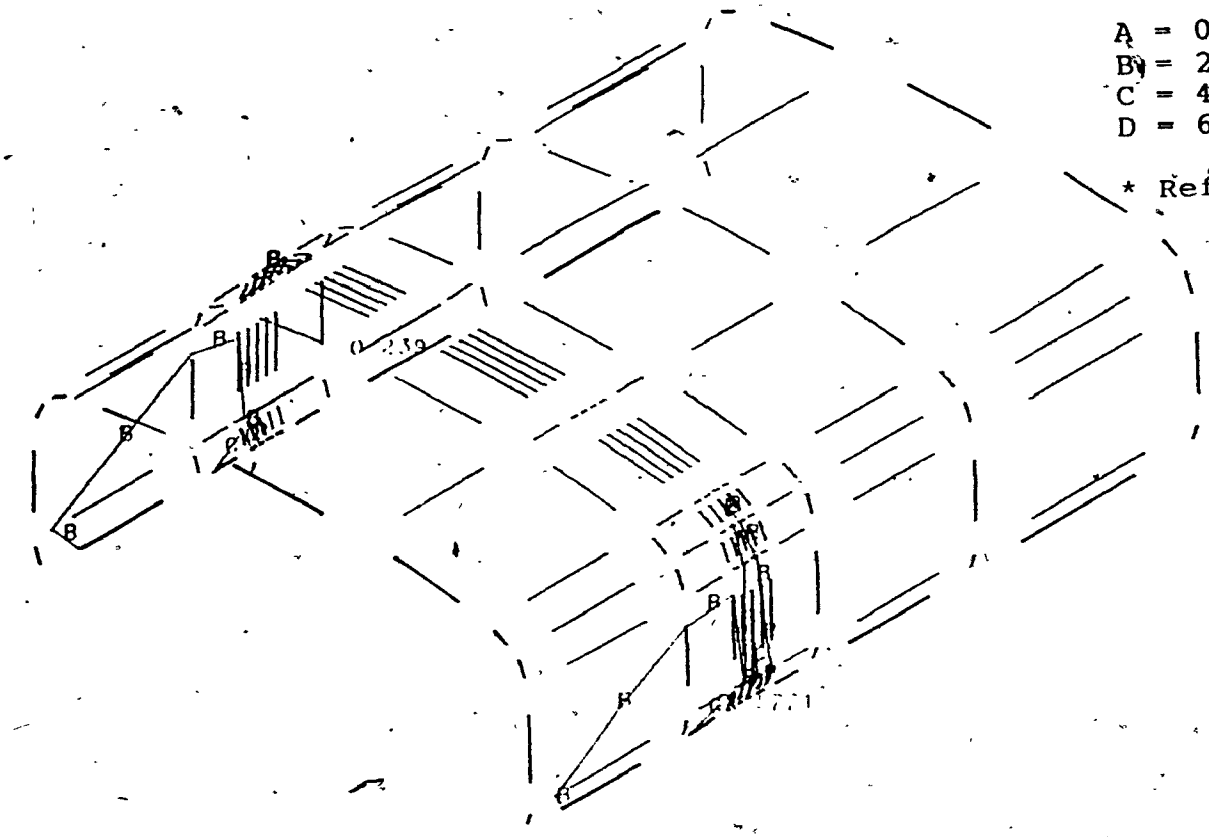

Figure 3.8: Stress Contours for Rear Top Half of
Tanker A - Torsion Load
(Top thickness = 0.250 in., Bottom Thickness = 0.250 in.)
(Baffle Hole Diam. = 20.0 in., Baffle Shape Rad. = 4.0 in.)
(For conversion to SI Units: 1 in = 0.0254 m; 1 psi = 0.00689 MPa)

and on the baffles respectively. Figures 3.10 and 3.12 show stress contours of the most highly stressed areas on the supports and the top of the tank which experience a maximum stress of 1,382 psi (9.5 MPa) and 3,732 psi (25.73 MPa) respectively. As in tanker A, the stresses are symmetrical about the center of the tank.

Although the stresses on the bottom and on the first and last baffles are above the acceptable level of 5,667 psi (39.07 MPa), all four areas of the tanker experience lower stresses as compared to the same areas on Tanker A. This is expected as Tanker B has a more rounded cross-section than Tanker A.

3.3.2 Case 2: Torsion

In this section, the second proposed tanker , i.e., Tanker B was applied with the same torsion load as Tanker A to determine its stress level. The most highly stressed area on the bottom of the tank is again on the rear pad area as in Model A. The maximum value is 6,386 psi (44.03 MPa), a level above the acceptable stress value. The first baffle is the most highly stressed baffle with a maximum Von Mises stress of 6,782 psi (46.76 MPa) occurring on the bottom of the baffle. The maximum stress on the top part of the tank is 3,998 psi (27.56 MPa) and occurs on the rear half . The support area is most highly stressed on the

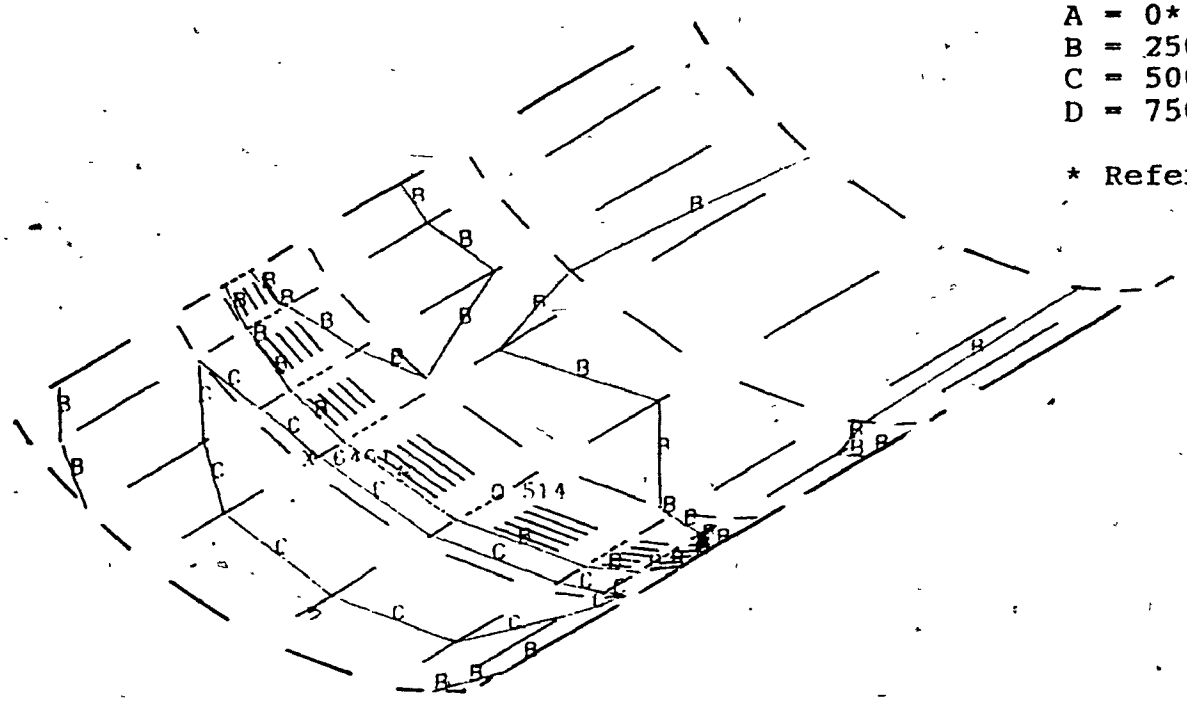

A = 0*
B = 2500
C = 5000
D = 7500

* Refers to stress value in psi.

Figure 3.9: Stress Contours for Rear Bottom Half of
Tanker B - Dead Weight Load
(Top thickness = 0.187 in., Bottom Thickness = 0.250 in.)
(For conversion to SI Units: 1 in = 0.0254 m; 1 psi = 0.00689 MPa)

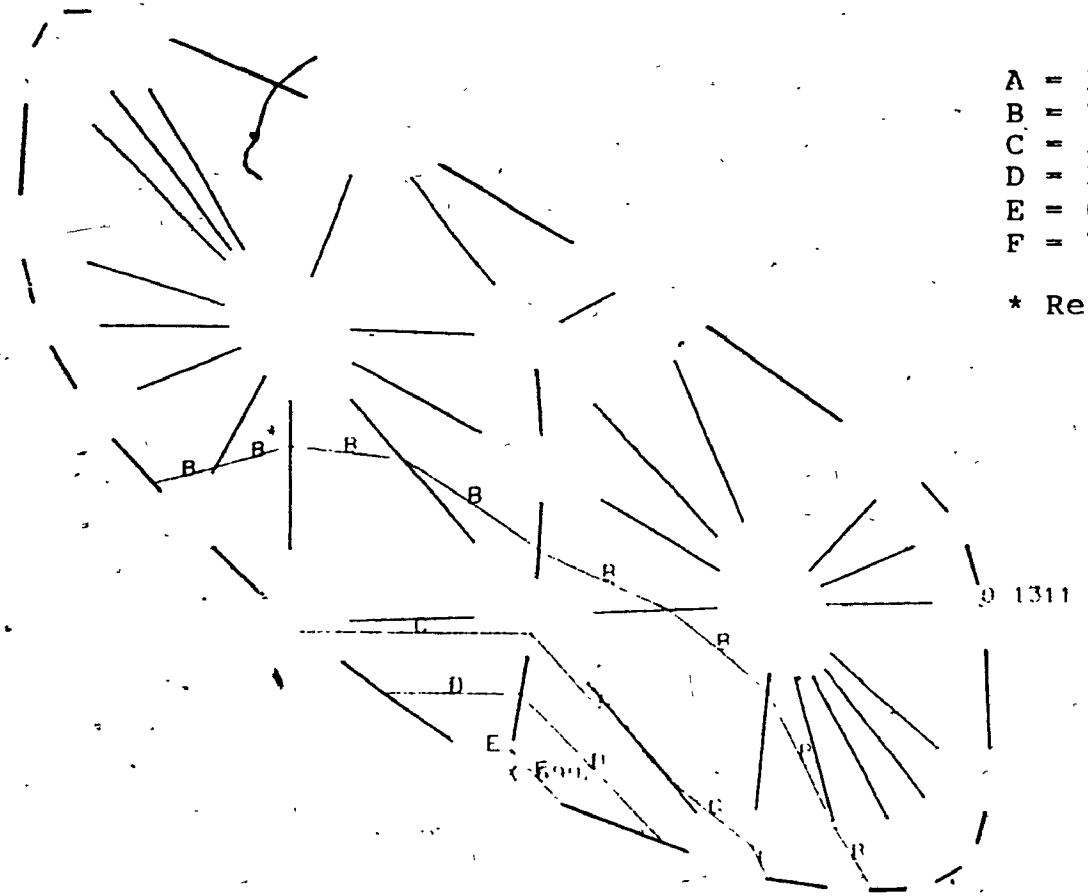

Figure 3.10: Stress Contours for the First Baffle of
Tanker B - Dead Weight Load
(Top thickness = 0.187 in., Bottom Thickness = 0.250 in.)
(For conversion to SI Units: 1 in = 0.0254 m; 1 psi = 0.00689 MPa)

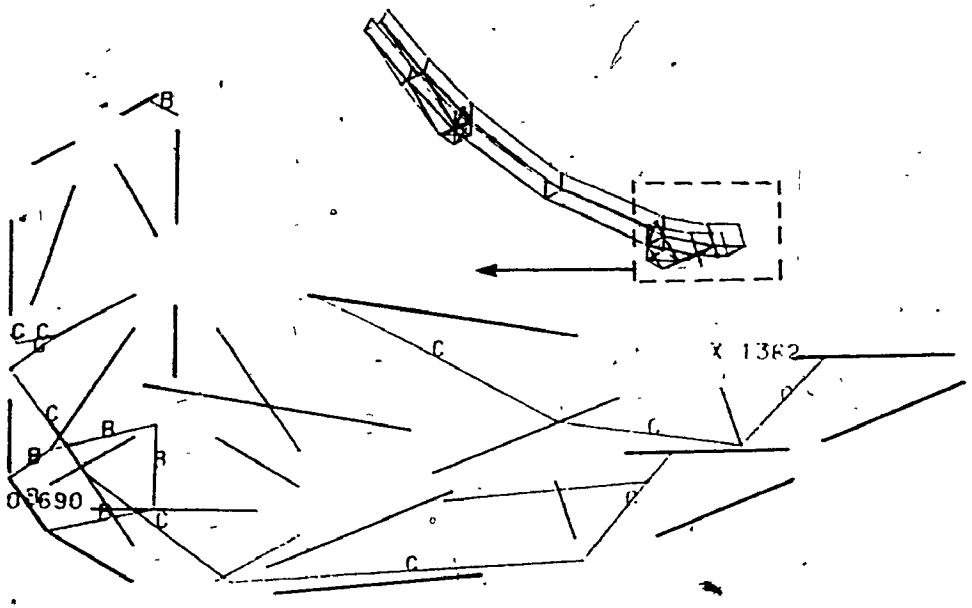

A = 400*
B = 800
C = 1200
D = 1600
E = 2000

* Refers to stress value in psi.

Figure 3.11: Stress Contours for the Right Rear Support of Tanker B - Dead Weight Load
(Top thickness = 0.187 in., Bottom Thickness = 0.250 in.)
(For conversion to SI Units: 1 in = 0.0254 m; 1 psi = 0.00689 MPa)

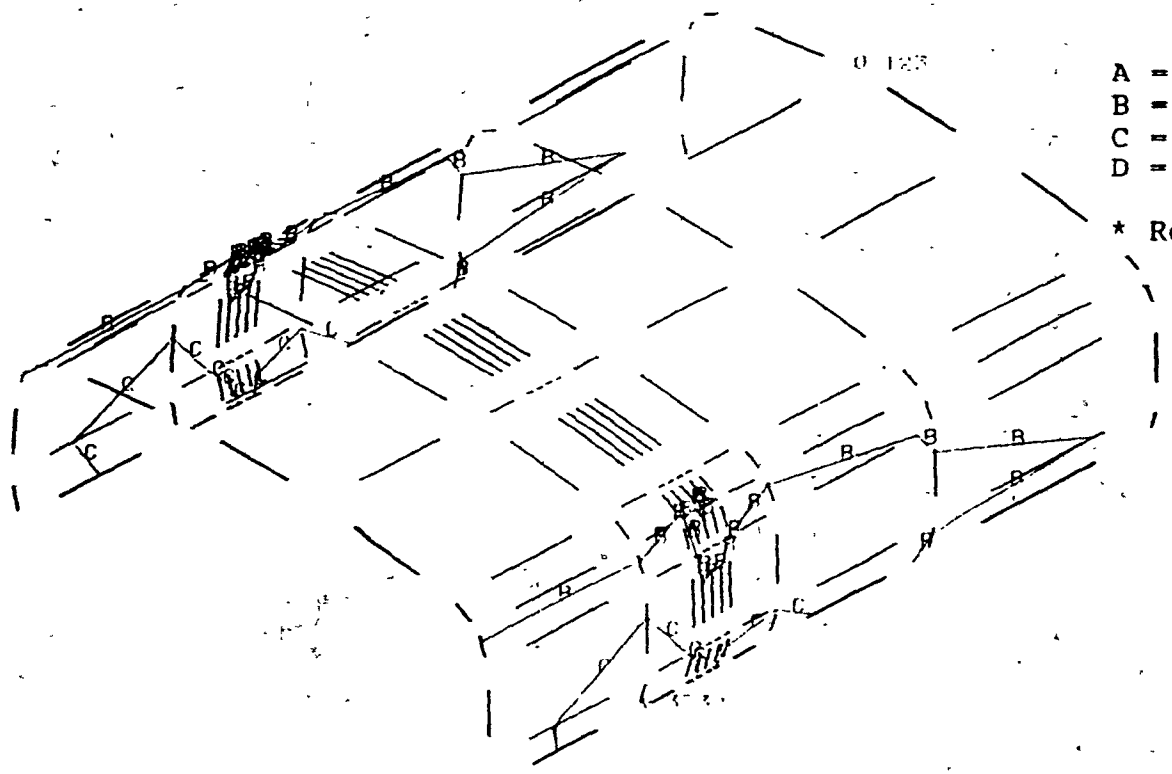

A = 0*
B = 1250
C = 2500
D = 3750

* Refers to stress value in psi.

Figure 3.12: Stress Contours for Rear Top Half of
Tanker B - Dead Weight Load
(Top thickness = 0.187 in., Bottom Thickness = 0.250 in.)
(For conversion to SI Units: 1 in = 0.0254 m; 1 psi = 0.00689 MPa)

left rear outrigger area with the highest stress of 4,153 psi (28.63 MPa). Again, as in the dead weight case, Tanker B experiences lower stresses than Tanker A for similar loading.

3.3.3 Parametric Variation for Tank Thickness

A parametric study similar to the one carried out for Tanker A was studied for Tanker B. The results of the parametric variation are shown in Table 3.3. The lowest maximum stress of 6,772 psi (46.67 MPa) occurs on the first baffle with both the top and bottom thicknesses of the tanker set to 0.250 in (0.00635 m). This is not a significant reduction in comparison to the maximum stress of 6,782 psi (46.76 MPa)which occurs on the first baffle with the top thickness set to 0.187 in (0.00475 m). The stresses on the top of the tank and on the support are also reduced by a small amount to 3,561 psi (24.55 MPa) and 4,127 psi (28.45 MPa) due to the change in the upper tank thickness to 0.250 in (0.00635 m).

3.3.4 Parametric Variation for the Baffles

As in the case of Tanker A, baffle geometry variation was carried out on Tanker B. Table 3.4 shows the results of the parameter variation on the baffles. The lowest stress case occurs with the baffle radius set to 4 in (0.1016 m) as in the case of Tanker A, and with a center hole diameter

Table 3.3 Tank Thickness Variation for Tanker B – Case 2 Loading

Case No.	Top Thickness (in)	Bottom Thickness (in)	Top Max. Stress (psi)	Bottom Max. Stress (psi)	First Baffle Max. Stress (psi)	Support Max. Stress (psi)
1	0.187	0.187	5,026	9,748	10,623	4,784
2	0.187	0.250	3,998	6,386	6,782	4,153
3	0.250	0.187	4,434	9,670	10,592	4,752
4	0.250	0.250	3,561	6,308	6,772	4,127

(For conversion to SI Units: 1 in = 0.0254 m; 1 psi = 0.00689 MPa)

Table 3.4 Baffle Variation for Tanker B – Case 2 Loading

(Tanker top thickness = 0.250 in.; bottom thickness = 0.250 in.)

Case No.	Hole Diameter (in)	Shape Radius (in)	Top Max. Stress (psi)	Bottom Max. Stress (psi)	First Baffle Max. Stress (psi)	Support Max. Stress (psi)
1	18.0	3.0	3,731	6,336	7,045	4,169
2	18.0	4.0	3,561	6,308	6,772	4,127
3	20.0	3.0	3,722	6,335	7,044	4,175
4	20.0	4.0	3,523	6,309	6,766	4,096

(For conversion to SI Units: 1 in = 0.0254 m; 1 psi = 0.00689 MPa)

of 20 in (0.508 m). Figures 3.13, 3.14, 3.15, and 3.16 show stress contour plots of the most highly stressed areas of Tanker B on bottom of tanker, on the first baffle, on the support and on the top of tanker (case 4 in Table 3). The maximum stresses on all four areas are not significantly reduced due to the baffle geometry variation. The stresses on bottom of the tank and on the first baffle are still above the acceptable level of 5,667 psi (39.07 MPa).

3.4 Tanker C

Tanker C is a double support type tanker with eight baffles and has a cross-section identical to Tanker A. Four baffles are directly positioned on top of the supports, with the interior two baffles placed equidistantly from the support.

3.4.1 Case 1: Dead Weight

In the case of the dead weight, this tanker was set on all four supports with the internal pressures of the liquid acting on it. The results show that the stresses throughout the tanker are significantly less compared to Tankers A and B. The highest stress of 4,549 psi (31.36 MPa) occurs on the bottom part of the first and last baffles. Unlike Tanker A and Tanker B, the top of the tanker experiences higher stress compared to the bottom of the tanker. This can be attributed to the extra strength provided by the

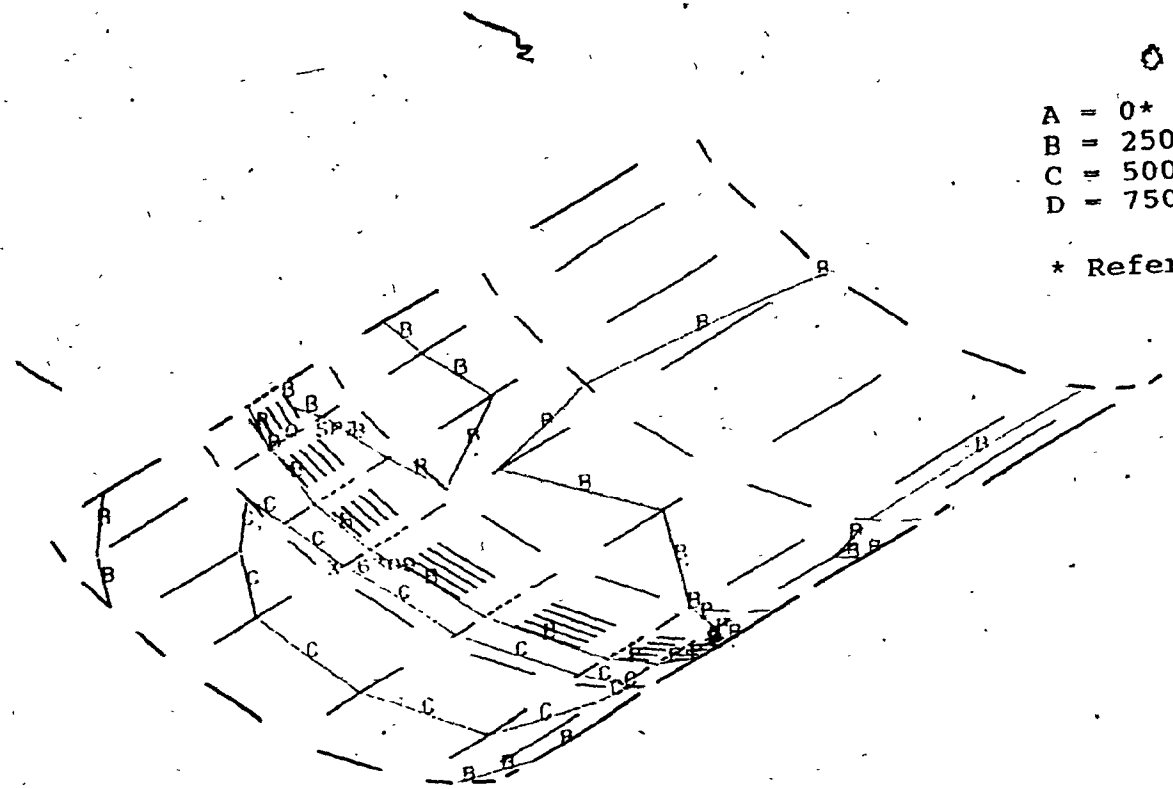

Figure 3.13: Stress Contours for Rear Bottom Half of
Tanker B - Torsion Load
(Top thickness = 0.250 in., Bottom Thickness = 0.250 in.)
(Baffle Hole Diam. = 20.0 in., Baffle Shape Rad. = 4.0 in.)
(For conversion to SI Units: 1 in = 0.0254 m; 1 psi = 0.00689 MPa)

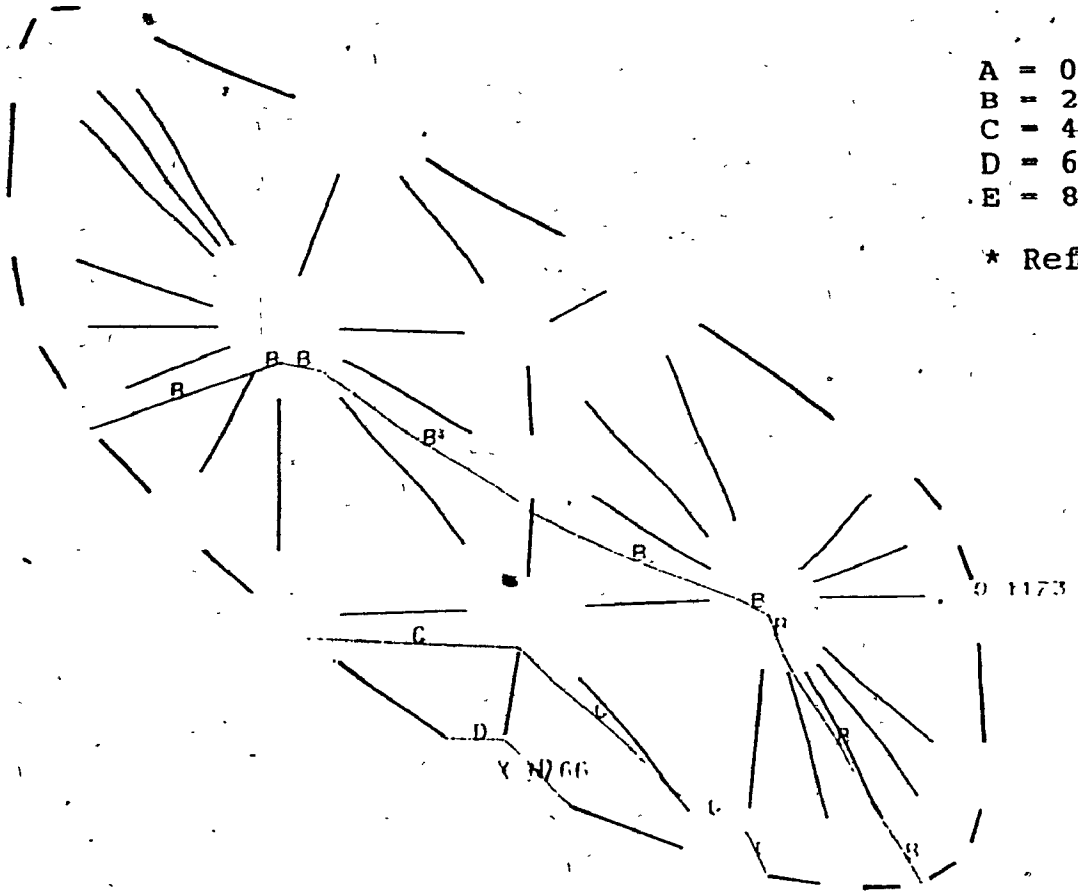

Figure 3.14: Stress Contours for the First Baffle of Tanker B - Torsion Load
(Top thickness = 0.250 in., Bottom Thickness = 0.250 in.)
(Baffle Hole Diam. = 20.0 in., Baffle Shape Rad. = 4.0 in.)
(For conversion to SI Units: 1 in = 0.0254 m; 1 psi = 0.00689 MPa)

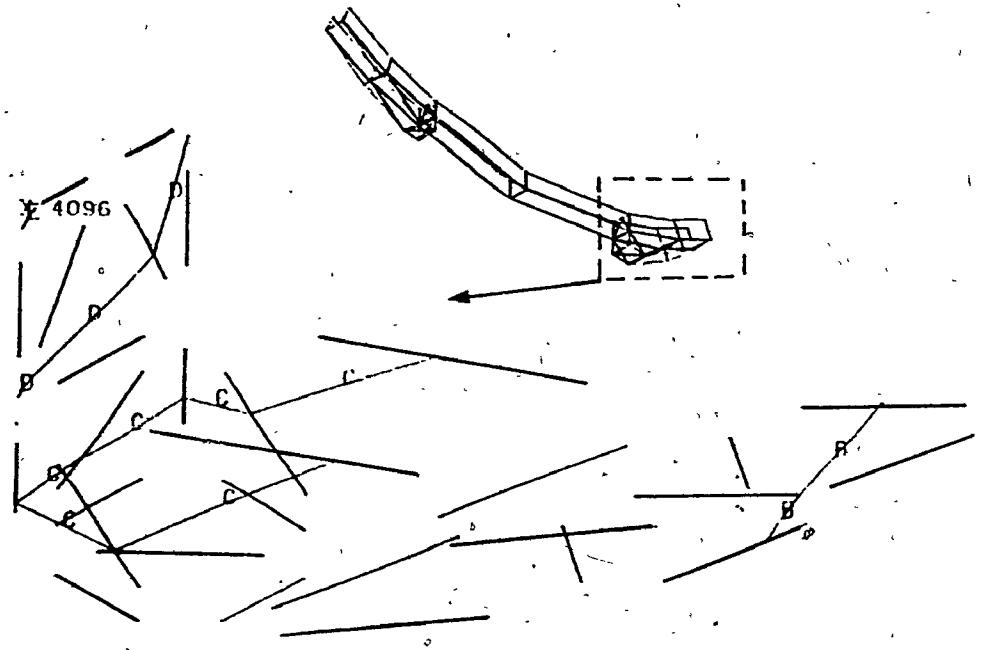

A = 0*
B = 1000
C = 2000
D = 3000
E = 4000

* Refers to stress value in psi.

Figure 3.15: Stress Contours for the Right Rear Support of Tanker B - Torsion Load
(Top thickness = 0.250 in., Bottom Thickness = 0.250 in.)
(Baffle Hole Diam. = 20.0 in., Baffle Shape Rad. = 4.0 in.)
(For conversion to SI Units: 1 in = 0.0254 m; 1 psi = 0.00689 MPa)

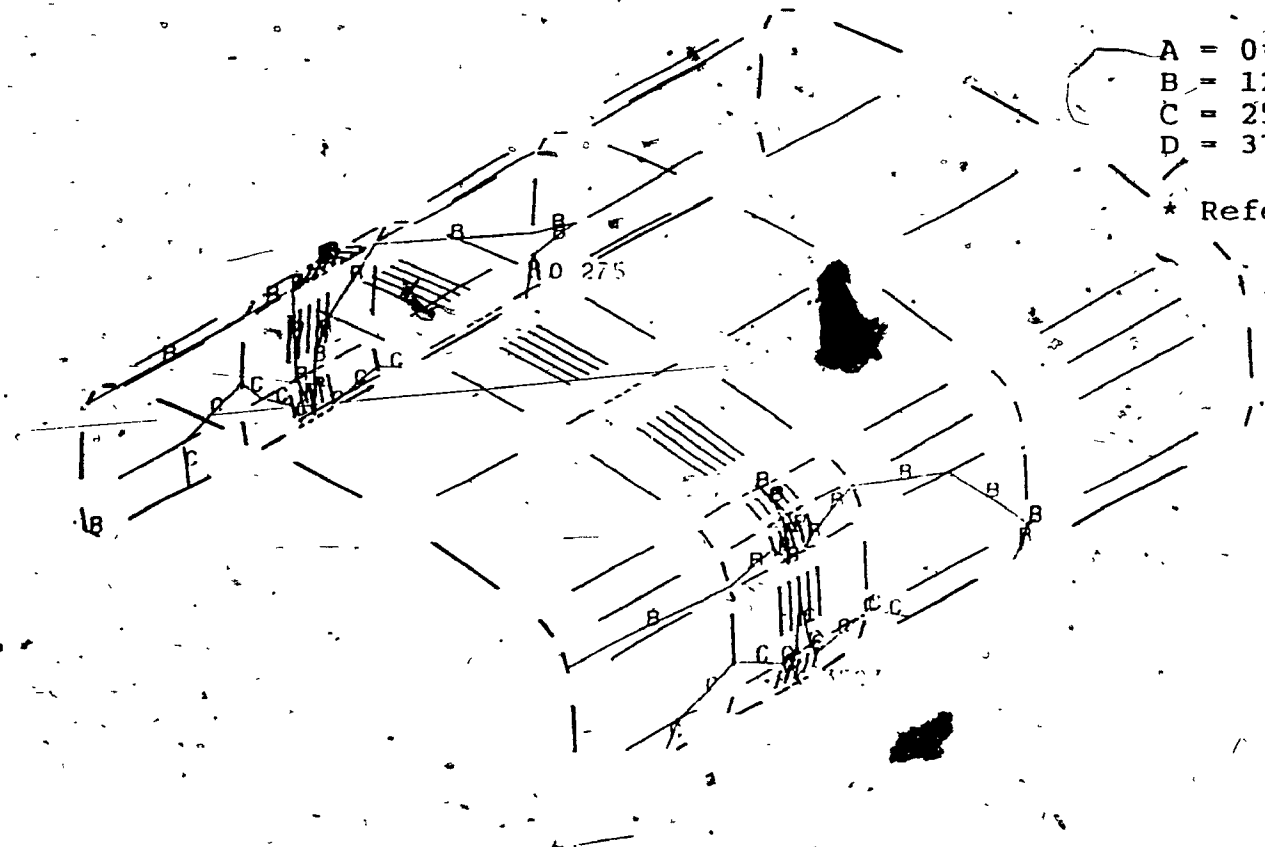

Figure 3.16: Stress Contours for Rear Top Half of
Tanker B - Torsion Load
(Top thickness = 0.250 in., Bottom Thickness = 0.250 in.)
(Baffle Hole Diam. = 20.0 in., Baffle Shape Rad. = 4.0 in.)
(For conversion to SI Units: 1 in = 0.0254 m; 1 psi = 0.00689 MPa)

double support to the tanker. The maximum stress on the top of the tanker is 3,699 psi (25.50 MPa) while the bottom of the tanker has a maximum stress of 2,180 psi (15.03 MPa). The maximum stress on the support structure is significantly less compared to single support cases and has a magnitude of only 855 psi (5.89 MPa). Figures 3.17, 3.18, 3.19, and 3.20 show the stress contours on the bottom of the tanker, the first baffle, the support structure and the top of the tanker.

As expected, the double support structure significantly reduces the Von Mises stresses throughout the tanker. These stresses are all below the acceptable level.

3.4.2 Case 2: Torsion

Tanker C was applied with the same torsion load as in the case of Tankers A and B. The most highly stressed area in the tanker is the first baffle with a maximum stress of 4,553 psi (31.39 MPa) occurring at the bottom of the baffle. The maximum stress on the top of the tank is 3,708 psi (25.56 MPa) while the bottom has a maximum stress of 2,178 psi (15.02 MPa). As in the case of the dead weight, the support structure does not experience a high stress with a maximum value of 880 psi (6.07 MPa) occurring on the front left angle. The stresses which occur on the different parts of the tanker for the dead weight case and the torsion case

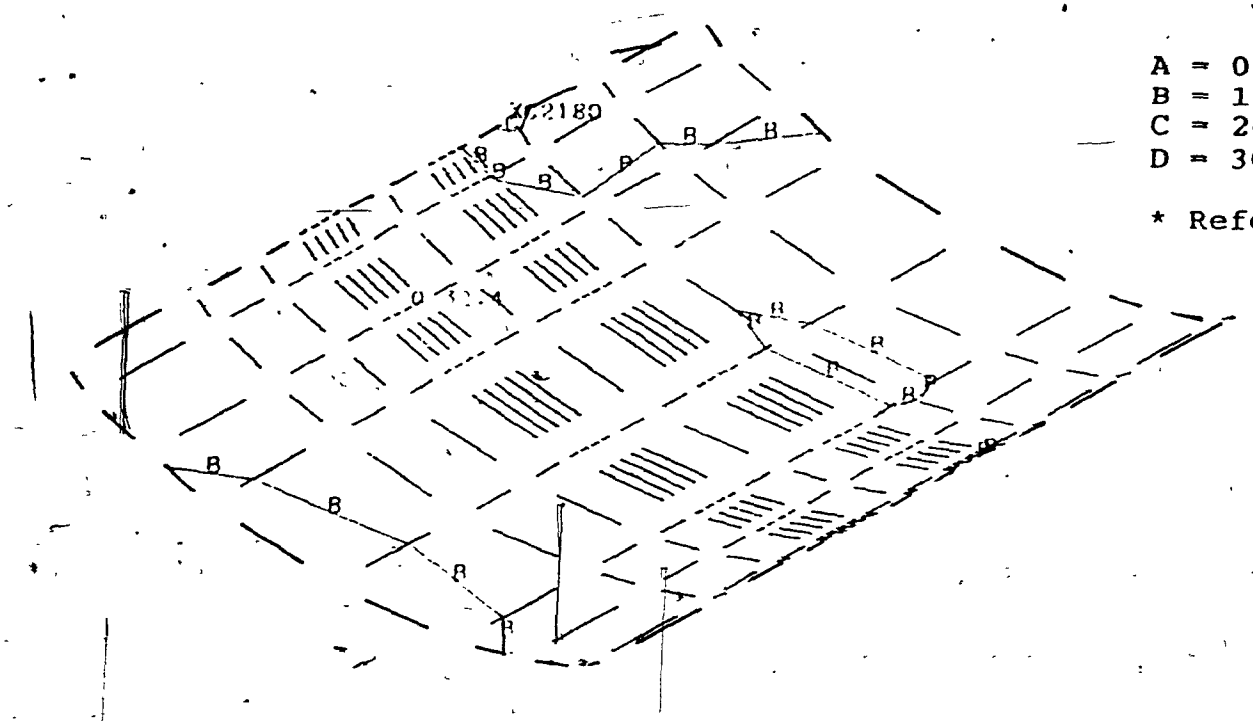

Figure 3.17: Stress Contours for Rear Bottom Half of Tanker C - Dead Weight Load
(Top thickness = 0.187 in., Bottom Thickness = 0.250 in.)
(For conversion to SI Units: 1 in = 0.0254 m; 1 psi = 0.00689 MPa)

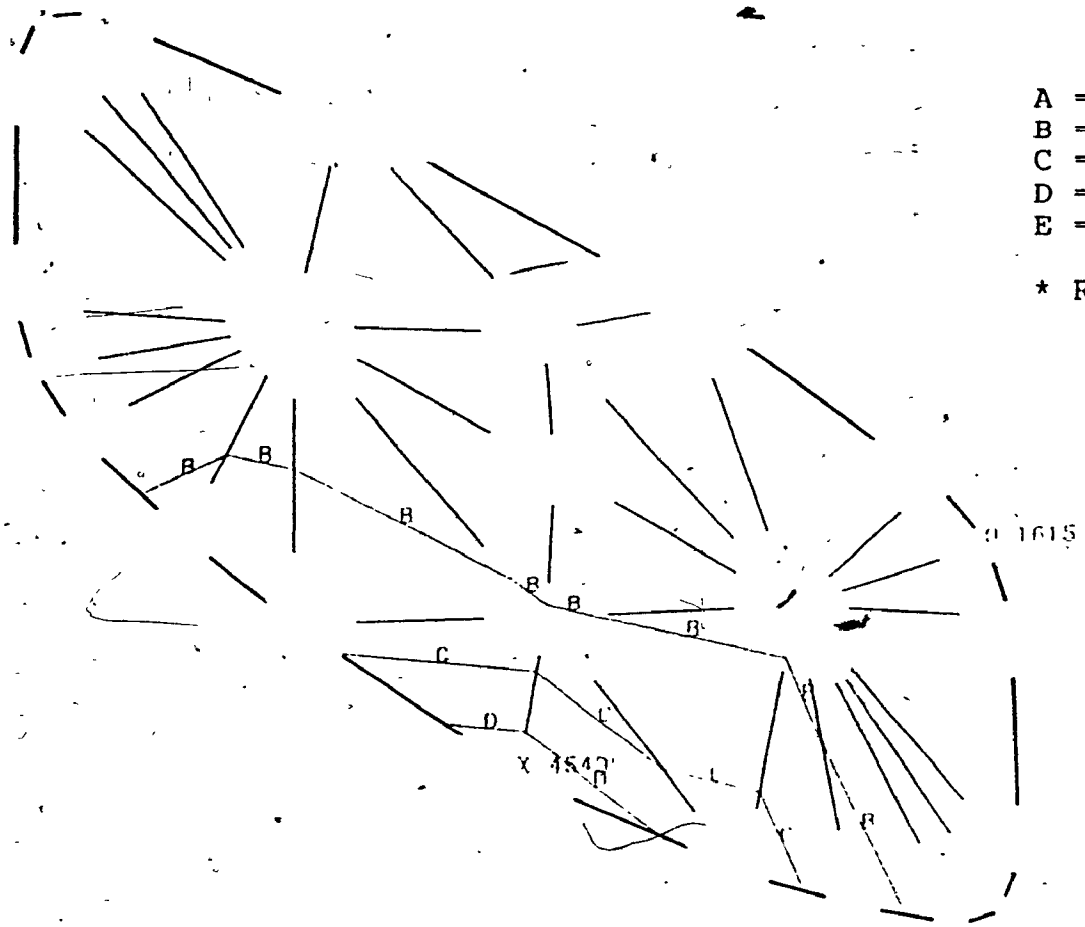

A = 1600*
B = 2400
C = 3200
D = 4000
E = 4800

* Refers to stress value in psi.

Figure 3.18: Stress Contours for the First Baffle of Tanker-C - Dead Weight Load
(Top thickness = 0.187 in., Bottom Thickness = 0.250 in.)
(For conversion to SI Units: 1 in = 0.0254 m; 1 psi = 0.00689 MPa)

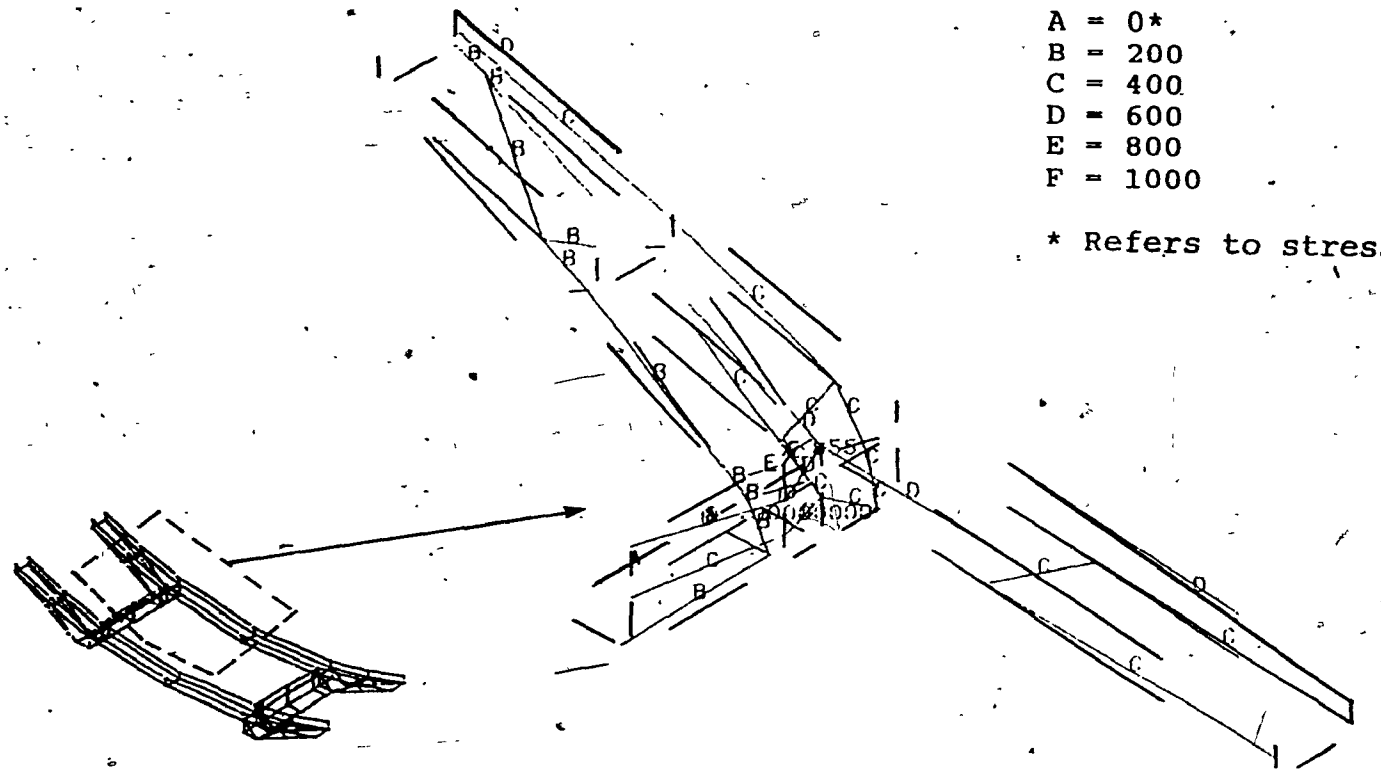

A = 0*
B = 200
C = 400
D = 600
E = 800
F = 1000

* Refers to stress value in psi.

Figure 3.19: Stress Contours for the Right Rear Support of Tanker C - Dead Weight Load
(Top thickness = 0.187 in., Bottom Thickness = 0.250 in.)
(For conversion to SI Units: 1 in = 0.0254 m; 1 psi = 0.00689 MPa)

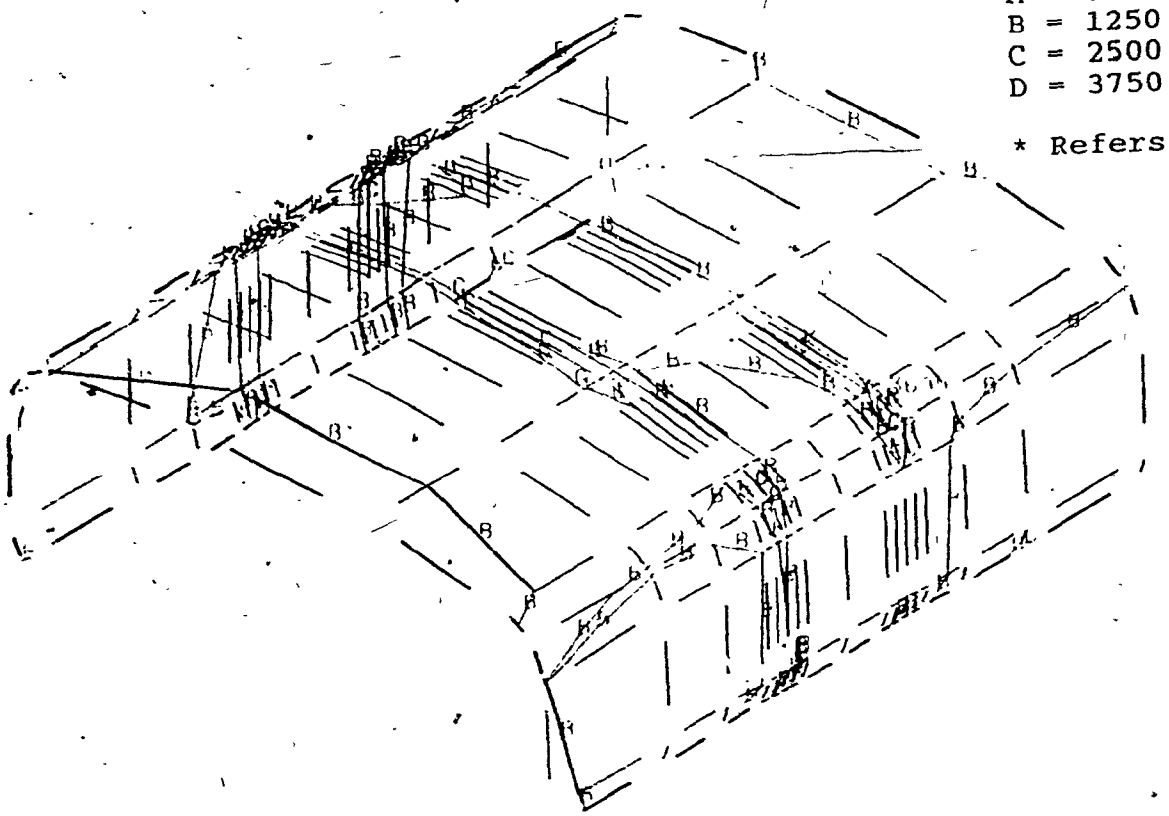

A = 0*
B = 1250
C = 2500
D = 3750

* Refers to stress value in psi.

Figure 3.20: Stress Contours for Rear Top Half of
Tanker C - Dead Weight Load
(Top thickness = 0.187 in., Bottom Thickness = 0.250 in.)
(For conversion to SI Units: 1 in = 0.0254 m; 1 psi = 0.00689 MPa)

are not very different. This can be attributed to the extra stiffness provided by the double supports and the extra angles included in the support configuration.

3.4.3 Parametric Variation for Tank Thickness

A parametric study similar to the one carried out for Tankers A and B was studied for Tanker C. The results of the parametric variation are shown in Table 3.5. The lowest maximum stress of 4,544 psi (31.40 MPa) occurred on the first baffle for the case when the top and bottom thicknesses are 0.250 in (0.00635 m). Referring to table 3.5, this case along with case 2 is found to have stress values below the critical value. Figures 3.21, 3.22, 3.23, and 3.24 show stress contour plots of the most highly stressed areas on the bottom of tanker, first baffle, support, and top of tanker. Case 3 where the top and bottom thicknesses are set to 0.187 in (0.00475 m) also experiences an acceptable stress level everywhere except on the first baffle which has a maximum stress of 5,887 psi (40.59 MPa).

3.4.4 Parametric Variation for the Baffles

The parametric variation for the baffles was carried out for case 1 in Table 3.5. Table 3.6 shows the results of the baffle geometry variation. The stresses on all the sections except on the baffle are acceptable for all the

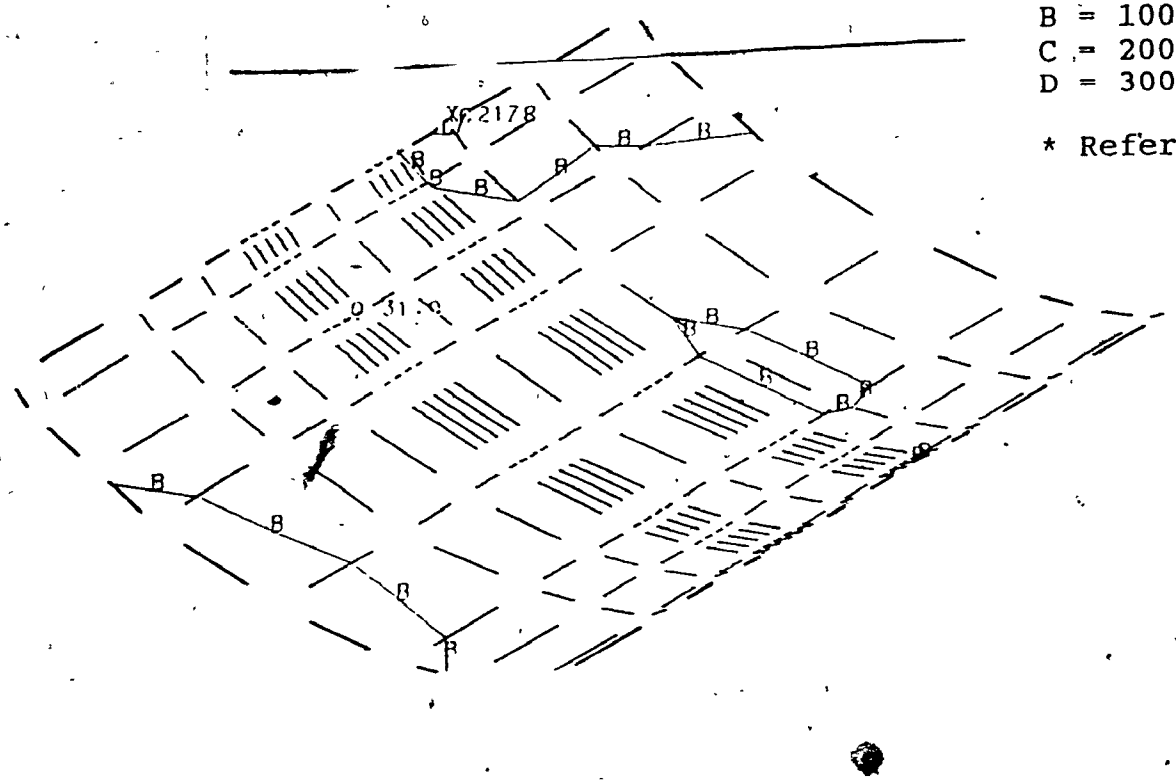

Figure 3.21: Stress Contours for Rear Bottom Half of
Tanker C - Torsion Load
(Top thickness = 0.187 in., Bottom Thickness = 0.250 in.)
(Baffle Hole Diam. = 18.0 in., Baffle Shape Rad. = 4.0 in.)
(For conversion to SI Units: 1 in = 0.0254 m; 1 psi = 0.00689 MPa)

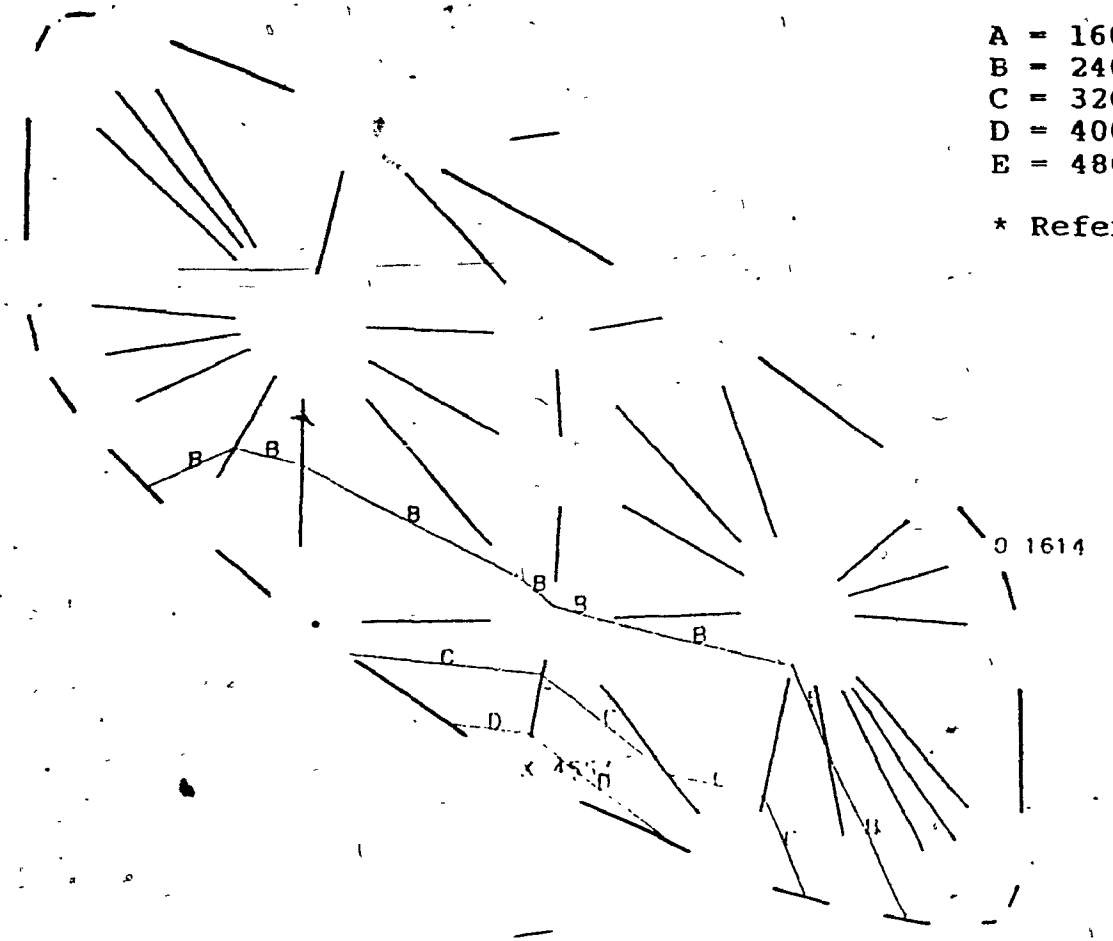

Figure 3.22: Stress Contours for the First Baffle of Tanker C - Torsion Load
(Top thickness = 0.187 in., Bottom Thickness = 0.250 in.)
(Baffle Hole Diam. = 18.0 in., Baffle Shape Rad. = 4.0 in.)
(For conversion to SI Units: 1 in = 0.0254 m; 1 psi = 0.00689 MPa)

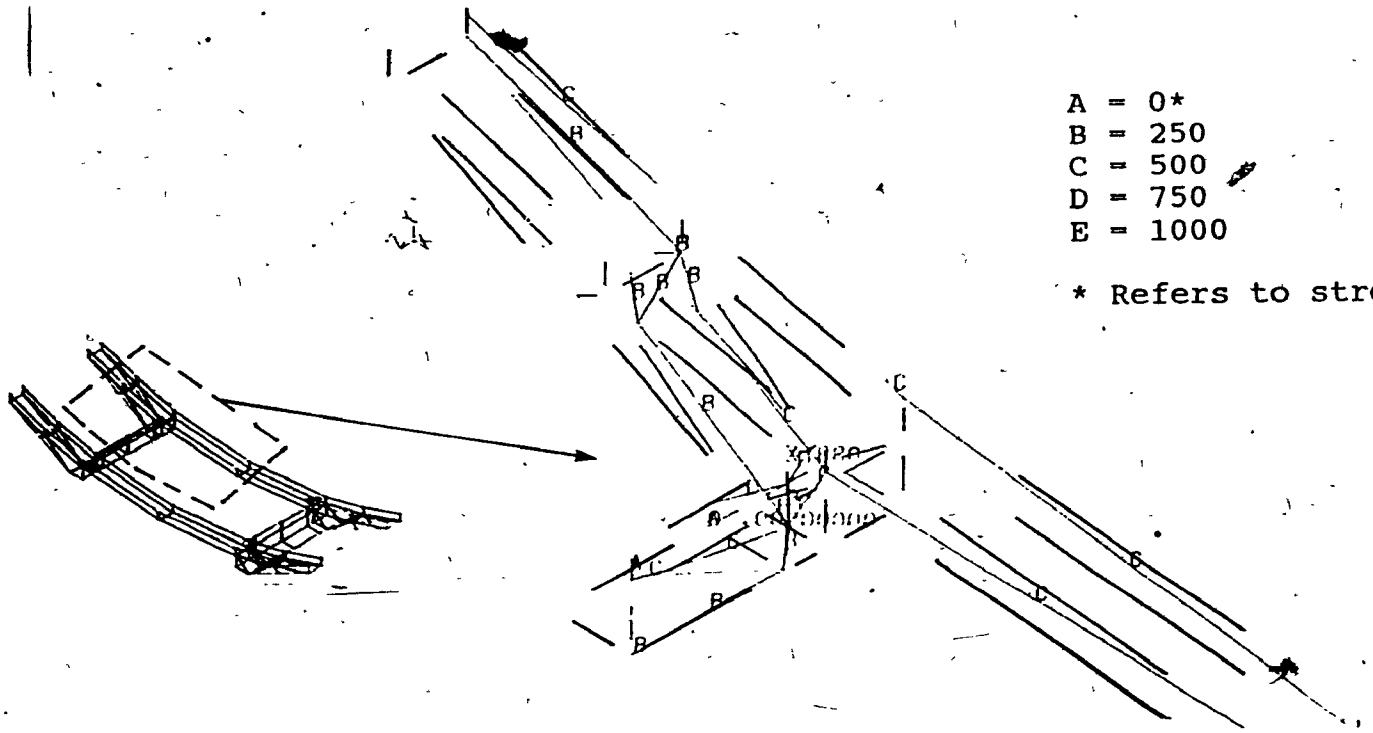

Figure 3.23: Stress Contours for the Right Rear Support of Tanker C - Torsion Load
(Top thickness = 0.187 in., Bottom Thickness = 0.250 in.)
(Baffle Hole Diam. = 18.0 in., Baffle Shape Rad. = 4.0 in.)
(For conversion to SI Units: 1 in = 0.0254 m; 1 psi = 0.00689 MPa)

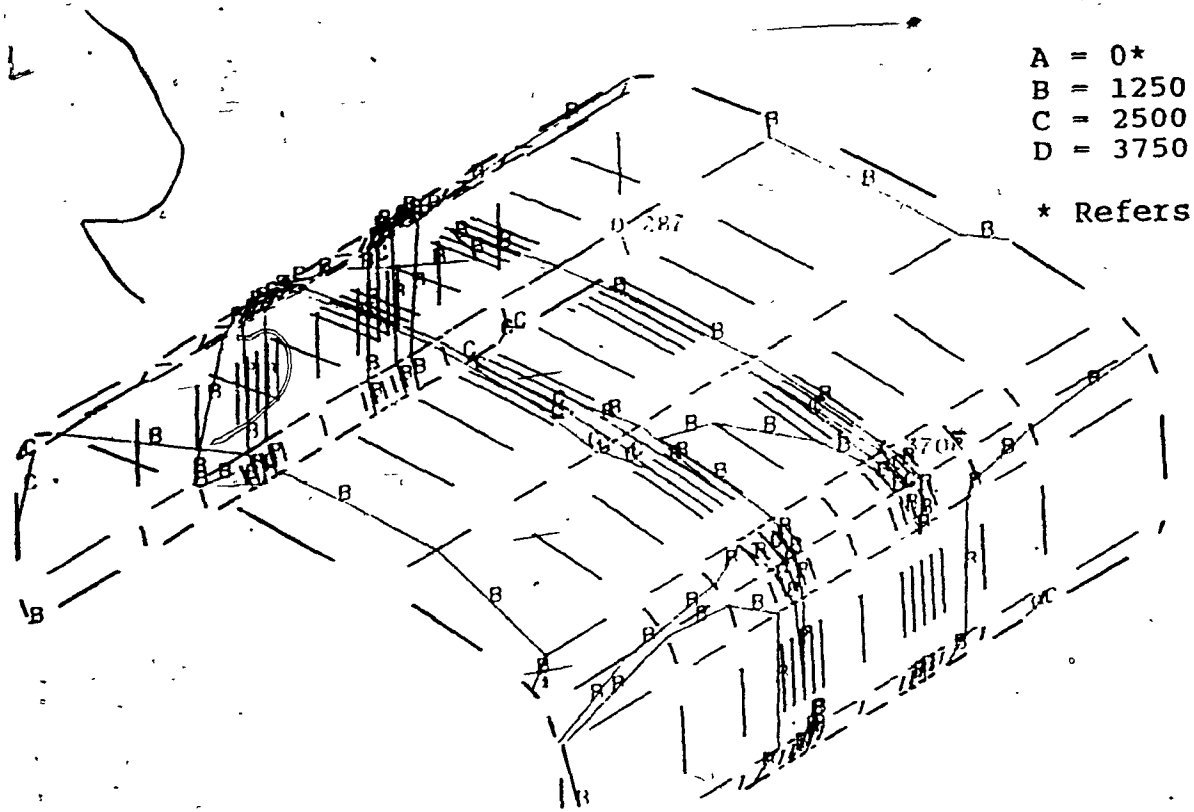

Figure 3.24: Stress Contours for Rear Top Half of
Tanker C - Torsion Load
(Top thickness = 0.187 in., Bottom Thickness = 0.250 in.)
(Baffle Hole Diam. = 18.0 in., Baffle Shape Rad. = 4.0 in.)
(For conversion to SI Units: 1 in = 0.0254 m; 1 psi = 0.00689 MPa)

Table 3.5 Tank Thickness Variation for Tanker C - Case 2 Loading

Case No.	Top Thickness (in)	Bottom Thickness (in)	Top Max. Stress (psi)	Bottom Max. Stress (psi)	First Baffle Max. Stress (psi)	Support Max. Stress (psi)
1	0.187	0.187	3,996	4,498	5,887	972
2	0.187	0.250	3,708	2,178	4,553	880
3	0.250	0.187	3,412	4,458	5,899	955
4	0.250	0.250	3,289	1,784	4,544	868

(For conversion to SI Units: 1 in = 0.0254 m; 1 psi = 0.00689 MPa)

Table 3.6 Baffle Variation for Tanker C – Case 2 Loading

(Tanker top thickness = 0.187 in.; bottom thickness = 0.187 in.)

Case No.	Hole Diameter (in)	Shape Radius (in)	Top Max. Stress (psi)	Bottom Max. Stress (psi)	First Baffle Max. Stress (psi)	Support Max. Stress (psi)
1	18.0	3.0	3,931	4,509	6,362	1,003
2	18.0	4.0	3,996	4,498	5,887	972
3	20.0	3.0	4,021	4,509	6,363	996
4	20.0	4.0	3,846	4,498	5,890	976

(For conversion to SI Units: 1 in = 0.0254 m; 1 psi = 0.00689 MPa)

baffle geometry variations. The lowest value of stress on the baffle corresponds to the case where the baffle is with a hole size of 18 in (0.4572 m) and shape radius of 4 in (0.1016 m).

3.5 Comparison of Results and Recommendations

The results of the parametric variation for Tankers A and B show that both of these tankers will not meet the critical stress criteria set for the design. Tanker C is found to experience stresses below the maximum acceptable level. The different variations of thicknesses on Tanker C show that only in the case where both the top and bottom thicknesses are set to 0.187 in (0.00475 m), does the maximum stress value exceeds the acceptable level. This occurs on the first baffle.

3.6 Summary

Three types of liquid tankers are analyzed in this chapter. To reduce the stress to an acceptable level, tank thickness variations as well as baffle shape radius, and manhole diameter variations are carried out on all three tankers. The results of this design parametric study are presented in this chapter.

CHAPTER 4

AUTOMATED SUBMODEL COMPONENT REANALYSIS

CHAPTER 4

AUTOMATED SUBMODEL COMPONENT REANALYSIS

4.1 General

As it can be seen from the previous section, it is often required in most design problems to reanalyze the model for minor structural changes. In applying the finite element method for analysis, even a minor design change usually means a full reanalysis of the modified model. Different methods have been proposed in the last two decades for simplyfing and reducing the computations required in this reanalysis. The most commonly used method for reanalysis is through the use of substructures in the creation of the model. Substructures give the designer the ability to modify and reanalyze a section of the model if it has been created as a substructure right from the beginning. Thus, the main limitation of this method for reanalysis purposes is that the substructures have to be defined a priori in the first analysis. They cannot be created after the modeling has been done without a lot of redundancy in the work. This sometimes causes difficulties as the designer often becomes aware of the critical region only after the first analysis as the highly stressed areas sometimes appear on unlikely parts of the model.

Other techniques often used include the Taylor series expansion for response variables [26] ,the Jacobi iteration

and the Gauss-Seidel iteration method [33]. They are approximate techniques and require iterative procedures for the solution. They normally work on the full finite element model and not on the sub-area of interest and thus often require a large amount of computation.

In this section, a new technique for reanalysis and the software which was developed for this purpose is presented. This technique can be utilized to provide a good approximation to the solution for design modifications within a sub-area of a finite element model. It combines St. Venant's principle, and the concept of submodelling for the reanalysis. In this technique, it is possible to extract a submodel from a full finite element model, and from this submodel a single- or multi-component reanalysis within the submodel can be carried out. It can be used for parametric variation analyses or sensitivity analyses of different design variables within a submodel of interest. It is an approximate procedure and requires an initial submodel boundary displacement solution and submodel element stiffness generation from the complete model. It allows design modifications to components within the submodel, and gives a displacement solution for these components. This solution gives a good approximation to the displacement solution of these same components, obtained by analysis carried out on the complete model with

similar design modifications.

As opposed to substructuring, this technique provides flexibility to the user to study the effect of component variation within the submodel after the initial finite element analysis of the full model has been performed only once. This way, the user can select only the highly stressed area for the reanalysis. Different variations to design parameters within the submodel can thus be analyzed at the submodel level without having to reanalyze the full finite element model.

4.2 Submodelling Concept

The submodelling concept originates from the St. Venant's principle which states that localized effects tend to disappear rapidly as the forces involved are transmitted away from the the region of application [32]. This principle in finite element analysis allows the use of the displacements generated in a original base model as boundary displacement constraints in a submodel. This submodel must have approximately similar geometry and stiffness as the area of interest of the original model. An illustration of this principle is shown in Figure 4.1. In theory, either forces or displacements can be applied to the boundary nodes of the submodel.

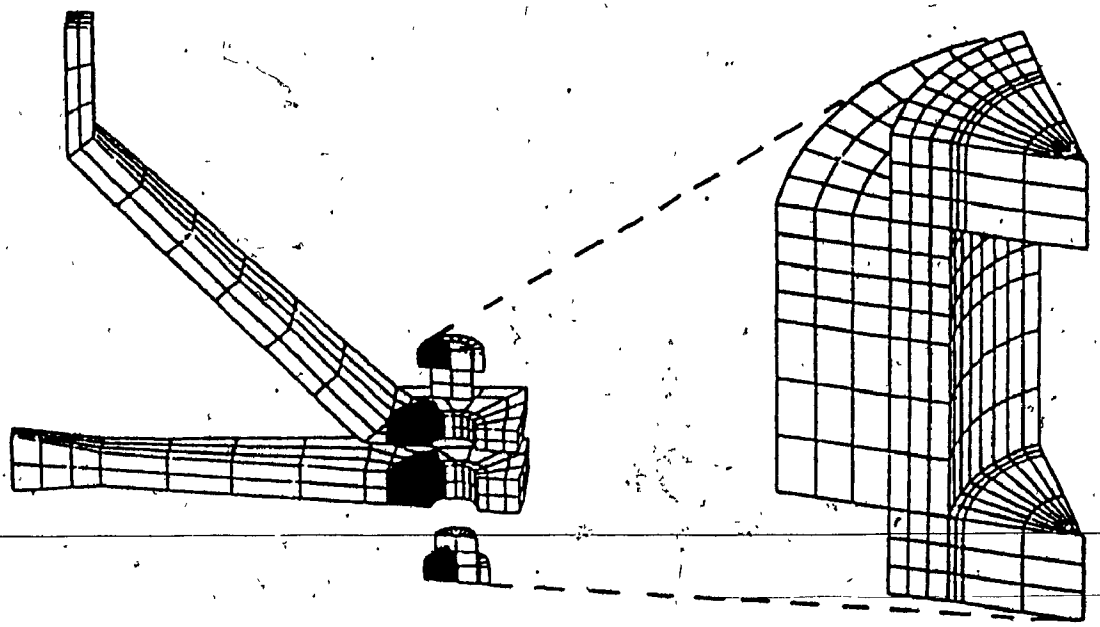

Figure 4.1: Illustration of St. Venant's Principle (Ref. [9])

Based on St. Venant's principle, one can thus isolate an area of interest within a finite element model after the initial run and utilize this area as a submodel for detailed analysis. The displacement solution of this cut boundary, as generated by the initial run can be applied along the boundary nodes of this submodel. The forces acting inside this region must be maintained as in the full model. This application of the cut boundary loads will give similar displacement and stress distribution as calculated for the same region in the initial run of the full model. The solution generated due to minor design variations on components within the submodel will be quite close to the solution of the same region on the full model subjected to the same component design variations.

4.3 Mathematical Formulation for Component Reanalysis

For finite element static analysis, the equation solved is the following

$$[K]\{Y\} = \{P\} \qquad (4.1)$$

where [K] is the global stiffness matrix of the submodel,

{Y} is the unknown displacement solution,

{P} is the load on the structure

The global matrix [K] is calculated by the summation of

the individual element stiffness matrices in global coordinates. Often when a small change is carried out to the structure, only some of the element stiffnesses change. Thus, only a part of the global matrix changes.

If the global matrix can be assembled in such a way that all the elements which are modified are at the top left corner of the matrix, only this section of the global matrix will change upon the modification. Thus a partitioning technique can be applied which utlizes the change of only a small section of the global matrix for a modified components reanalysis.

The global matrix partioning can be done in the following way :

$$K = \left[\begin{array}{ccc|ccc} k_{1,1} & \cdots & k_{1,r} & k_{1,r+1} & \cdots & k_{1,n} \\ \vdots & & \vdots & \vdots & & \vdots \\ k_{r,1} & \cdots & k_{r,r} & k_{r,r+1} & \cdots & k_{r,n} \\ \hline k_{r+1,1} & \cdots & k_{r+1,r} & k_{r+1,r+1} & \cdots & k_{r+1,n} \\ \vdots & & \vdots & \vdots & & \vdots \\ k_{n,1} & \cdots & k_{n,r} & k_{n,r+1} & \cdots & k_{n,n} \end{array}\right]$$

Rewriting gives

$$K = \left[\begin{array}{c|c} K11 & K12 \\ \hline K21 & K22 \end{array}\right]$$

where the matrices [K12], [K21] and [K22] do not change and the matrix [K11] may vary from design to design.

Thus, we can write Equation (4.1) as :

$$[K11]\{Y1\} + [K12]\{Y2\} = \{P1\} \qquad (4.2)$$

$$[K21]\{Y1\} + [K22]\{Y2\} = \{P2\} \qquad (4.3)$$

where $\{P1\} = \{p_1,\ldots,p_r\}$ and $\{P2\} = \{p_{r+1},\ldots,p_n\}$ and $\{Y1\} = \{y_1,\ldots,y_r\}$ and $\{Y2\} = \{y_{r+1},\ldots,y_n\}$.

From equation 4.3 , we can write

$$\{Y2\} = [K22]^{-1}(\{P2\} - [K21]\{Y1\}) \qquad (4.4)$$

substituting into equation (4.2) and rearranging

$$\{Y1\} = ([K11 - K12K22^{-1}K21]^{-1}[P1 - K12K22^{-1}P2] \qquad (4.5)$$

The first step for the solution is to determine the inverse of [K22]. Once this has been calculated, all subsequent solutions involving the change in stiffness of the components of interest ([K11] matrix), only require the computation of the inverse of the matrix $[K11-K12K22^{-1}K21]$.

4.4 Submodel Component Reanalysis Software Description

A software for submodel component reanalysis was developed to demonstrate the effectiveness and validity of utilizing St. Venant's principle together with the above described partitioning technique. This software as described in the following sections utilizes the submodel stiffness data and the element node numbering extracted from Ansys F.E. software, as the only inputs for the reanalysis. The stiffness data is extracted from the Ansys generated stiffness file **FOR002.DAT** [9]. Minor variations to geometry such as thickness can be carried out from within the software, while structural changes require the recalculation of the modified element stiffnesses within Ansys.

As shown in Figure 4.2, the reanalysis cycle begins after the Ansys analysis . From the data generated by the first analysis run, the element stiffness matrices are extracted using the subroutine Readstif. Using submodel element numbering and nodal listing, bandwidth reduction for the submodel global matrix is independently carried out in a seperate subroutine.

The next routine used in the reanalysis cycle is the partitioned matrix assembly routine which uses the element data, the reduced bandwidth nodal listing, and the submodel

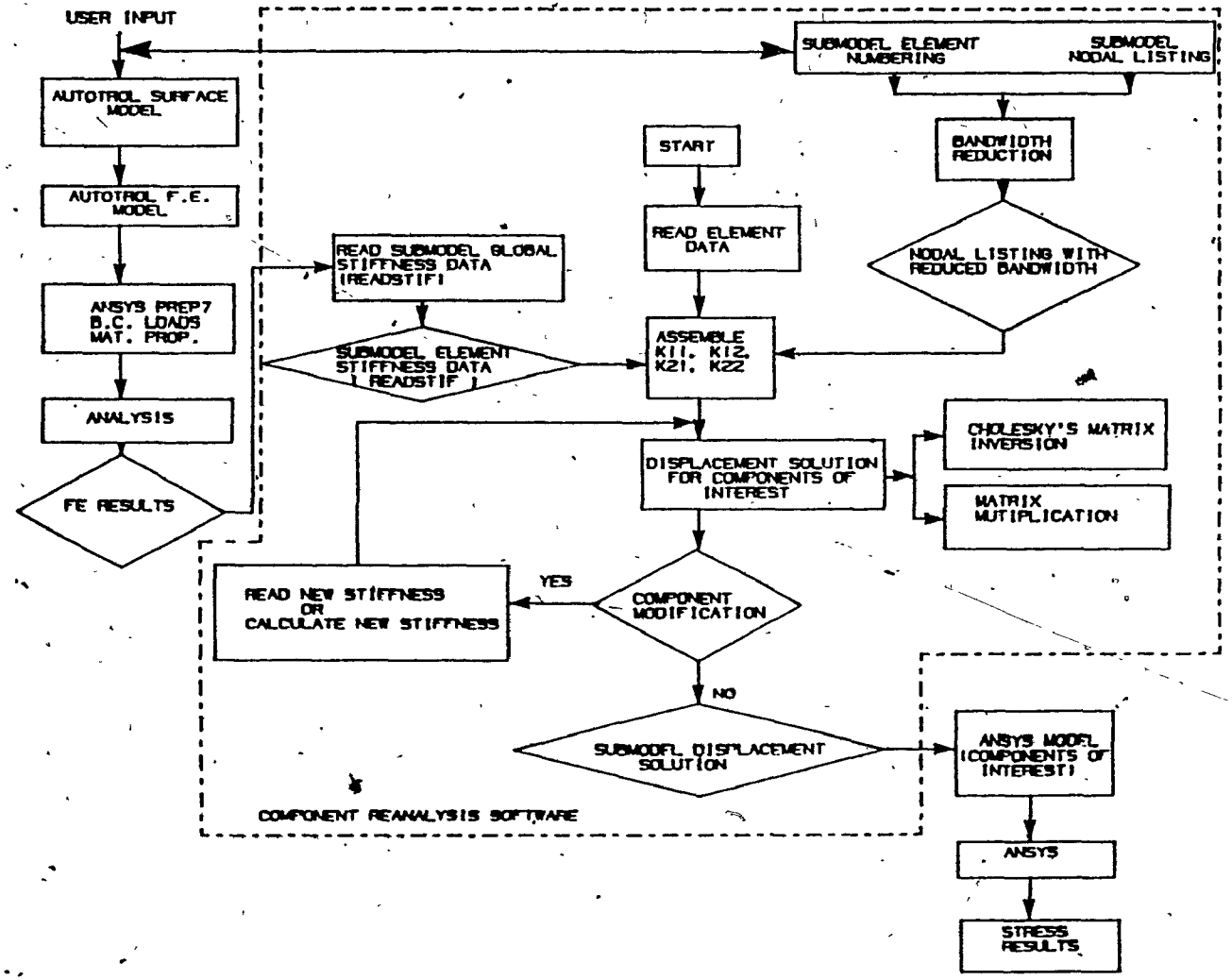

Figure 4.2: Automated Submodel Reanalysis Software

element stiffness data. The partitioned matrix assembly is carried out by placing those element stiffness matrices which correspond to components of interest in the top left partition ([K11]) and the rest of the element stiffness matrices are assembled and placed in [K12], [K21], and [K22] positions.

The assembled partitioned matrix is then used by an another routine to calculate actual displacement of the components of interest in the submodel utilizing the Equation 4.5 as described in the previous section. This routine utilizes two other routines; one for matrix inversion using Cholesky's decomposition method; and another for matrix multiplication using reduced link list storage. Next step in the reanalysis cycle is to calculate [K22] for the displacement solution using equation 4.5. For variations in design of the components of interest within the submodel, a new [K11] matrix can be calculated or assembled within this routine. For the assembly of the [K11], a database with an interface routine has been incorpporated with the software. The new [K11] matrix is then sent to the solution routine for the reanalysis calculation based on Equation 4.5.

On completion of the reanalysis, the displacement solution for the components of interest can then be sent as

input to Ansys as the boundary condition for a model composed of only the components of interest analyzed. The stress solution for these components of interest can then be generated using Ansys.

4.4.1 Element Stiffness Generation and Extraction

An Ansys analysis run produces number of files describing the model geometry, loading conditions, boundary conditions, calculated elemental stiffnesses, etc . They are stored in a series of **FOR0nn.DAT** files in either ASCII or binary format. The element stiffness matrices are stored in the file **FOR002.DAT** in binary format by Ansys during an analysis run. The **AUX2** routine available within Ansys can be used to dump file **FOR002.DAT** in ASCII format. This data can then be accessed by a user written Fortran program. The stiffnesses of the submodel elements can then be reordered or placed in any format in a data file for usage by a reanalysis program.

After an initial Ansys run of the full model, the program **Readstif** is used to extract the element stiffness matrices of the submodel of interest from the Ansys data file. These stifnesses are in global coordinates and thus do not have to undergo any type of conversion. The program Readstif then writes this data into a file with a known format so that it can be read by the reanalysis software.

4.4.2 Data Input

Data input into the reanalysis software includes a file containing the node numbering of all the elements of interest, the stiffness file extracted from Ansys, and the bandwidth optimized nodal listing of the submodel. The element list file can be automatically created using the Prep7 utility provided by Ansys. This file also has to be used as an input to the bandwidth optimization routine. The output from the bandwidth optimization routine is file containing a sorted list of the degrees of freedom to be inputted into the reanalysis software.

The data required for the parametric variation (sensitivity analysis) can be inputted into either interactively or through a file if the reanalysis is to be carried out in batch mode.

4.4.3 Bandwidth Optimization

Since the assembled global matrices are normally sparse, many schemes have been proposed to make use of the sparsity during the matrix manipulation in the solution phase. They are known as profile reduction ordering schemes and can significantly reduce the number of computations in the solution or during inversion of a large sparse symmetric matrix [28]. Since symmetric matrices can be stored in a banded form, the main principle of these

routines is to re-order the matrix so as to place all non-zero data as close to the diagonal as possible, i.e. to reduce the bandwidth of the matrix.

The most widely used algorithm for bandwidth reduction is the Cuthill-Mckee ordering scheme [28] which was proposed by Cuthill and Mckee in 1969. This scheme utilizes the following observation. Let y be a node of interest , and z be a neighbour of y used on the same element. To minimize the bandwidth of the row associated with z, it is apparent that the node z should be ordered as soon as possible after y.

Using this idea, an algorithm was developed and implemented in the reanalysis software. In this algorithm the node which has the highest degree amongst all the nodes in the nodal list (i.e. the node used in the most number of elements) is used as a starting node. The algorithm then tries to determine the next node to be placed in the reordered list such that it is a connecting node to the first node and has the highest degree amongst all the connecting node. The next few nodes are chosen from the connecting nodes of the second node until the list of all connecting nodes for the second node are exhausted. This follows on for the node with the second highest degree connected to the starting node. This method of ordering is

done until the full nodal list is reordered. A flowchart describing this algorithm is given in Appendix I.

After the ordering , nodes belonging to the components of interest are extracted and placed in the same order in the beginning of the list. The rest of the nodes are placed after the nodal list corresponding to the component of interest. Thus, there are now two sorted list of nodes: the first one corresponding to the components of interest and the second one corresponding to the rest of the submodel.

4.4.4 Partitioned Global Matrix Assembly

The process for global matrix assembly can be symbolically written as

$$[K] = \sum_{i} [Ki]$$

where the matrix [Ki] is the stiffness matrix of the ith element and the summation goes over all elements in the assemblage.

As shown in section 4.3, the global matrix is partitioned into four sub-matrices i.e. [K11], [K12], [K21], and [K22]. These are matrices created by partitioning the global matrix along a specific degree-of-freedom. To reduce computational time, an algorithm was developed which during global matrix assembly stores the

data in a partitioned form. The routine developed from this algorithm utilizes the reduced bandwidth degree-of-freedom list as the storage order for the global assembly. Details of this assembly procedure are given in Appendix II.

As the matrices [K11] and [K22] are symmetrical along the diagonal, a compacted storage procedure is used in this scheme. The diagonal elements are thus stored along the 1st column with only the elements on the right of the diagonal being stored beside it.

4.4.5 Submodel Component Reanalysis

The actual solution of the submodel component reanalysis was implemented in a subroutine which utilizes Equation 4.5 . This subroutine calls for a matrix inversion and sparse matrix multiplication routines. It also provides the user with the ability to modify the submodel component parameter variations for reanalysis. The parameter variations can either be inputted interactively or via a batch mode. This routine inverts only once the matrix [K22] , and utilizes it for all subsequent calculations for submodel component reanalysis.

4.4.6 Matrix Inversion Using Cholesky's Decomposition Method

Cholesky's method which utilizes matrix decomposition and factorization was implemented before the matrix

inversion in the reanalysis. It is a modified version of the Gauss Jordan's method used for solving a set of linear equations. It is one of the faster methods for matrix inversion when used with reduced bandwidth matrices. Appendix III describes the derivation of the final equations used in the inversion subroutines utilizing this method.

4.4.7 Matrix Multiplication Using Sparse Matrix Compacted Storage

Due to the requirement of large number of multiplications in the reanalysis procedure, an algorithm using a compacted matrix storage multiplication scheme was developed. This algorithm works only on the non-zero elements of the matrices, reducing significantly the unnecessary computations.

In this algorithm, the non-zero elements of the matrices to be multiplied are first placed in single-dimensioned arrays. Another single dimensional array containing pointers for the position of each element in the original matrix is also created. The two single dimensional arrays are then multiplied together by multiplying and adding only those elements indicated by the pointer arrays, thus reducing the large number of computations which would have resulted from adding and multiplying the zero elements in the original two matrices.

4.4.8 Stress Analysis of Submodel Using Finite Element Software

Once the displacement solution of the modified components within a submodel has been generated by the reanalysis software, it can then be utilized to generate the stress solution for the components. To generate the stress solution, the finite element models of the individual modified components have to be created within Ansys or any other finite element program. The displacement solution from the reanalysis software are inputted as constraints into the finite element model for the stress evaluation.

4.5 Validation of Technique

For validation purposes, two examples involving the second baffle on Tanker A, and the support on Tanker C are done. The validation involves comparing the stress results of a component as generated by an analysis run of the full model on Ansys, with that of the same component stress results as generated after extracting a submodel from the Ansys run, and reanalysing this component using the renalysis software.

4.5.1 Baffle Validation in Tanker A

For the baffle validation a full Ansys analysis is carried out for Tanker A for the torsion load case. A

submodel around and including the second baffle is extracted from the Ansys generated data, and inputted to the reanalysis software. The reanalysis is carried out for the baffle and the displacement results are inputted to an Ansys model consisting of only the second baffle for the stress evaluation.

Figure 4.3 shows the stress contours generated on the second baffle obtained via submodel reanalysis software in conjunction with an Ansys run for the second baffle. Figure 4.4 shows the Von Mises stress contours on the second baffle generated from an Ansys run of the complete model of Tanker A.

From these two stress contour plots, it can be seen that the maximum stress occurs at the same point in both cases and that the stress contours are similar throughout the baffle. The magnitude of the maximum stress obtained through the submodel reanalysis has an error of only 0.8%.

4.5.2 Support Structure Validation in Tanker C

As in the previous section, a full Ansys analysis was carried out for Tanker C, for the torsion load case. A submodel around and including the rear support was extracted from the Ansys generated data, and inputted to the reanalysis software. The reanalysis was carried out for

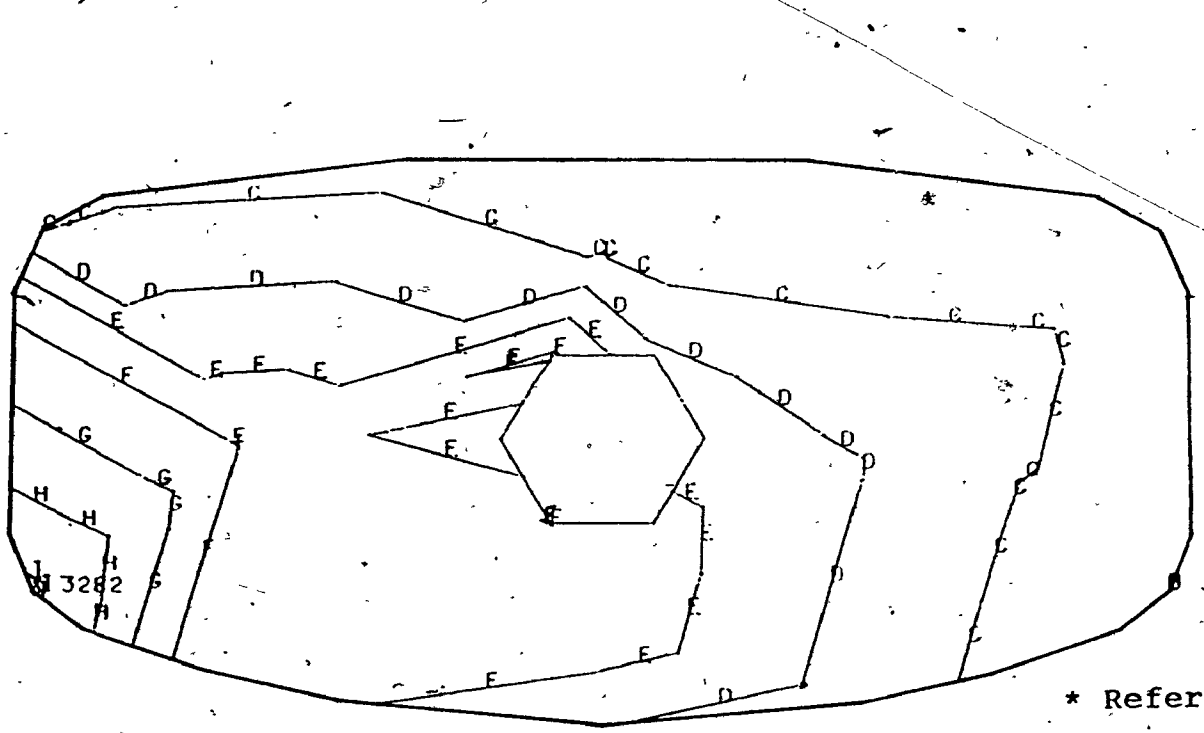

Figure 4.3: Stress Contours for the Second Baffle of Tanker A - Submodel Analysis for Torsion Load (Baffle Thickness = 0.0187 in, Shape Radius = 4 in, Hole Diameter = 18 in)
(For conversion to SI Units: 1 in = 0.0254 m; 1 psi = 0.00689 MPa)

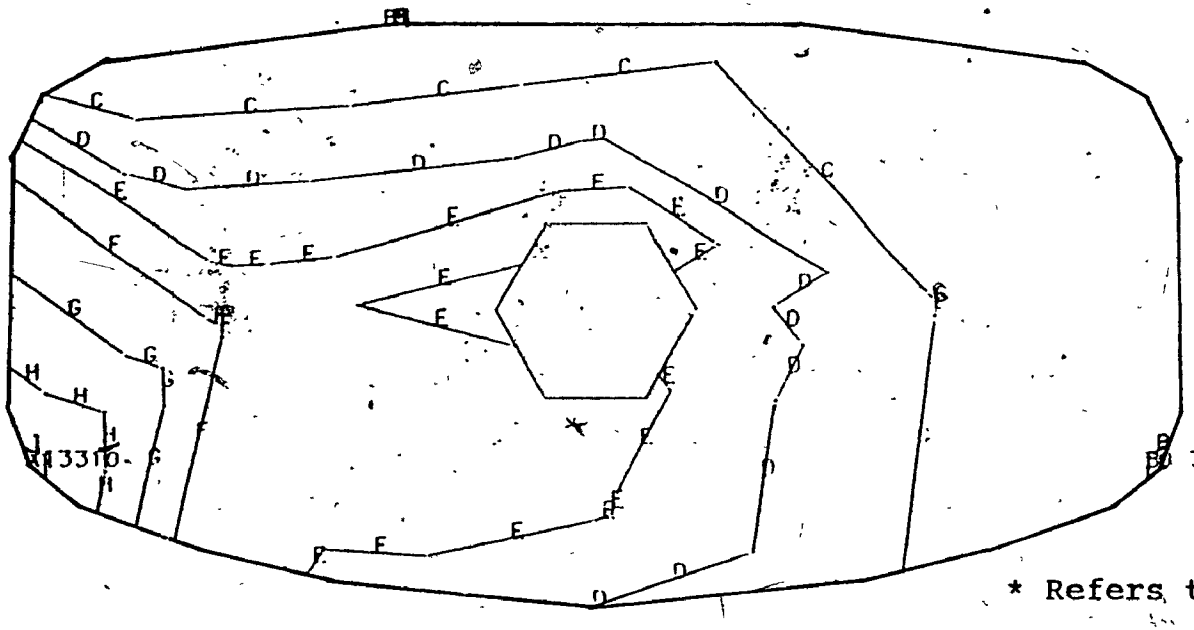

Figure 4.4: Stress Contours for the Second Baffle of Tanker A
- Complete Ansys Model Analysis for Torsion Load
(Baffle Thickness = 0.0187 in, Shape Radius = 4 in,
Hole Diameter = 18 in)
(For conversion to SI Units: 1 in = 0.0254 m; 1 psi = 0.00689 MPa)

the support and the displacement results again inputted to an Ansys model consisting of only the rear support.

Figure 4.5 shows the Von Mises stress contours on the high stress area of the support generated via submodel reanalysis technique in conjunction with Ansys software. Figure 4.6 shows the stress contours on the same area from an Ansys run of the complete model.

From these two stress contour plots, it can be seen that although the location of the maximum stress point is shifted more towards the corner in the case of stress contours obtained from the complete model, the stress contours themselves are similar in the entire region. The magnitude of the maximum stress value for the two cases are quite close with an error of only 10.9% .

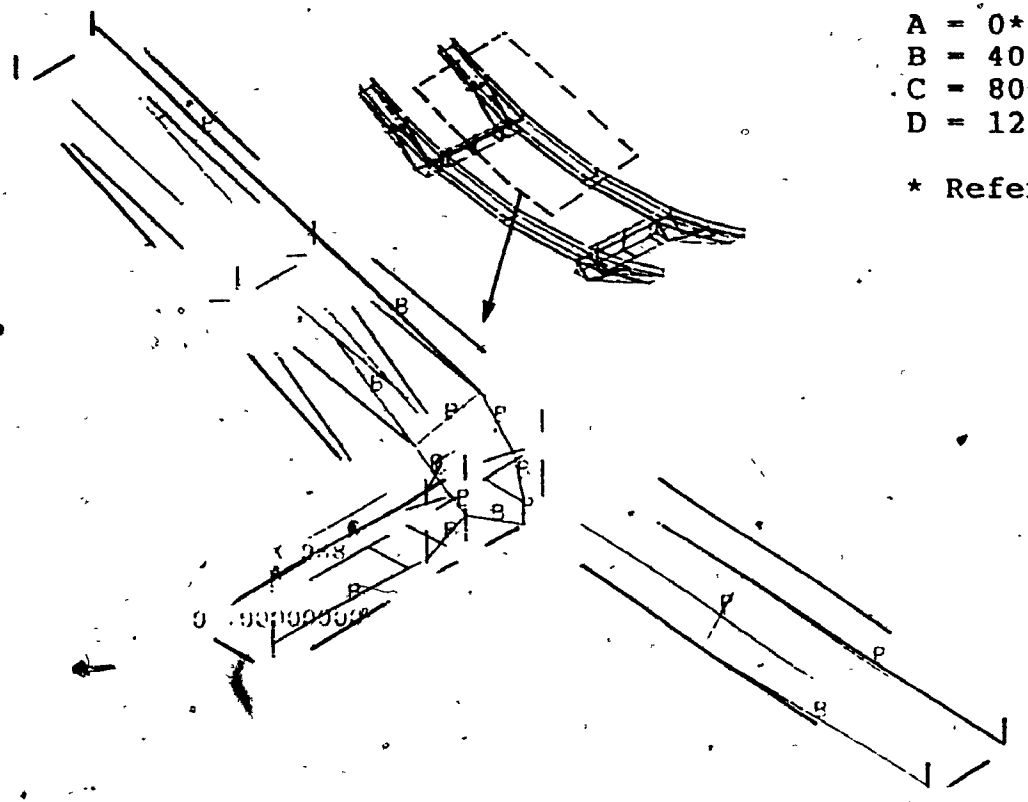

A = 0*
B = 400
C = 800
D = 1200

* Refers to stress value in psi.

Figure 4.5: Stress Contours for the Support Structure of Tanker C - Submodel Analysis for Torsion Load
(Channel Thickness = 0.375 in, Angle Thickness = 0.375 in, Outrigger Thickness = 0.375 in)
(For conversion to SI Units: 1 in = 0.0254 m; 1 psi = 0.00689 MPa)

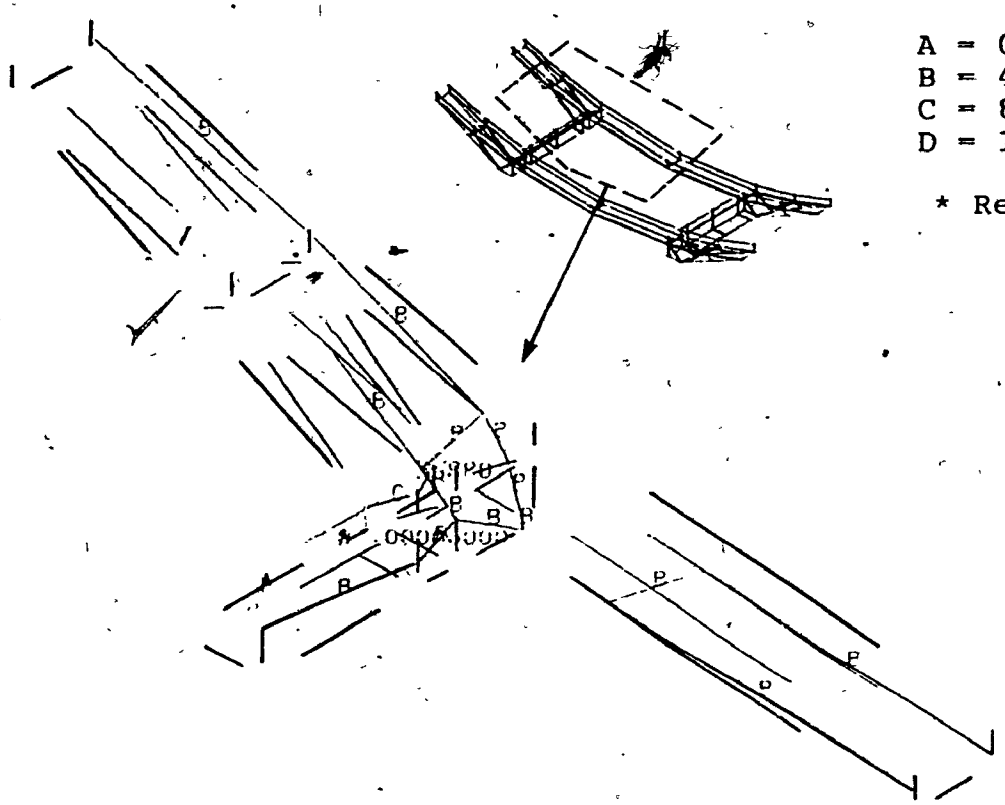

Figure 4.6: Stress Contours for the Support Structure of Tanker C - Complete Ansys Model Analysis for Torsion Load
(Channel Thickness = 0.375 in, Angle Thickness = 0.375 in, Outrigger Thickness = 0.375 in)
(For conversion to SI Units: 1 in = 0.0254 m; 1 psi = 0.00689 MPa)

4.6 Summary

In this chapter, a technique for the reanalysis of components within a submodel, extracted from a complete finite element model was presented. Using this technique, the components of interest within a submodel could be modified, and the solution to these components calculated, without having to recalculate the solution for the full model. St. Venant's principle and the method of matrix partitioning for component reanalysis in a submodel were utilized in this technique. A software utilizing this technique was developed and described. Numerical algorithms utilized by this software for the reanalysis were also presented. Finally two examples were presented for validation of the technique.

CHAPTER 5

CASE STUDIES ON REANALYSIS OF SUBMODEL COMPONENT PARAMETRIC VARIATIONS

CHAPTER 5

CASE STUDIES ON REANALYSIS OF SUBMODEL COMPONENT PARAMETRIC VARIATIONS

5.1 General

It is often necessary to introduce minor structural changes to a submodel component or to a submodel and to evaluate the changes in the stresses on the modified components using the finite element technique. Using the finite element model of the complete structure for analysis of minor changes, often it is tideous and time consuming and requires a large amount of disk storage space for the input, output, and the intermediate analysis data in each run. In chapter 4, a technique is described by which minor structural changes on a submodel can be studied by using a reanalysis technique on an area of interest in the submodel.

To demonstrate the effectiveness of this technique, two case studies are presented on the effect of minor structural changes on the areas of interest. The first case study is for parametric variation of the second baffle in the Tanker A. The second case study is for parametric variation of the support structure of tanker C. All reanalysis runs on both case studies are validated by comparing with results from finite element analysis of a complete model. The validation is based on the maximum

displacements for each of the six directions and on the lowest maximum stress in each of the case studies.

5.2 Case Study 1 - Baffle Variation in Tanker A

To study the variations of the second baffle parameters in Tanker A, a submodel is selected from the complete model of Tanker A as shown in Figure 5.1. Part of the tanker shell, the support underneath the baffle, and the baffle are taken as part of the submodel. The parametric variations in this case study are: baffle thickness, baffle shape radius, and baffle manhole diameter. The stresses occuring on the baffle are examined for these parametric variations.

The input data to the submodel is taken as the displacement solution to the boundary nodes generated by the complete model (base model) of Tanker A for torsional loading obtained from an Ansys analysis run. The stiffnesses of the submodel elements were extracted and inputted into the renalysis software. The modifications carried out to the baffle and the maximum stress on the baffle in each case carried out using the reanalysis technique are shown in Table 5.1. As shown in the Table, there are 18 individual cases. Case 1 to 9 uses a baffle with a thickness of 0.187 in (0.00475 m). The shape radius is varied from 3 in (0.0762 m) to 5 in (0.127 m) in steps

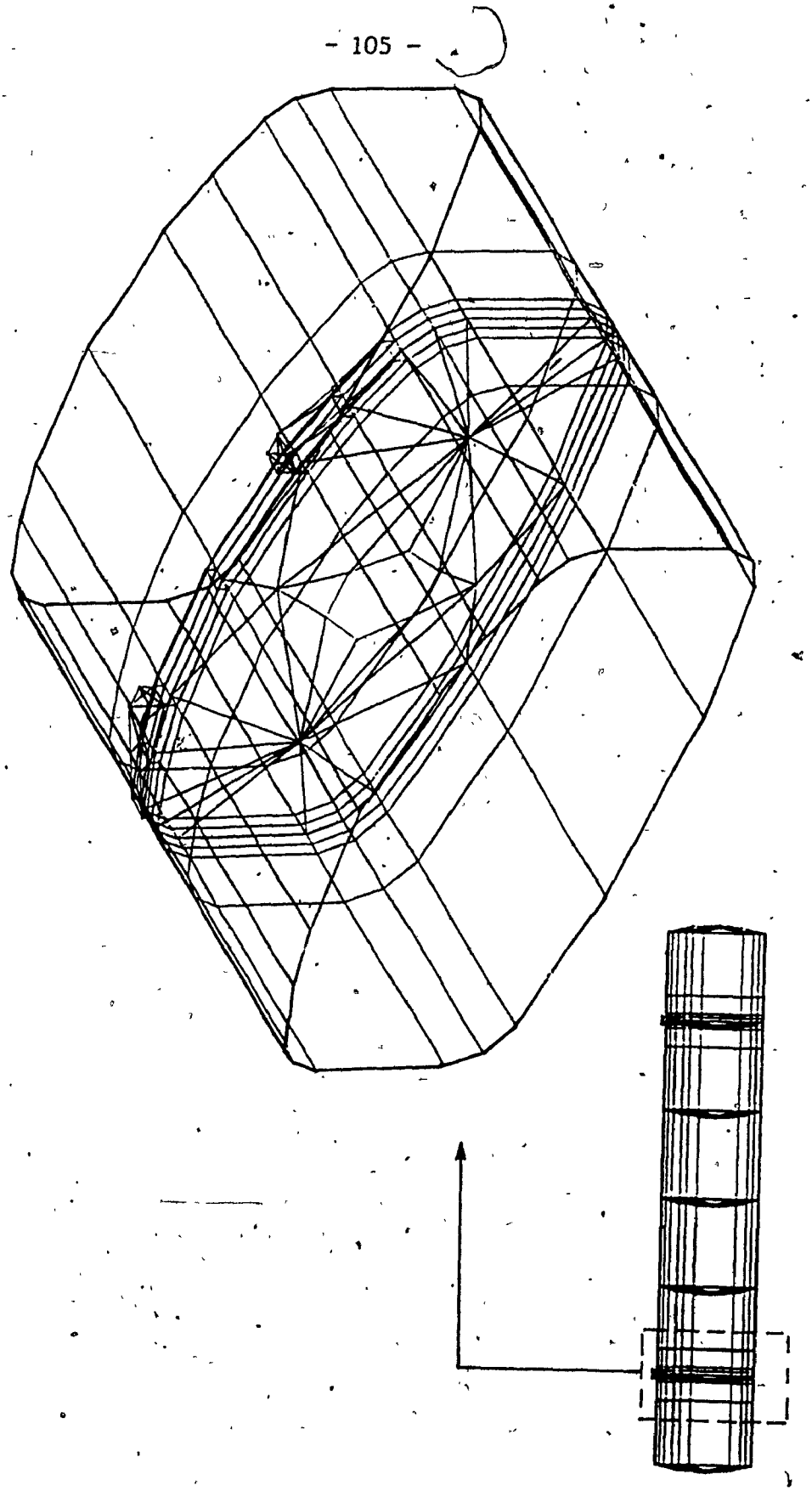

Figure 5.1: Submodel Extracted from Tanker A

Table 5.1 Geometry Variation for Baffle 2 in Tanker A

Case No.	Baffle Thickness (in)	Shape Radius (in)	Hole Diameter (in)	Maximum Stress (psi)
1	0.187	3	16	3436
2	0.187	3	18	3433
3	0.187	3	20	3459
4	0.187	4	16	3263
5	0.187	4	18	3281
6	0.187	4	20	3336
7	0.187	5	16	3254
8	0.187	5	18	3303
9	0.187	5	20	3305
10	0.250	3	16	2802
11	0.250	3	18	2800
12	0.250	3	20	2831
13	0.250	4	16	2596
14	0.250	4	18	2629
15	0.250	4	20	2682
16	0.250	5	16	2590
17	0.250	5	18	2634
18	0.250	5	20	2549

(For conversion to SI units: 1 in = 0.0254 m;

1 psi = 0.00689 Mpa)

of 1 in (0.0254 m) and the center hole diameter is varied from 16 in (0.406 m) to 20 in (0.508 m) in steps of 2 in (0.0508 m). Case 10 to 18 has a baffle thickness of 0.250 in (0.00635 m) with the same variations to shape radius and center hole diameter as in case 1 to 9.

5.2.1 Nodal Displacement Pattern

Figure 5.2a, 5.3a, 5.4a, 5.5a, 5.6a, and 5.7a show the maximum nodal displacement for the area of interest within the submodel (baffle) in the three translational and the three rotational directions plotted for variations in shape radius , center hole diameter, and the thickness for cases 1 to 18. In all six directions, the maximum displacement on the structure is lower with the baffle thickness of 0.187 in (0.00475 m) as compared with a baffle thickness of 0.250 in (0.00635 m). The lowest value of the maximum x- and y-transalational displacements occur with the center hole diameter of 20 in (0.508 m) and shape radius of 4 in (0.1016 m). For the lowest maximum displacement in z-transational, and x- and z-rotational modes, it is found that thickness is again to be 0.187 in (0.0475 m) with a hole diameter of 16 in (0.406 m) and a shape radius of 3 in (0,0762 m). The lowest maximum y-rotational occurs with a thickness of 0.187 in (0.0475 m), hole diameter of 16 in (0.406 m) and shape radius of 5 in (0.127 m).

The displacement solution of the reanalysis software was then extracted and inputted into an Ansys model composed only of the baffle and the stress contour plots were obtained. For the purpose of comparison, an Ansys complete model with similar parametric changes was run and the results are presented in Figures 5.2b, 5.3b, 5.4b, 5.5b, 5.6b, and 5.7b. It can be seen that the maximum displacement plots from submodel reanalysis have a similar pattern to the plots obtained from the Ansys complete model analysis. Further the location of the maximum displacements are approximately identical in the two analyses. The magnitude of the maximum nodal displacement error is less than 30%.

5.2.2 Comparison of Stress Contours

From Table 5.1, the submodel reanalysis show that the parametric changes (case 1 to 18), vary the maximum stress in the region between 2549 psi (17.56 MPa) and 3459 psi (23.81 MPa). Figure 5.8. shows the changes in maximum stress value for cases 1 to 18 corresponding to the three parametric changes on the baffle.

For the case of submodel reanalysis, the stress contour plot of the maximum Von Mises stress on the baffle for a thickness of 0.250 in (0.00635 m), a shape radius of 5 in (0.127 m) and a hole diameter of 20 in (0.508 m) is shown in Figure 5.9. The maximum stress value is 2549 psi (17.56

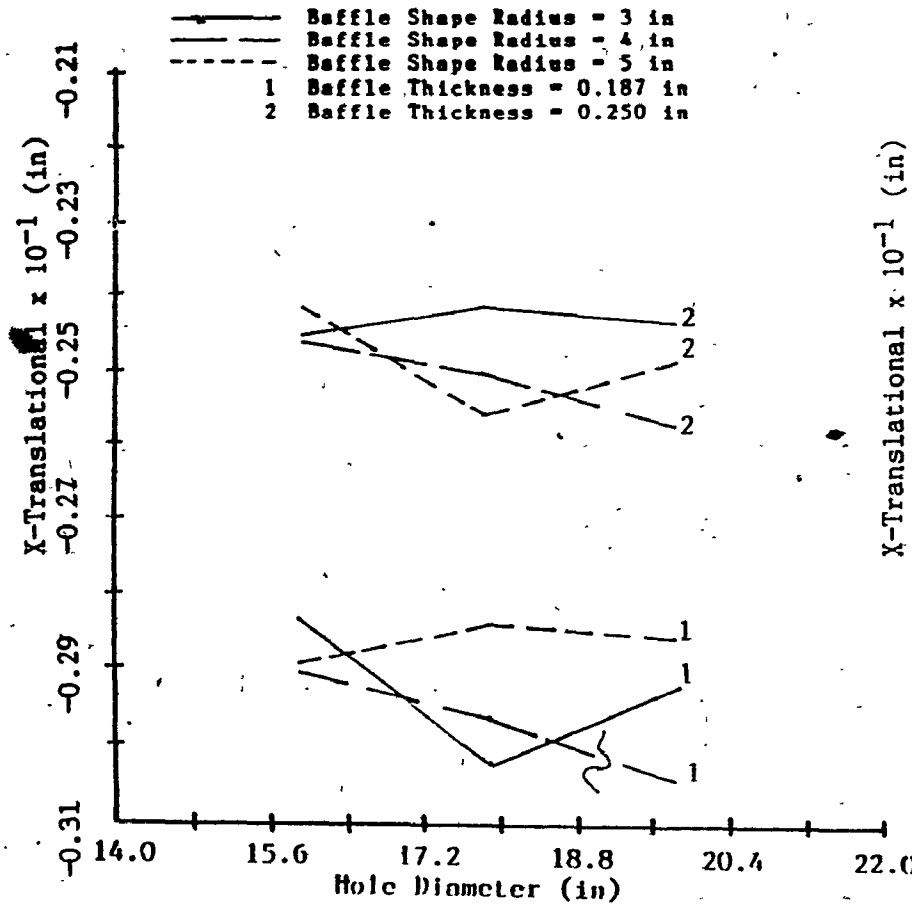

Figure 5.2a: Submodel Analysis - Maximum X-Translational Displacement for Second Baffle of Tanker A

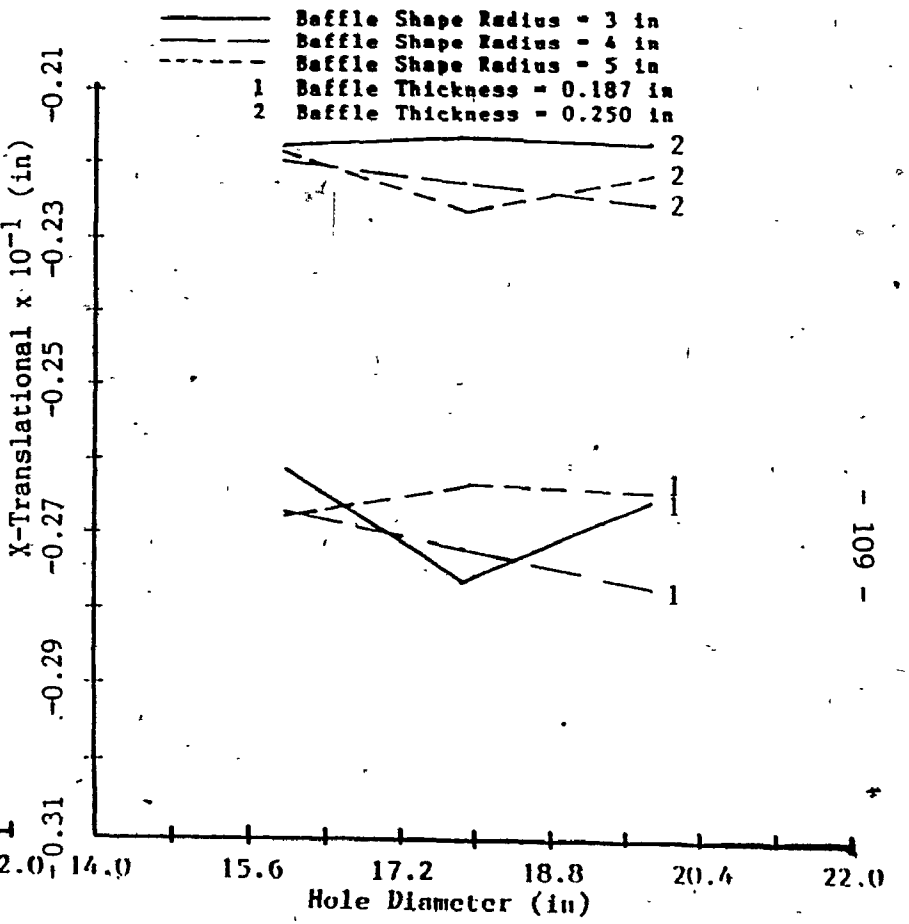

Figure 5.2b: Ansys Complete Model Analysis - Maximum X-Translational Displacement for Second Baffle of Tanker A

(For conversion to SI Units: 1 in = 0.0254 m)

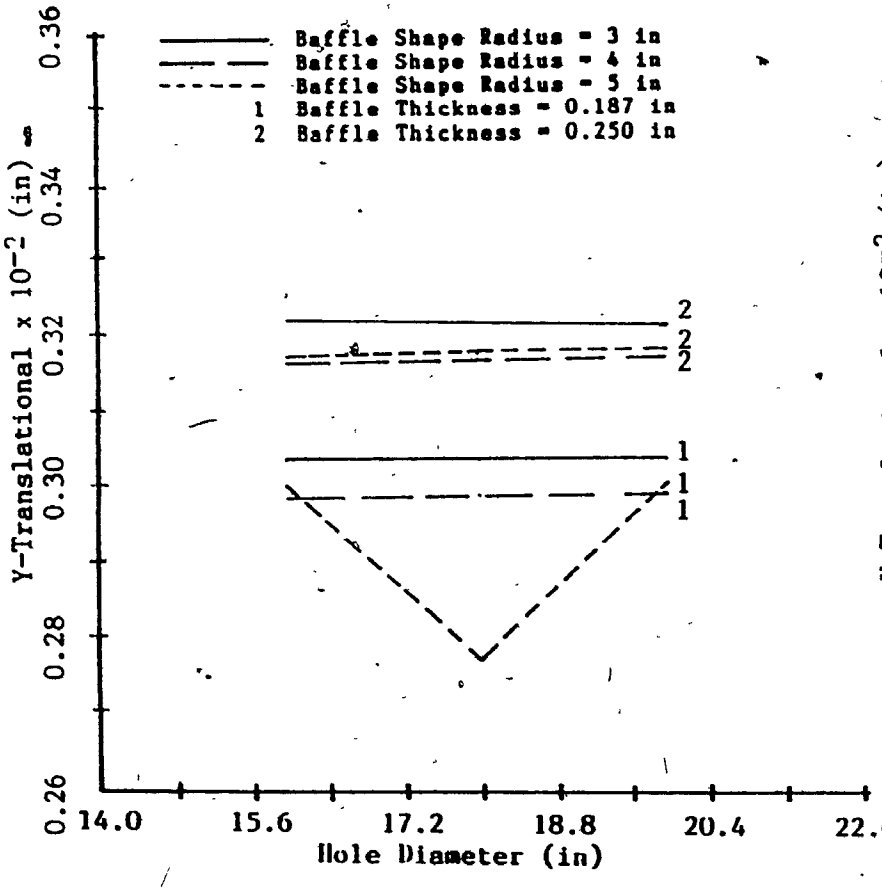

Figure 5.3a: Submodel Analysis - Maximum Y-Translational Displacement for Second Baffle of Tanker A

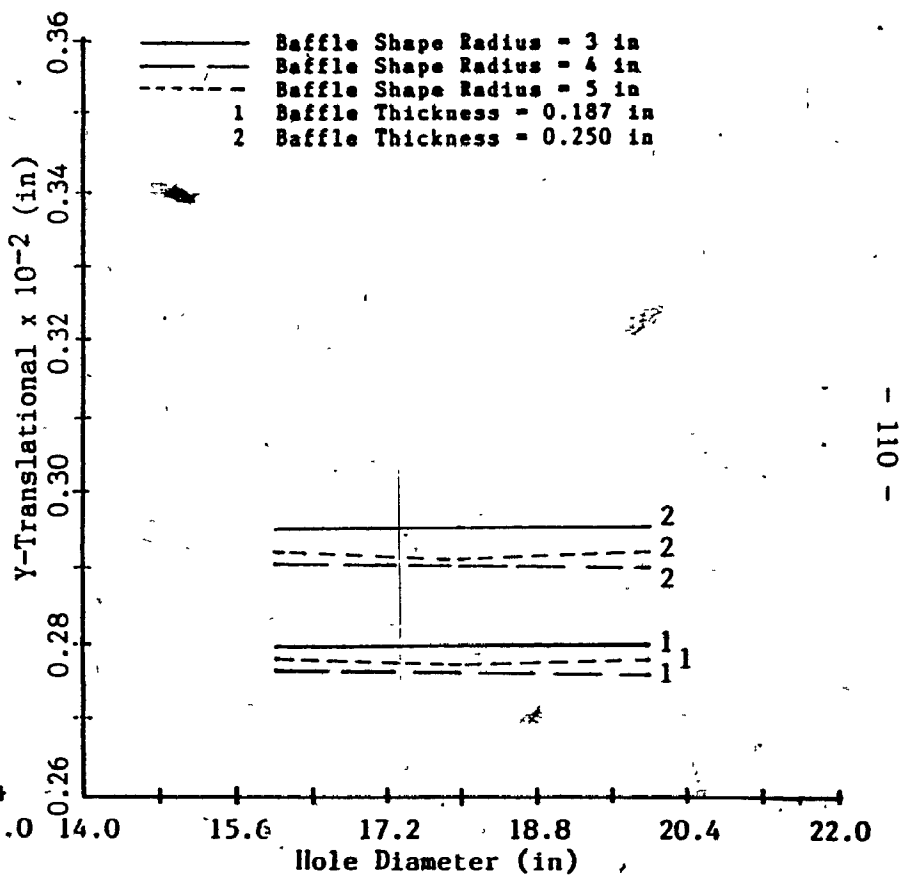

Figure 5.3b: Ansys Complete Model Analysis - Maximum Y-Translational Displacement for Second Baffle of Tanker A

(For conversion to SI Units: 1 in = 0.0254 m)

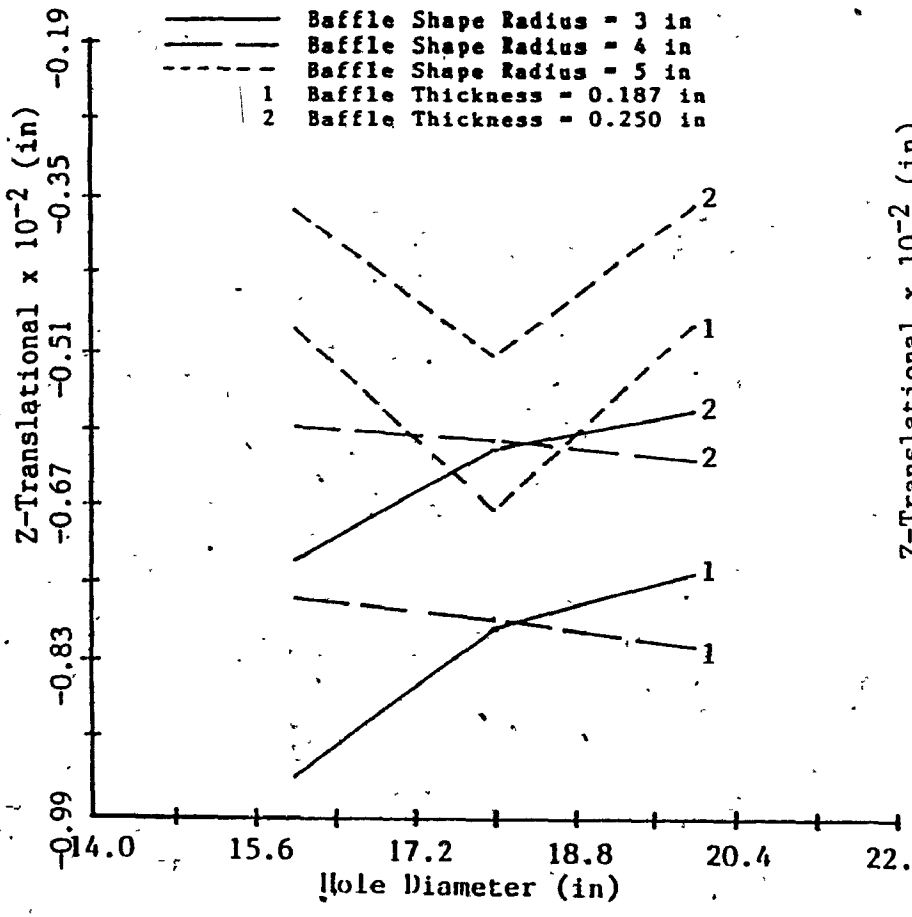

Figure 5.4a: Submodel Analysis - Maximum Z-Translational Displacement for Second Baffle of Tanker A

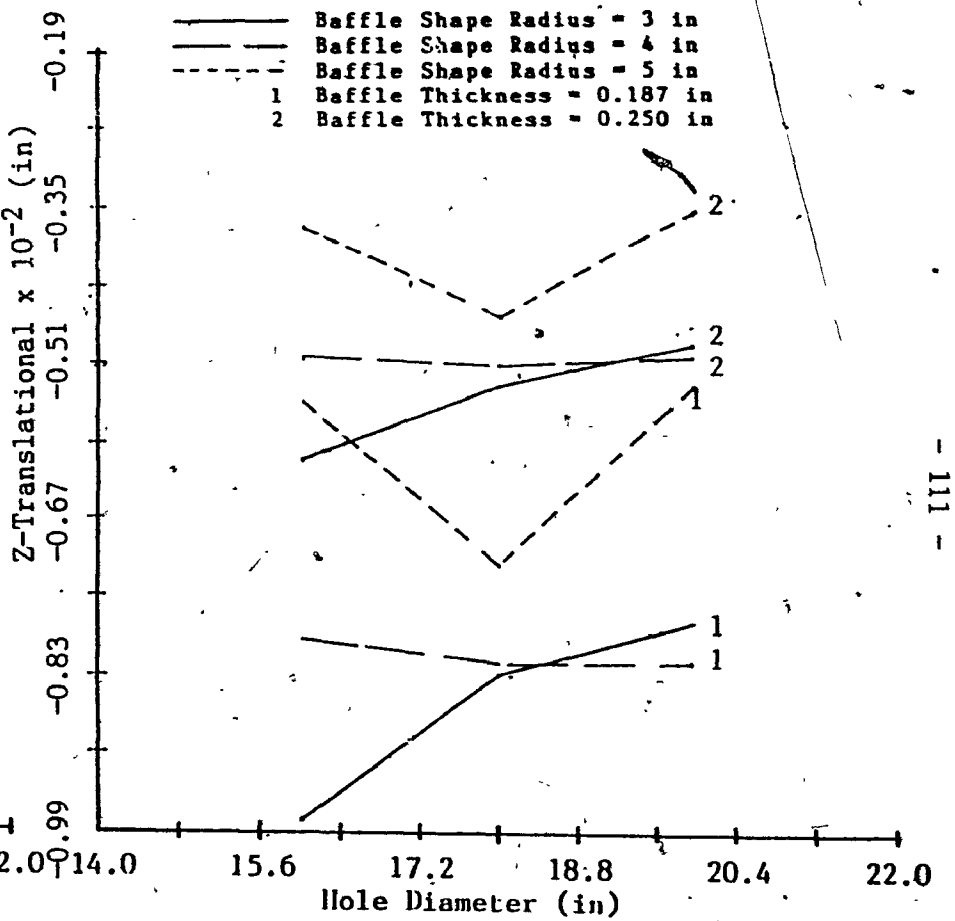

Figure 5.4b: Ansys Complete Model Analysis - Maximum Z-Translational Displacement for Second Baffle of Tanker A

(For conversion to SI Units: 1 in = 0.0254 m)

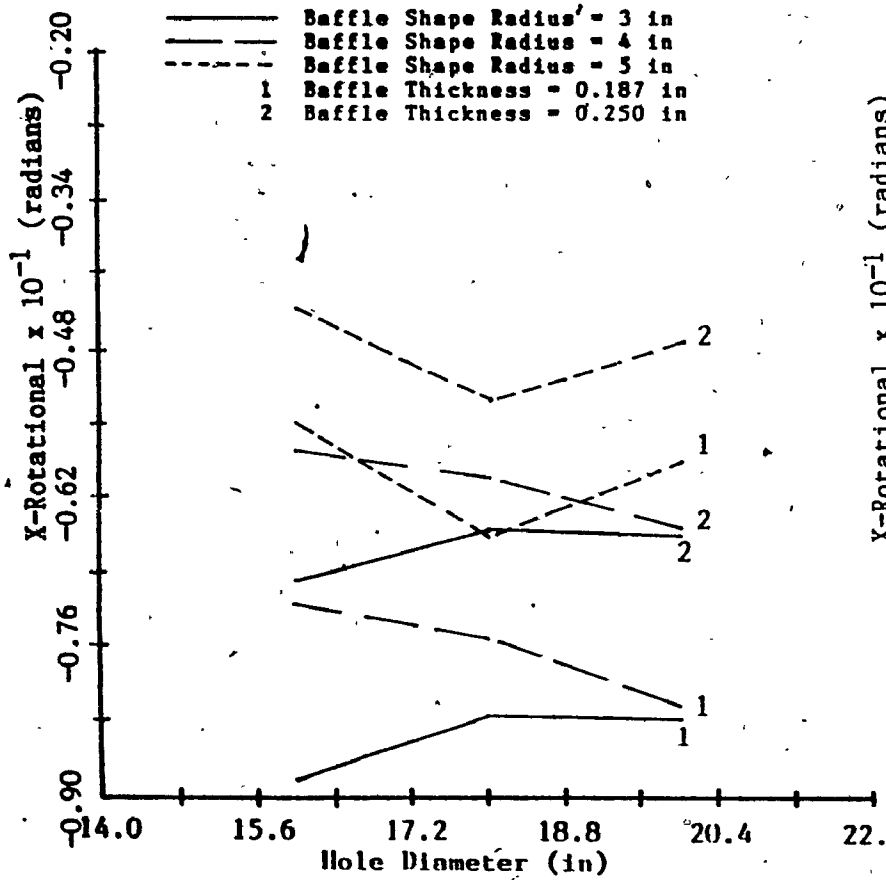

Figure 5.5a: Submodel Analysis - Maximum X-Rotational Displacement for Second Baffle of Tanker A

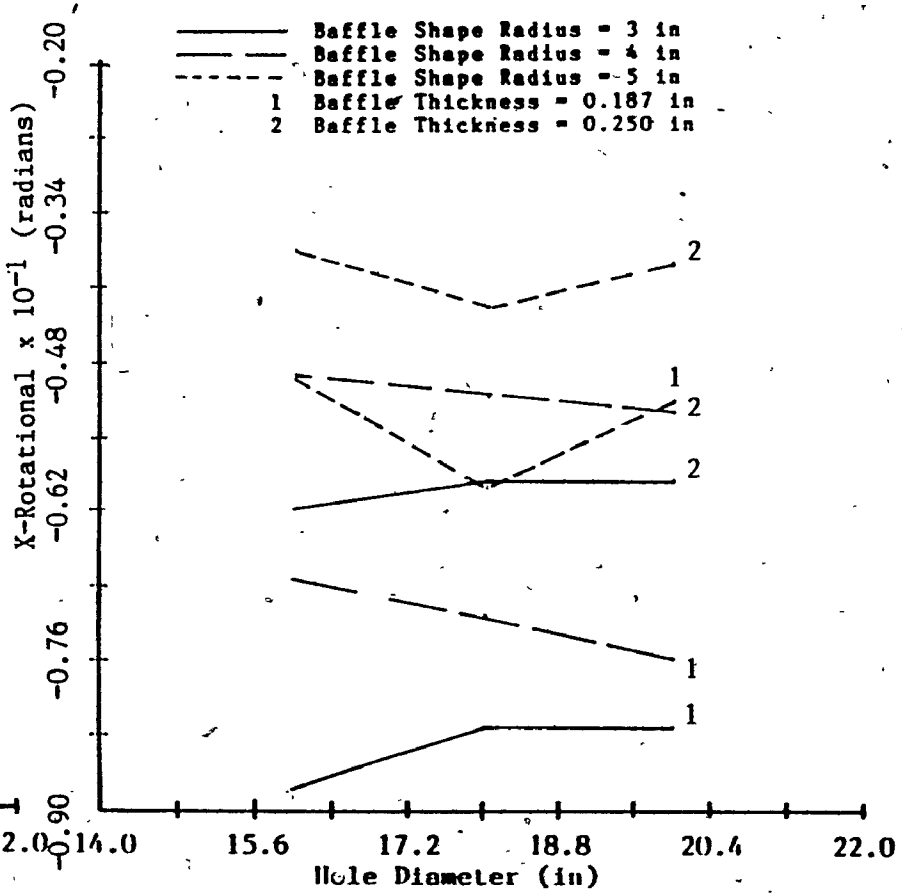

Figure 5.5b: Ansys Complete Model Analysis - Maximum X-Rotational Displacement for Second Baffle of Tanker A

(For conversion to SI Units: 1 in = 0.0254 m)

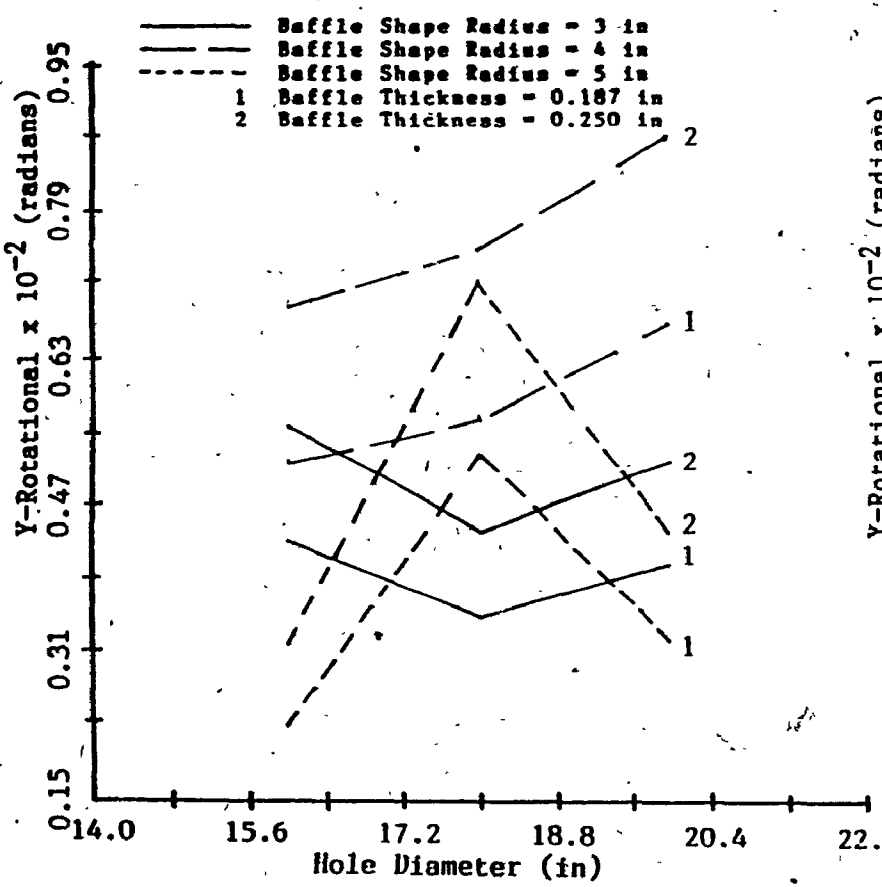

Figure 5.6a: Submodel Analysis - Maximum Y-Rotational Displacement for Second Baffle of Tanker A

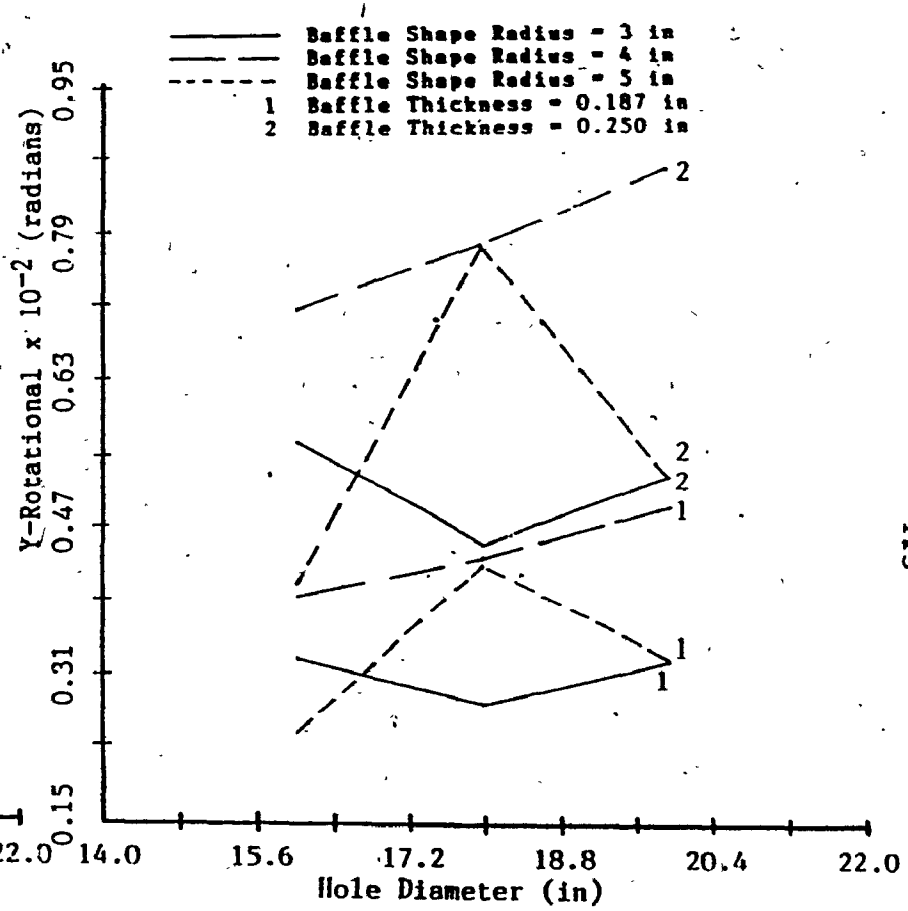

Figure 5.6b: Ansys Complete Model Analysis - Maximum Y-Rotational Displacement for Second Baffle of Tanker A

(For conversion to SI Units: 1 in = 0.0254 m)

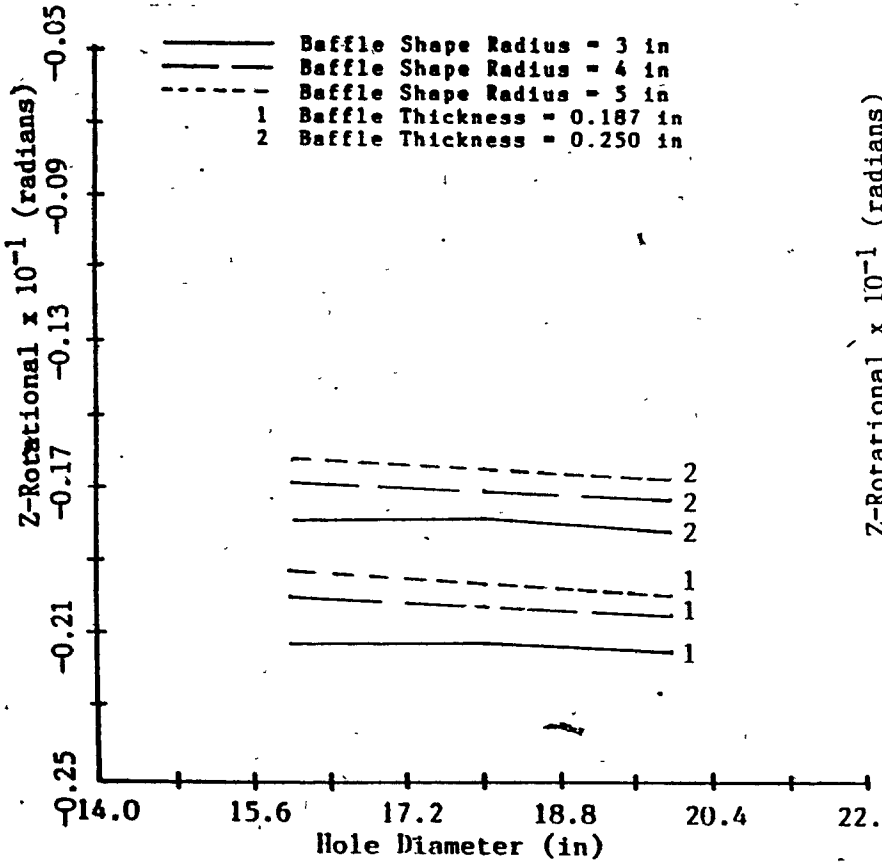

Figure 5.7a: Submodel Analysis - Maximum Z-Rotational Displacement for Second Baffle of Tanker A

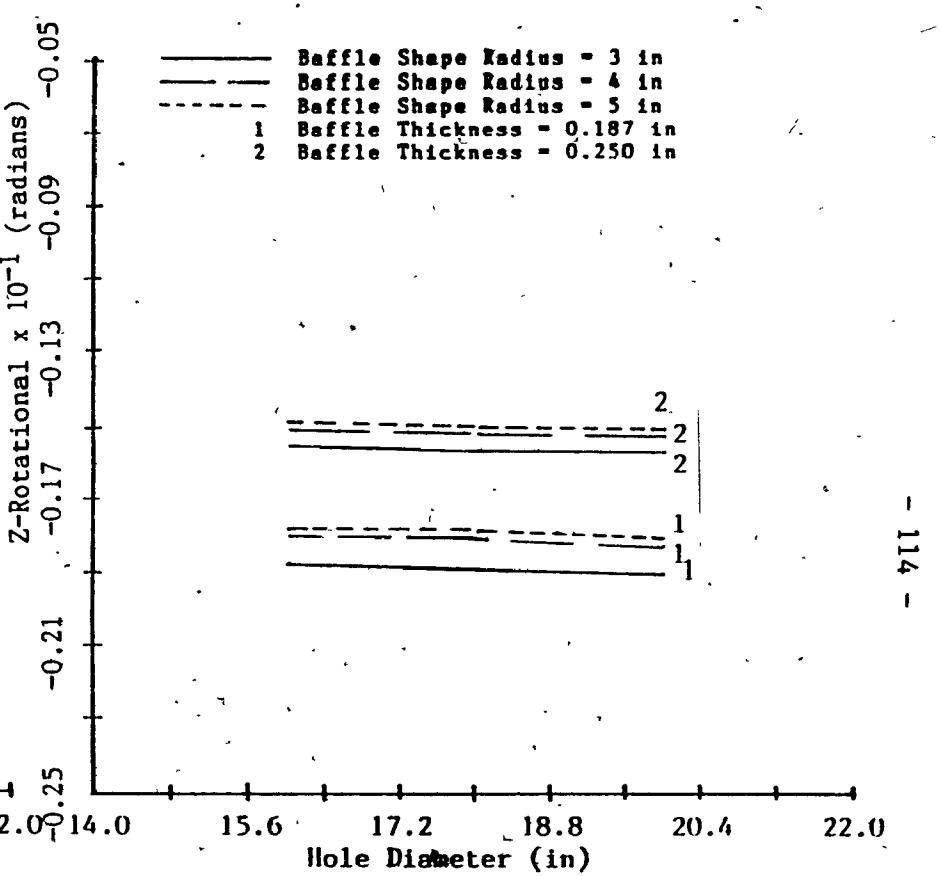

Figure 5.7b: Ansys Complete Model Analysis - Maximum Z-Rotational Displacement for Second Baffle of Tanker A

(For conversion to SI Units: 1 in = 0.0254 m)

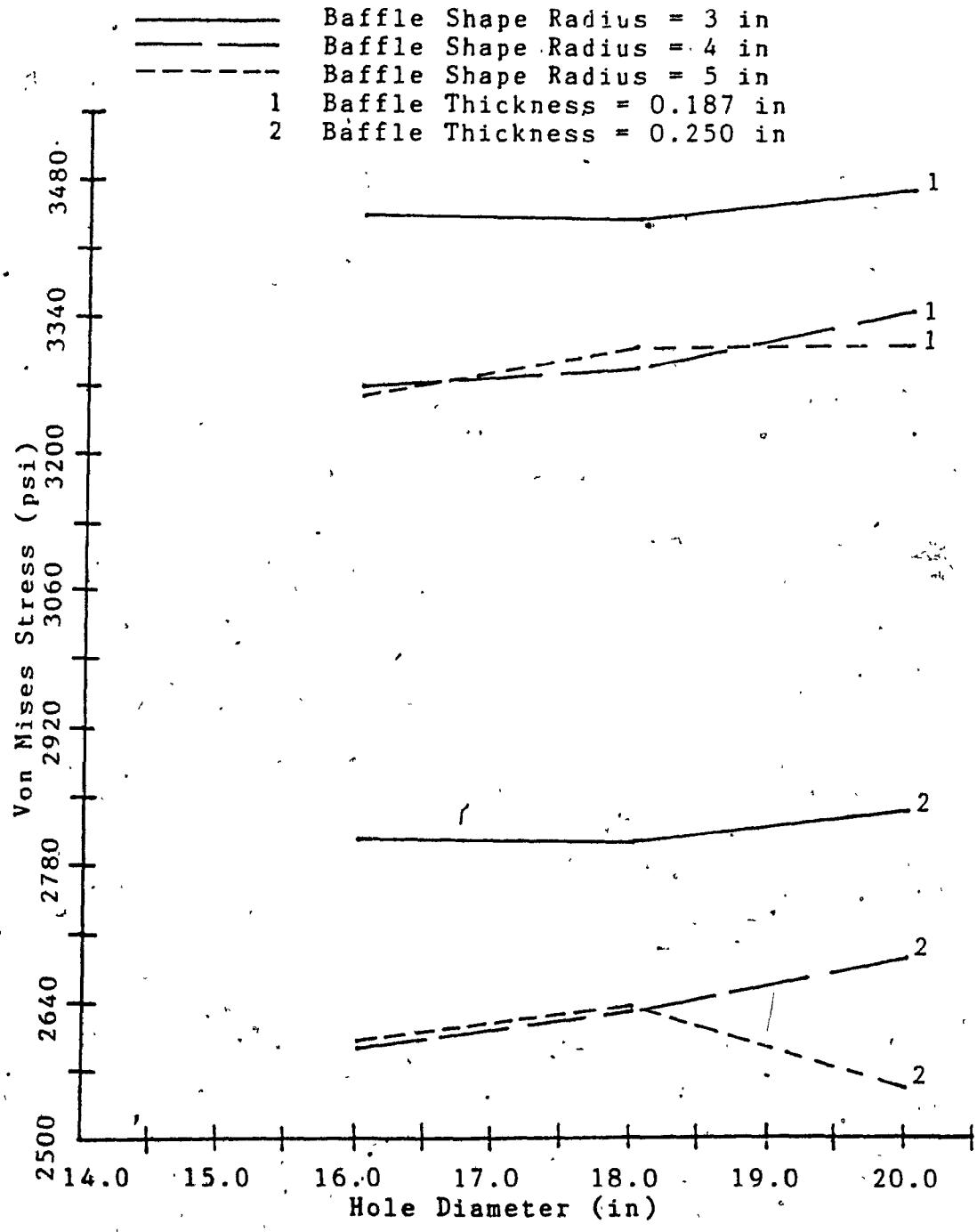

Figure 5.8: Submodel Analysis - Maximum Von Mises Stress for Second Baffle of Tanker A

(For conversion to SI Units: 1 psi = 0.00689 MPa)

MPa) (case 18 - Table 5.1). A complete model analysis using Ansys for the same baffle gives a value of 2647 psi (18.24 MPa) for the maximum stress and the stress contours are shown in Figure 5.10. It can be seen that the maximum stress occurs at the same point in both analyses with an error magnitude of 3.6%.

5.3 Case Study 2 - Support Structure Variations in Tanker C

To study the change in stress value for variations in the thickness of the support structure in Tanker C, a submodel of the area around the support was extracted from the model of Tanker C. Figure 5.11 shows the submodel chosen for the support reanalysis. The three components of the support considered for parametric variations are: outriggers, angles, and channels.

As in case study 1, the input data to the submodel is taken as the displacement solution to the boundary nodes generated by the complete model (base model) of Tanker C under torsional loading obtained from the Ansys analysis run. The stiffnesses of the submodel elements were extracted and inputted into the renalysis software. The modifications to the three components of the support structure and the maximum stress generated in each case calculated using the reanalysis technique are shown in Tables 5.2.

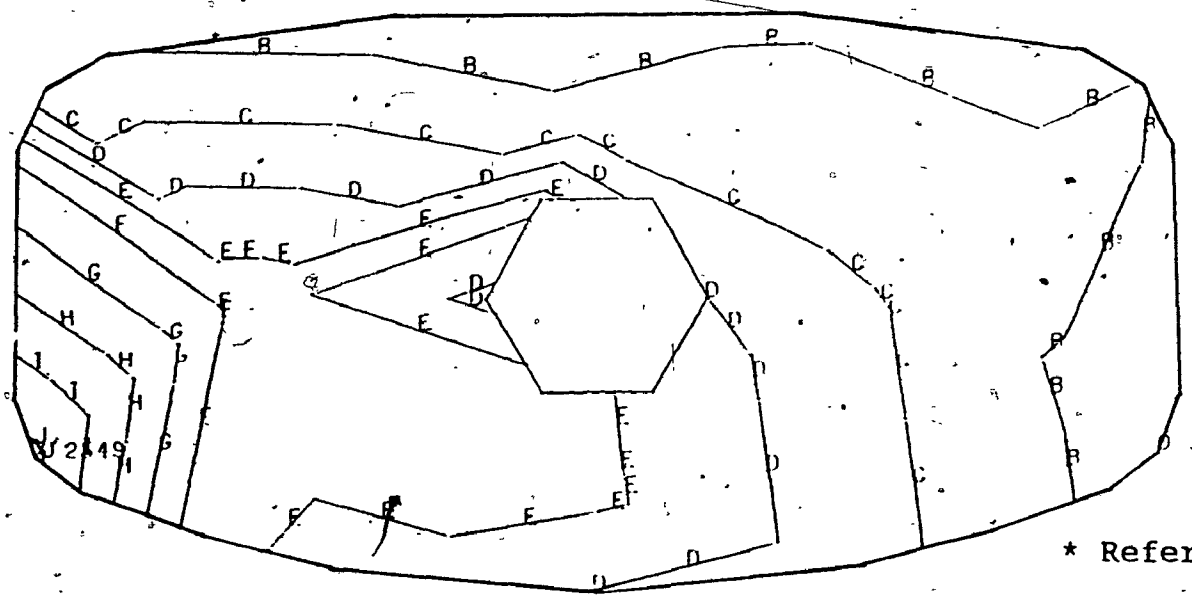

Figure 5.9: Stress Contours for the Second Baffle of Tanker A
- Submodel Analysis for Torsion Load
(Baffle Thickness = 0.0250 in, Shape Radius = 5 in,
Hole Diameter = 20 in)
(For conversion to SI Units: 1 in = 0.0254 m; 1 psi = 0.00689 MPa)

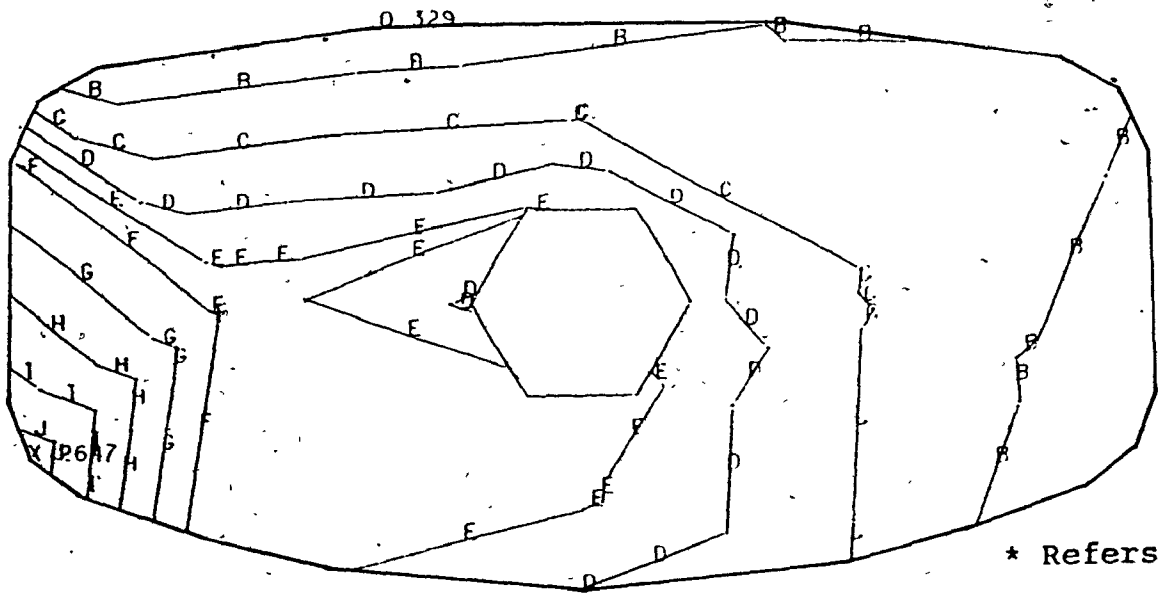

A = 0*
B = 400
C = 800
D = 1200
E = 1600
F = 2000
G = 2400
H = 2800
I = 3200
J = 3600
K = 4000

* Refers to stress value in psi.

Figure 5.10: Stress Contours for the Second Baffle of Tanker A
- Complete Ansys Model Analysis for Torsion Load
(Baffle Thickness = 0.0250 in, Shape Radius = 5 in,
Hole Diameter = 20 in)
(For conversion to SI Units: 1 in = 0.0254 m; 1 psi = 0.00689 MPa)

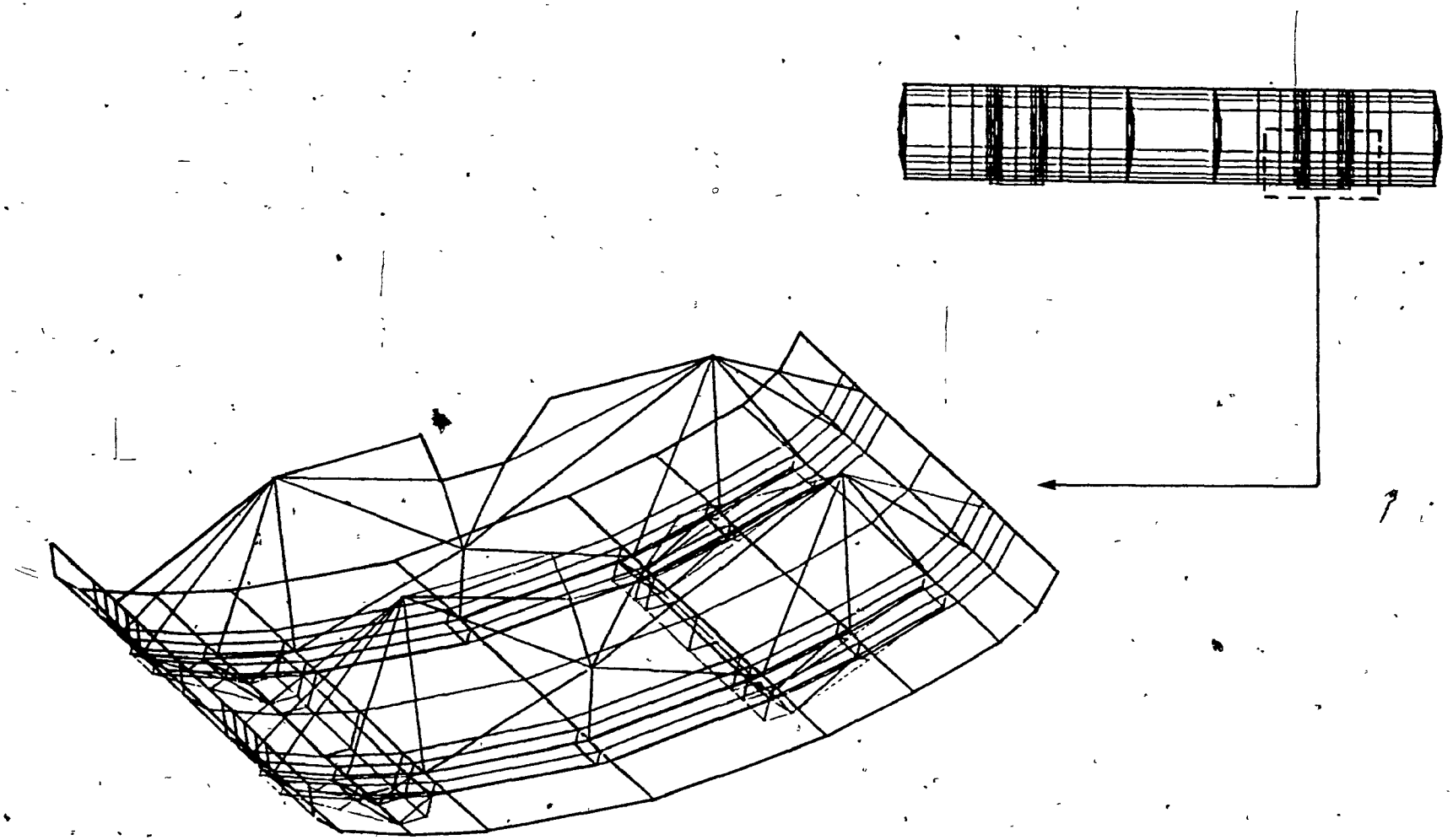

Figure 5.11: Submodel Extracted from Tanker C

Table 5.2 Thickness Variation on the First Support on Tanker C

Case No.	Channel Thickness (in)	Angle Thickness (in)	Outrigger Thickness (in)	Maximum Stress (psi)
1	0.375	0.325	0.350	991
2	0.375	0.325	0.375	990
3	0.375	0.325	0.400	988
4	0.375	0.350	0.350	963
5	0.375	0.350	0.375	962
6	0.375	0.350	0.400	961
7	0.375	0.375	0.350	988
8	0.375	0.375	0.375	988
9	0.375	0.375	0.400	987
10	0.375	0.400	0.350	1014
11	0.375	0.400	0.375	1013
12	0.375	0.400	0.400	1012
13	0.375	0.425	0.350	1039
14	0.375	0.425	0.375	1039
15	0.375	0.425	0.400	1038
16	0.350	0.325	0.375	1002
17	0.375	0.325	0.375	989
18	0.400	0.325	0.375	978
19	0.350	0.350	0.375	968
20	0.375	0.350	0.375	962
21	0.400	0.350	0.375	961
22	0.350	0.375	0.375	987
23	0.375	0.375	0.375	988
24	0.400	0.375	0.375	989
25	0.350	0.400	0.375	1014
26	0.375	0.400	0.375	1013
27	0.400	0.400	0.375	1013
28	0.350	0.425	0.375	1039
29	0.375	0.425	0.375	1039
30	0.400	0.425	0.375	1038

(For conversion to SI units: 1 in = 0.0254 m; 1 psi = 0.00689 Mpa)

In cases 1 to 15, the channel thickness is kept fixed as 0.375 in (0.00953 m) , and the angle thickness is varied from 0.325 in (0.00826 m) to 0.425 in (0.0108 m) in steps of 0.025 in (0.000635 m). The outrigger thickness varied from 0.350 in (0.00889 m) to .400 in (0.0102 m) in steps of 0.025 in (0.000635 m) for each variation of angle thickness. In cases 16 to 30, the outrigger thickness is kept constant at 0.375 in (0.00953 m), with the angle thickness again varying from 0.325 in (0.00826 m) to 0.425 in in steps of 0.025 in (0.000635 m). The channel thickness is varied from 0.350 in (0.00889 m) to 0.400 in (0.0102 m) in steps of 0.025 in (0.000635 m)for each variation in angle thickness.

5.3.1 Nodal Displacement Pattern

Figures 5.12a, 5.13a, 5.14a, 5.15a, 5.16a, and 5.17a show maximum nodal displacements for the support structure, plotted for cases 1 to 15.

The maximum displacements on the structure for x- and y-translational, and z-rotational directions increased for an increase in angle and outrigger thickness. The maximum displacement for both z-translational and the x-rotational directions decreased while the y-rotational displacement remained fairly constant due to changes in parameters. Maximum nodal displacements for the support structure for

cases 16 to 30 (Table 5.2) are shown in Figures 5.18a - 5.23a. In these cases, where the outrigger is kept to a constant thickness, the displacement change in all 6 directions are very similar to changes shown in cases 1 to 15.

The displacement solution of the reanalysis software was then extracted and inputted into an Ansys model composed only of the support structure and the stress contour plots were obtained. For the purposes of comparison, an Ansys complete model with similar parametric changes was run and the results are presented in Figures 5.12b - 5.23b. It can be seen from these plots that the location of the maximum displacements are approximately identical in the two analyses. The magnitude of the maximum nodal displacement error is less than 48%.

5.3.2 Comparison of Stress Contours

The submodel reanalysis showed that the parametric changes (case 1 to 30), did not cause much variation to the maximum stress in the region. This can be seen in Figure 5.24 and 5.25 which show the maximum stress value corresponding to cases 1 to 15 and 16 to 30 respectively.

A stress contour plot of the minimum value of the maximun Von Mises stress which occurs in case 6 of the

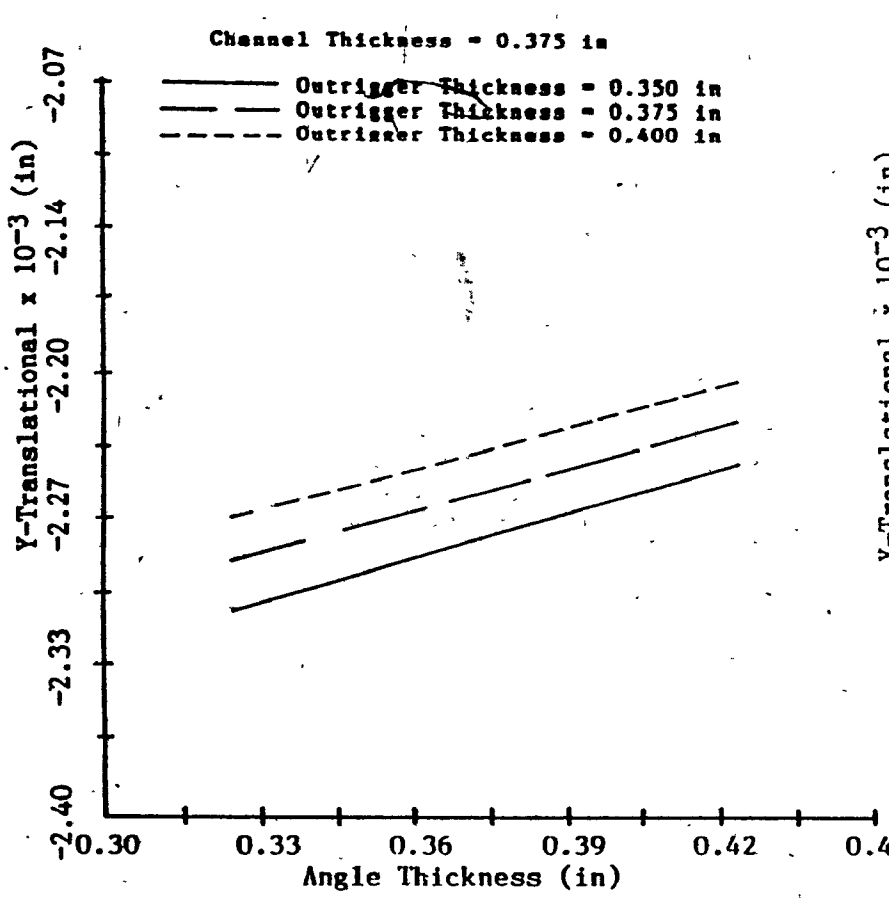

Figure 5.12a: Submodel Analysis (Case 1-15) - Maximum X-Translational Displacement for Support Structure of Tanker C

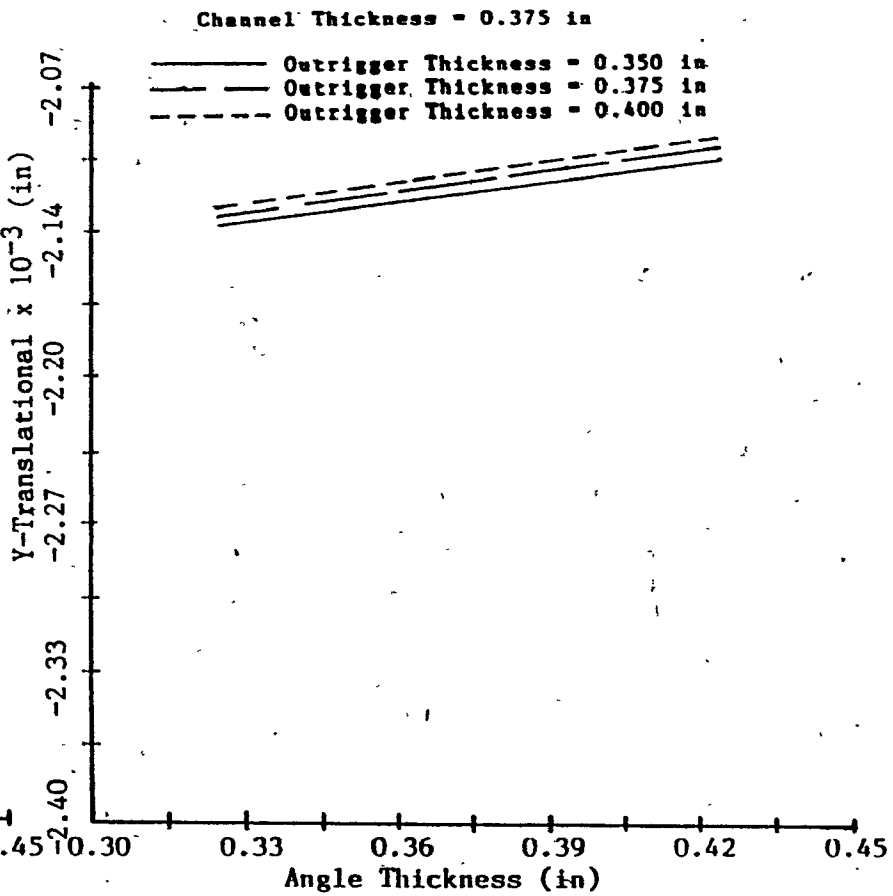

Figure 5.12b: Ansys Complete Model Analysis (Case 1-15) - Maximum X-Translational Displacement for Support Structure of Tanker C

(For conversion to SI Units: 1 in = 0.0254 m)

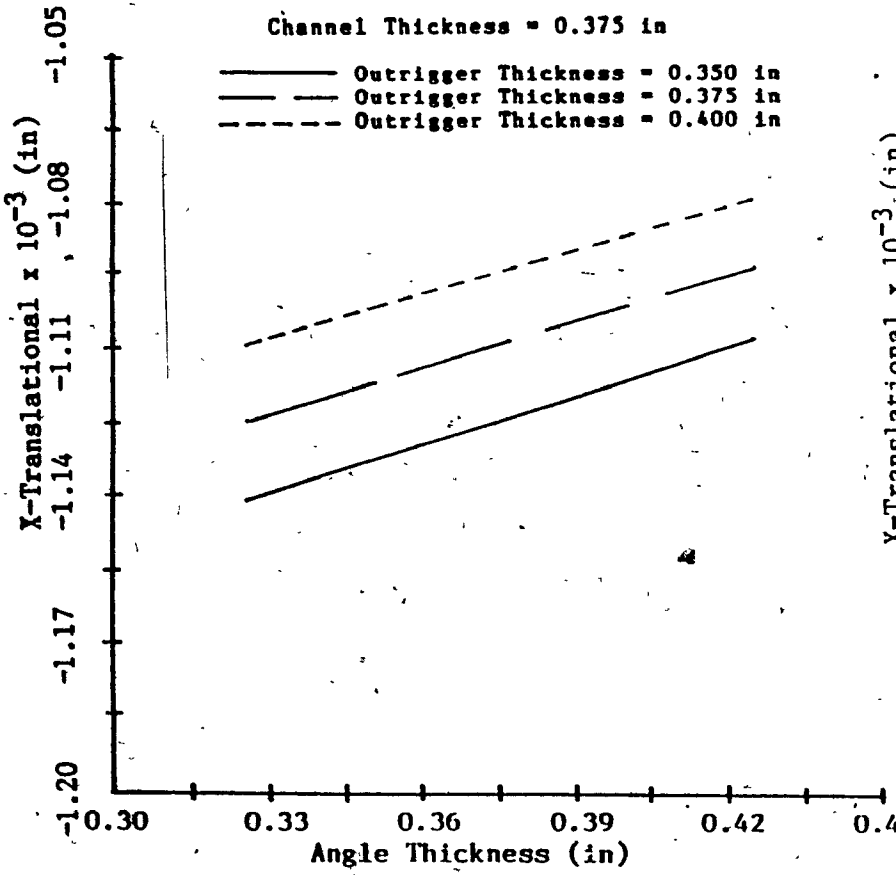

Figure 5.13a: Submodel Analysis (Case 1-15) - Maximum Y-Translational Displacement for Support Structure of Tanker C

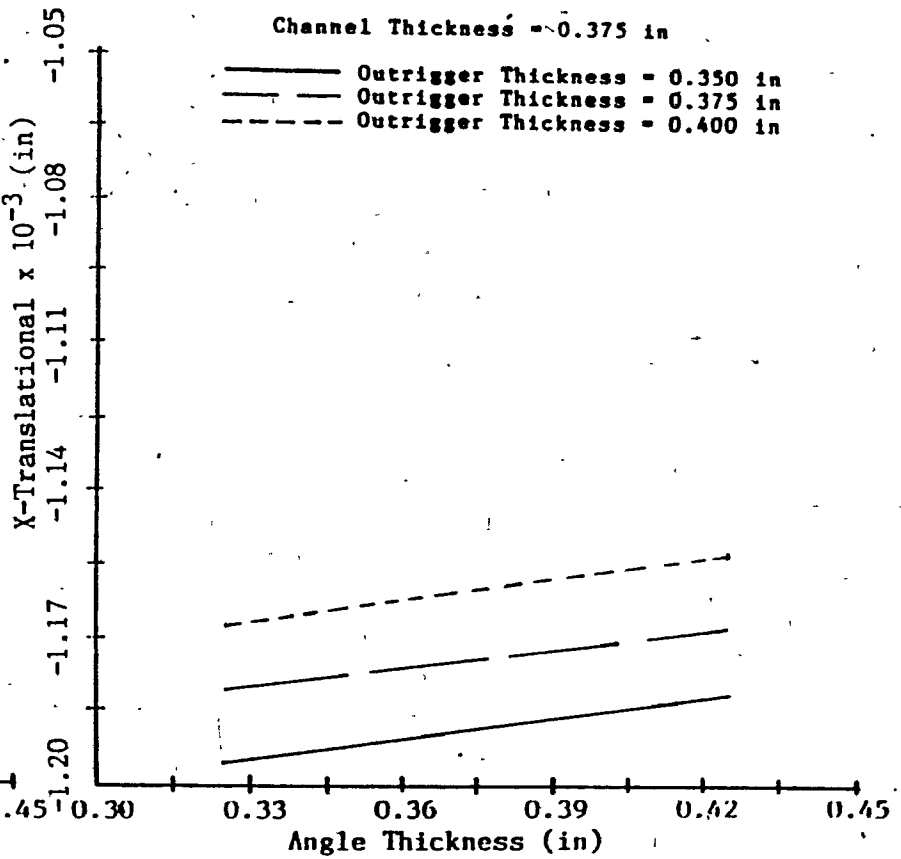

Figure 5.13b: Ansys Complete Model Analysis (Case 1-15) - Maximum Y-Translational Displacement for Support Structure of Tanker C

(For conversion to SI Units: 1 in = 0.0254 m)

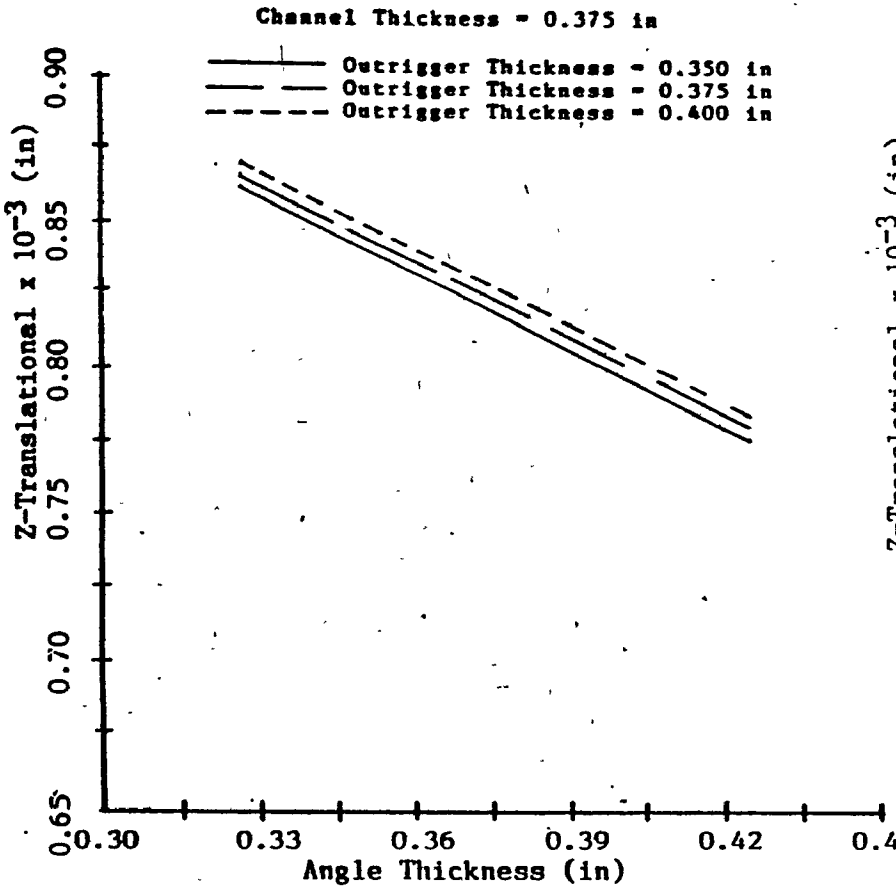

Figure 5.14a: Submodel Analysis (Case 1-15) - Maximum Z-Translational Displacement for Support Structure of Tanker C

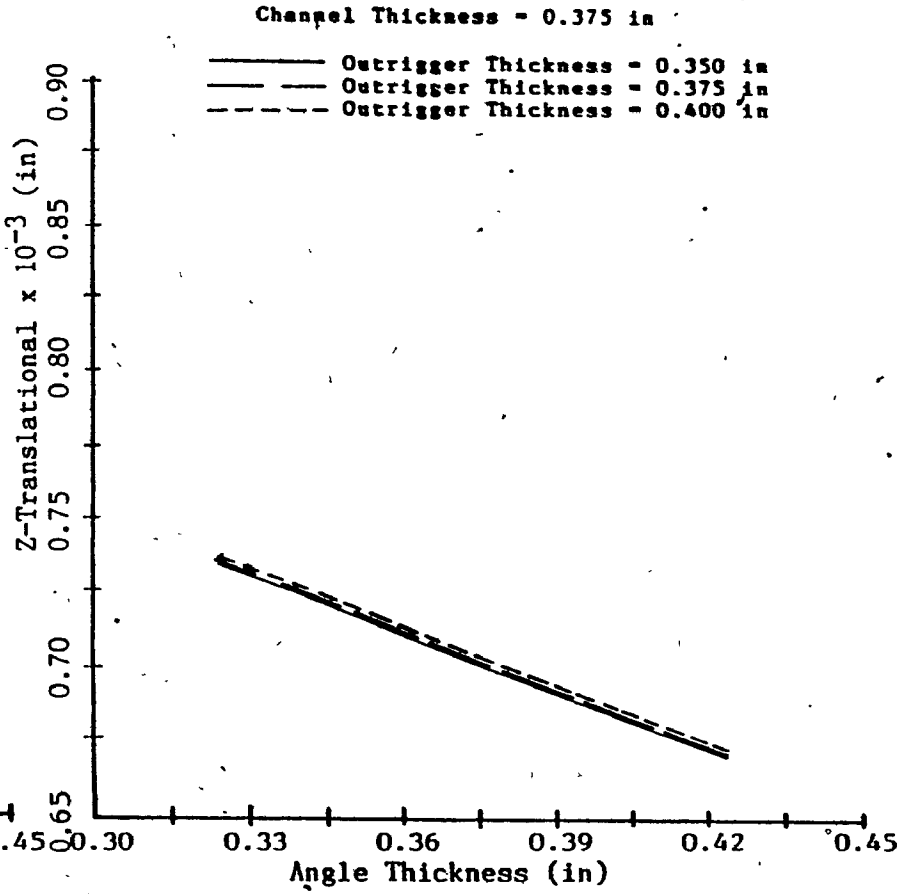

Figure 5.14b: Ansys Complete Model Analysis (Case 1-15) - Maximum Z-Translational Displacement for Support Structure of Tanker C

(For conversion to SI Units: 1 in = 0.0254 m)

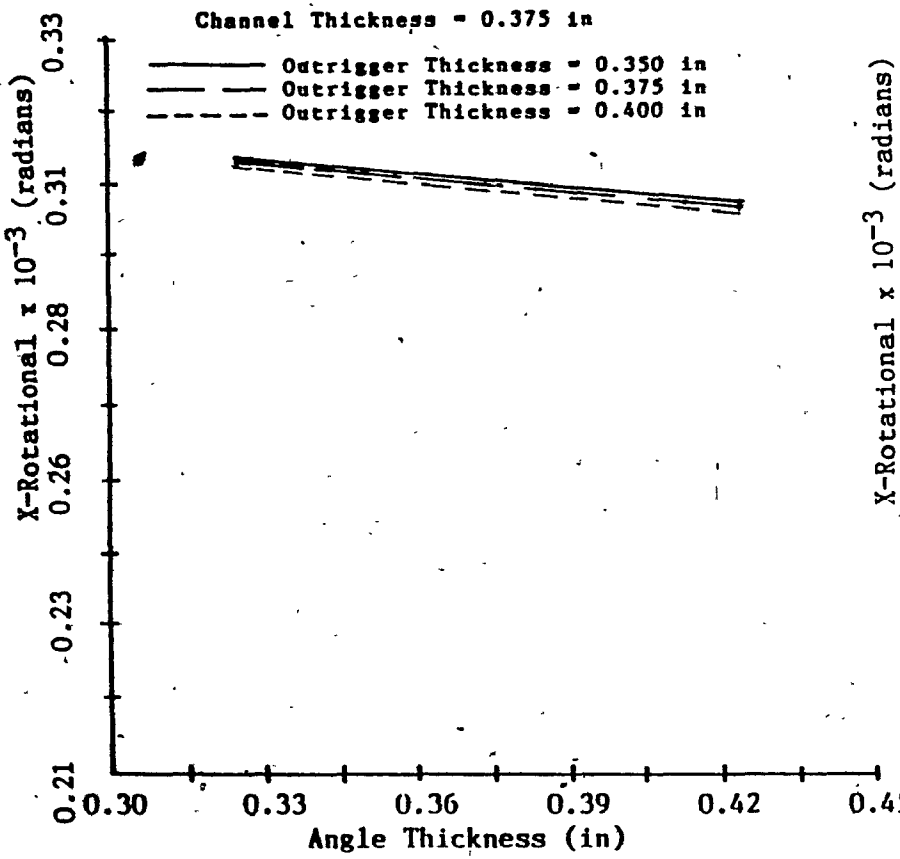

Figure 5.15b: Ansys Complete Model Analysis (Case 1-15) - Maximum X-Rotational Displacement for Support Structure of Tanker C

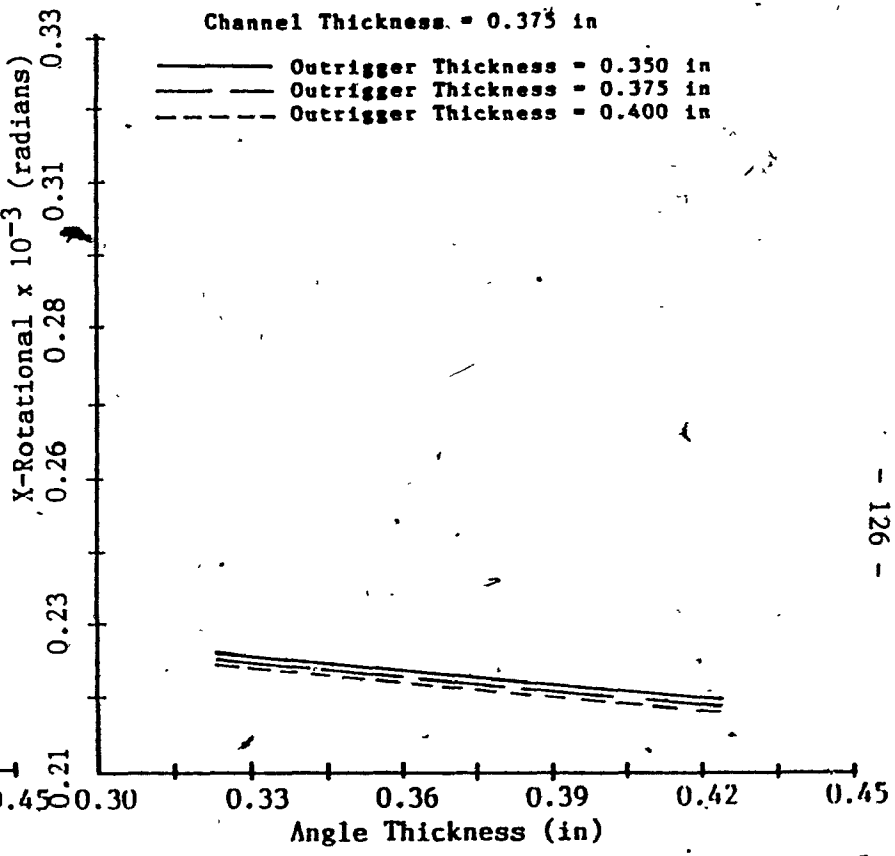

Figure 5.15a: Submodel Analysis (Case 1-15) - Maximum X-Rotational Displacement for Support Structure of Tanker C

(For conversion to SI Units: 1 in = 0.0254 m)

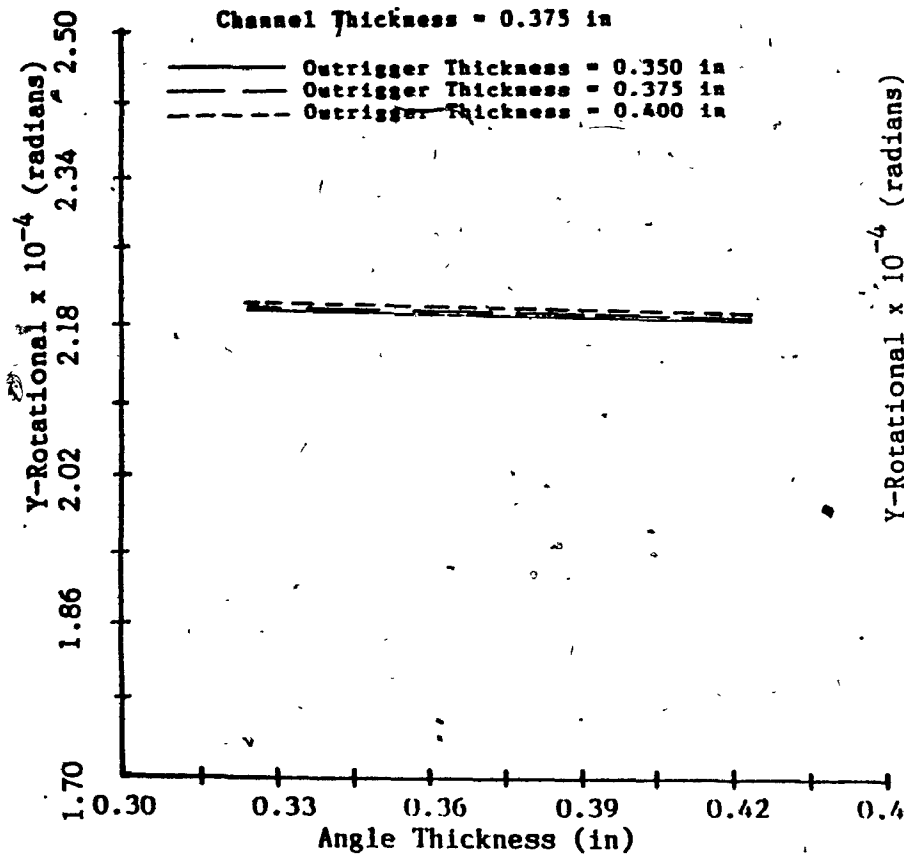

Figure 5.16a: Submodel Analysis (Case 1-15) - Maximum Y-Rotational Displacement for Support Structure of Tanker C

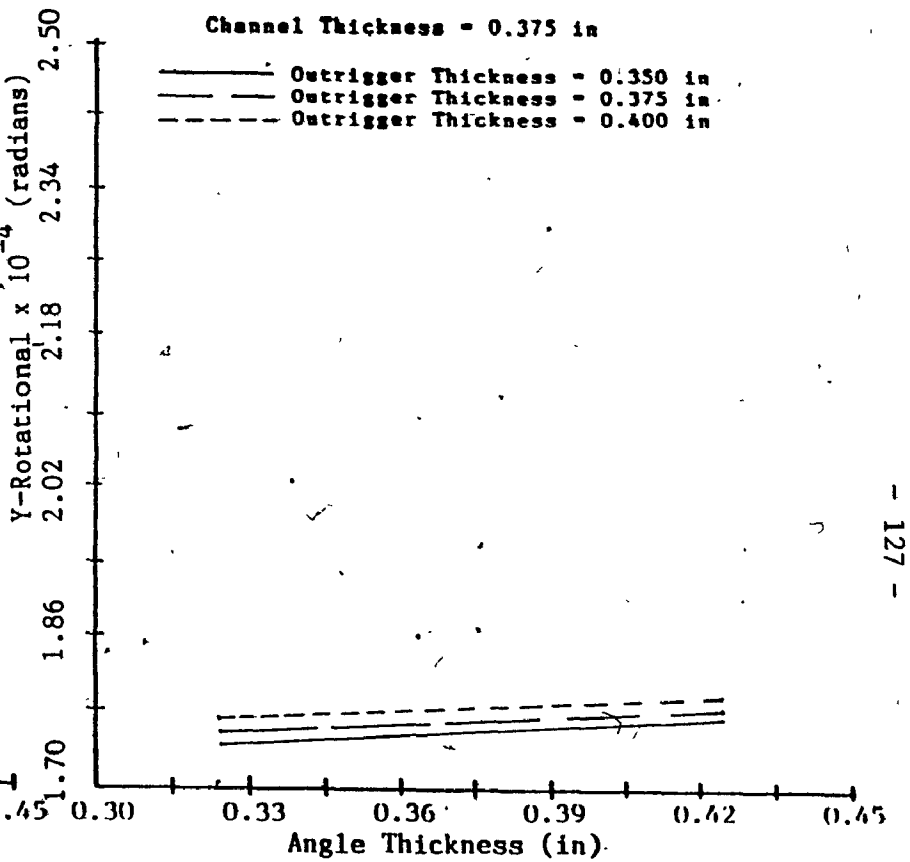

Figure 5.16b: Ansys Complete Model Analysis (Case 1-15) - Maximum Y-Rotational Displacement for Support Structure of Tanker C

(For conversion to SI Units: 1 in. = 0.0254 m)

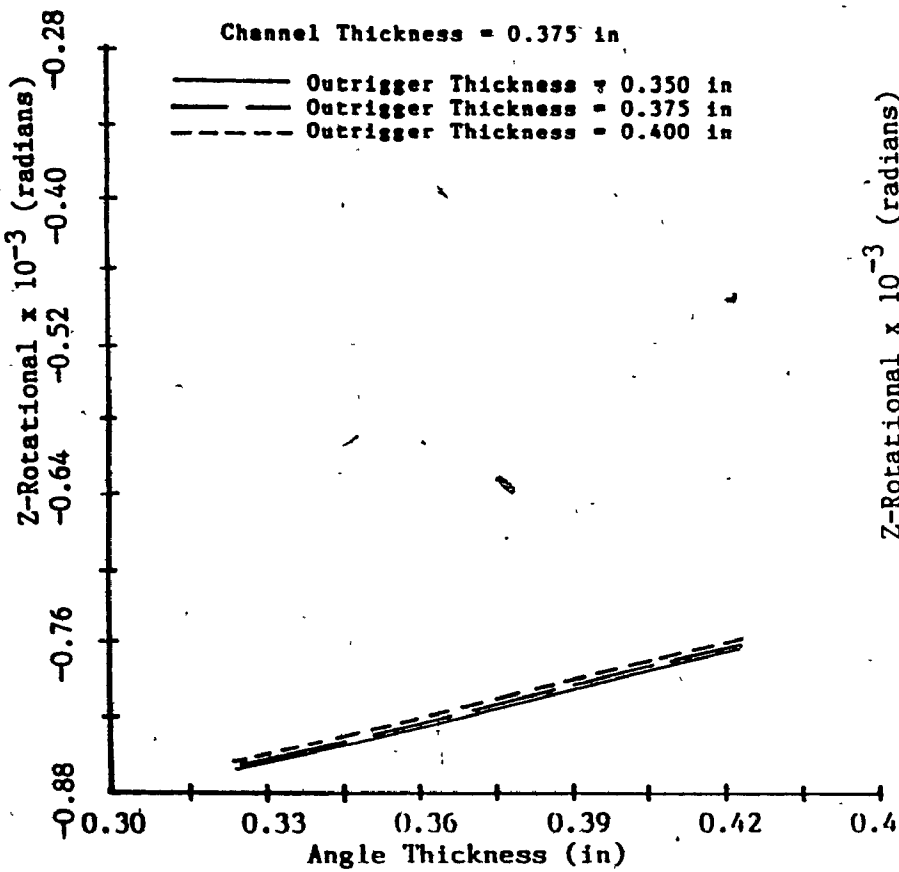

Figure 5.17a: Submodel Analysis (Case 1-15) - Maximum Z-Rotational Displacement for Support Structure of Tanker C

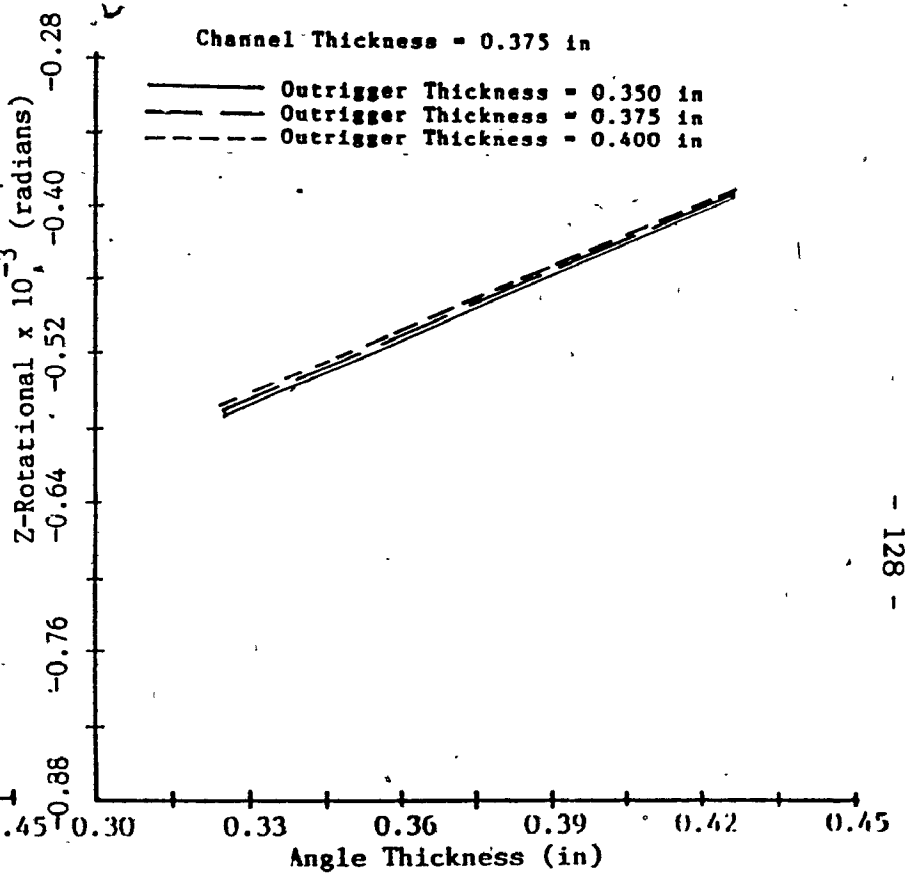

Figure 5.17b: Ansys Complete Model Analysis (Case 1-15) - Maximum Z-Rotational Displacement for Support Structure of Tanker C

(For conversion to SI Units: 1 in = 0.0254 m)

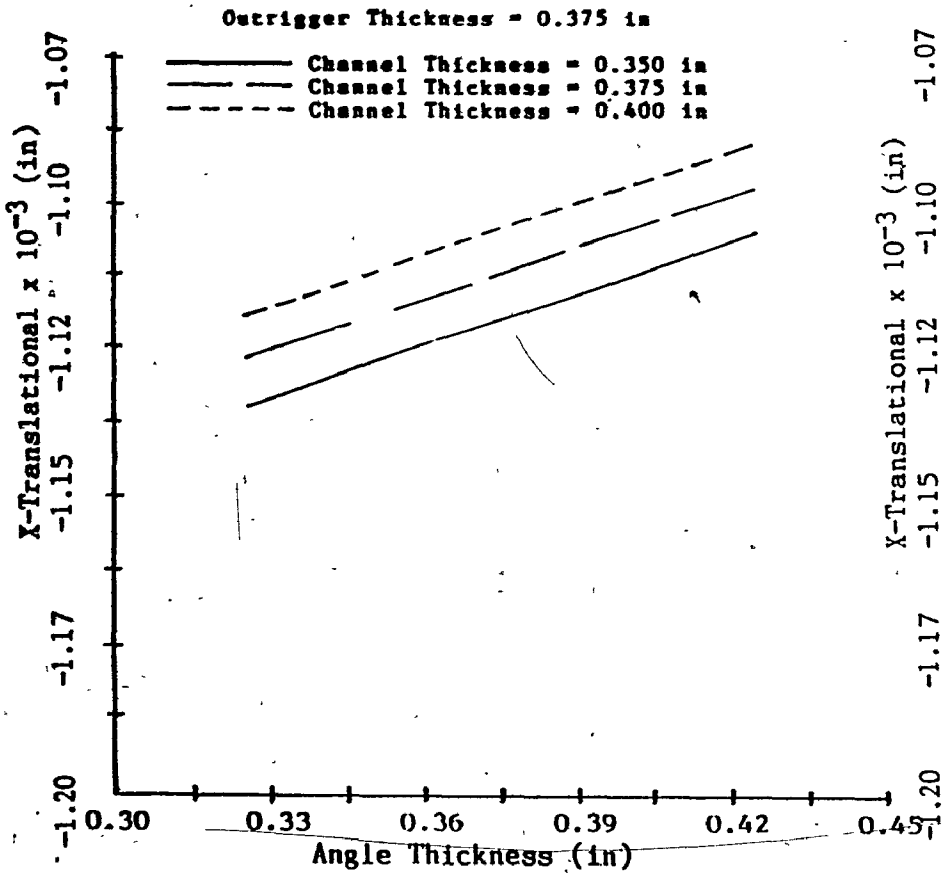

Figure 5.18a: Submodel Analysis (Case 16-30) - Maximum X-Translational Displacement for Support Structure of Tanker C

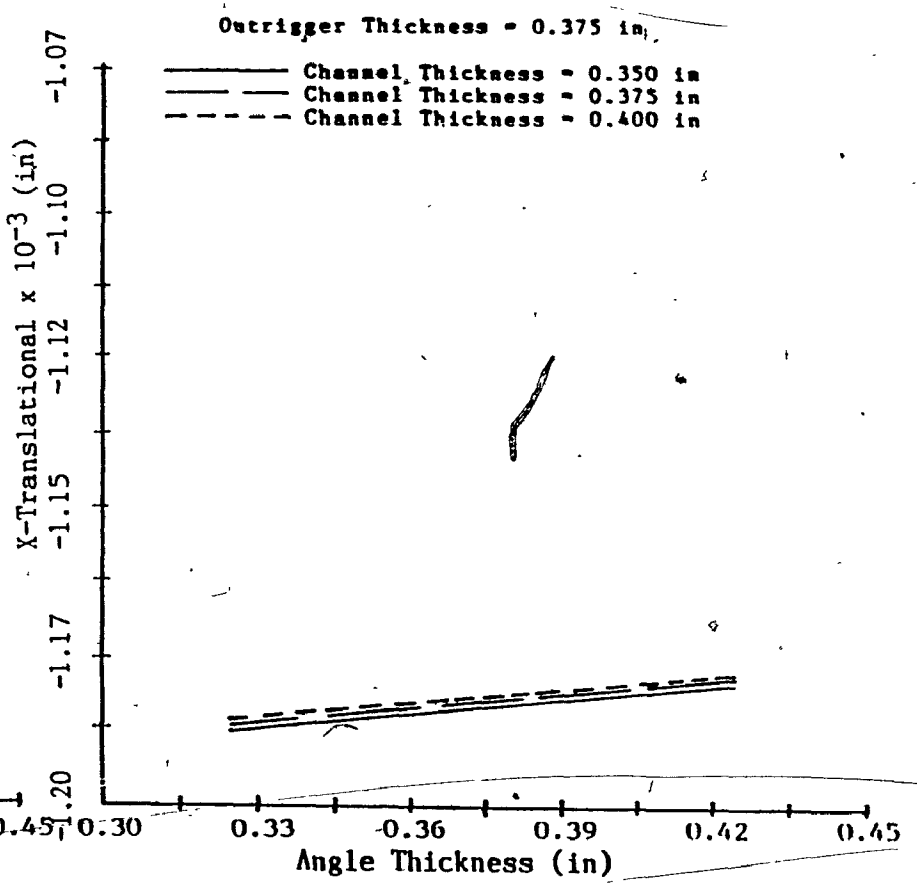

Figure 5.18b: Ansys Complete Model Analysis (Case 16-30) - Maximum X-Translational Displacement for Support Structure of Tanker C

(For conversion to SI Units: 1 in = 0.0254 m)

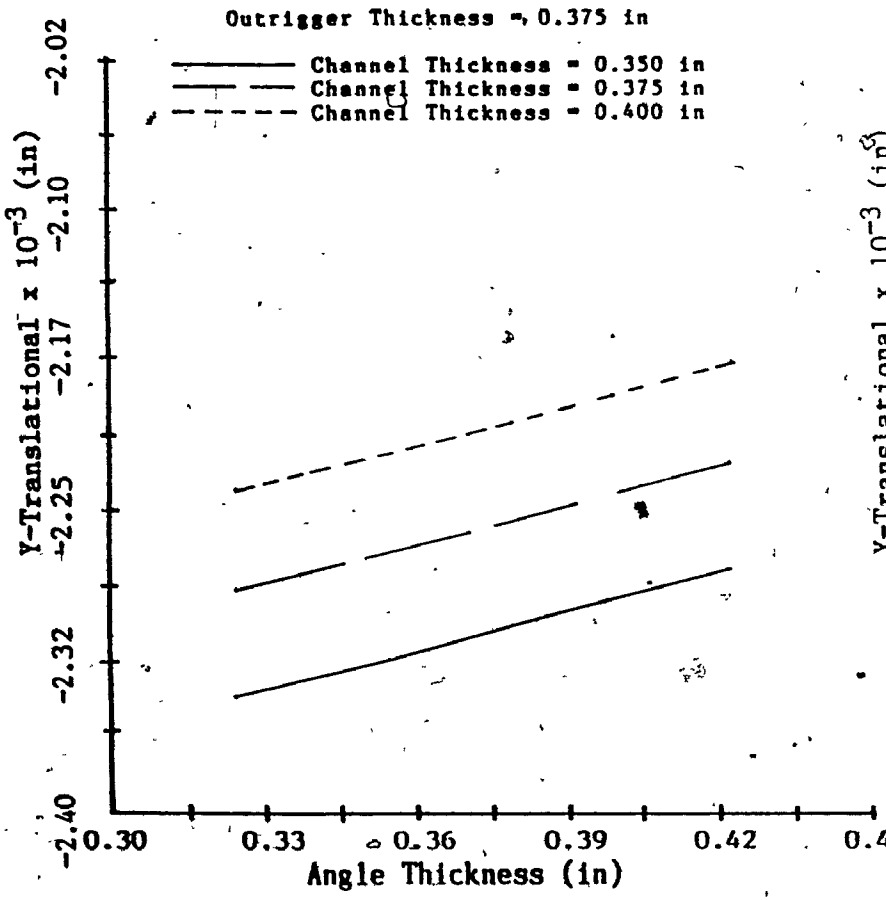

Figure 5.19a: Submodel Analysis (Case 16-30) - Maximum Y-Translational Displacement for Support Structure of Tanker C

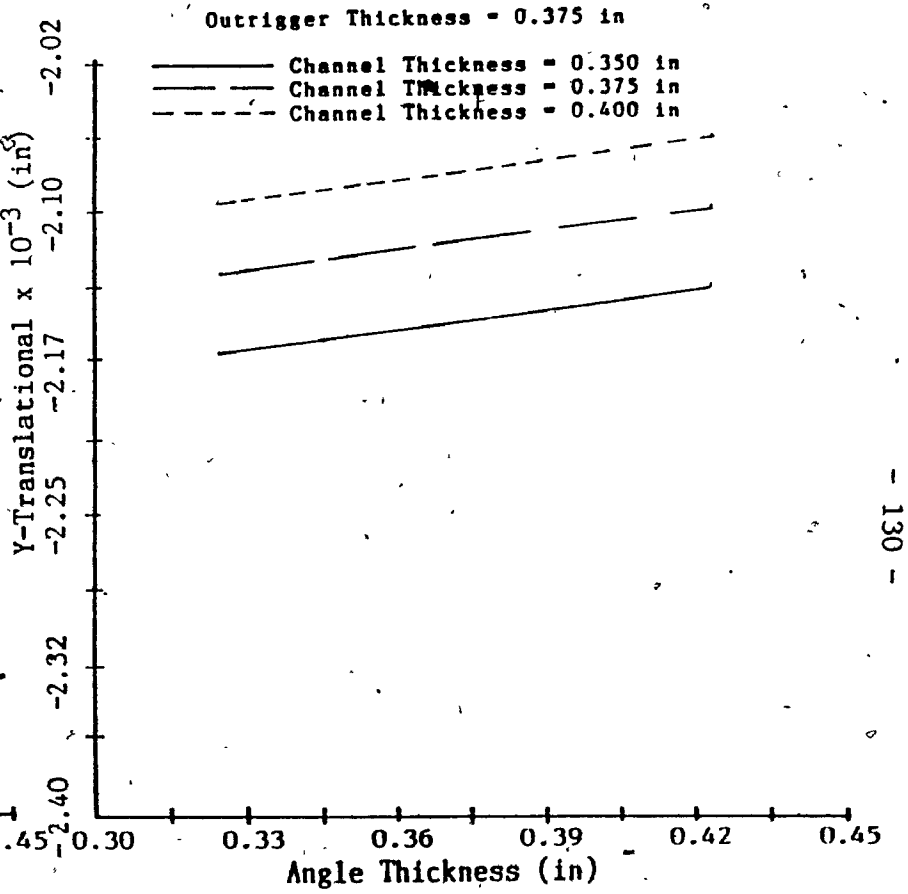

Figure 5.19b: Ansys Complete Model Analysis (Case 16-30) - Maximum Y-Translational Displacement for Support Structure of Tanker C

(For conversion to SI Units: 1 in = 0.0254 m)

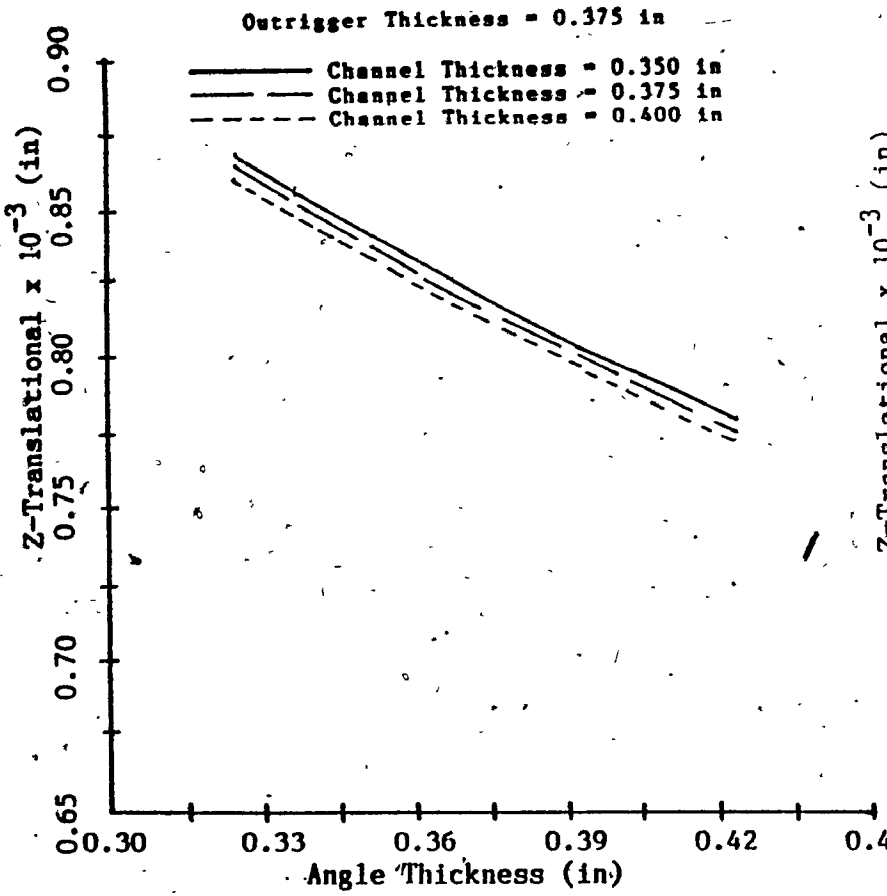

Figure 5.20a: Submodel Analysis (Case 16-30) - Maximum Z-Translational Displacement for Support Structure of Tanker C

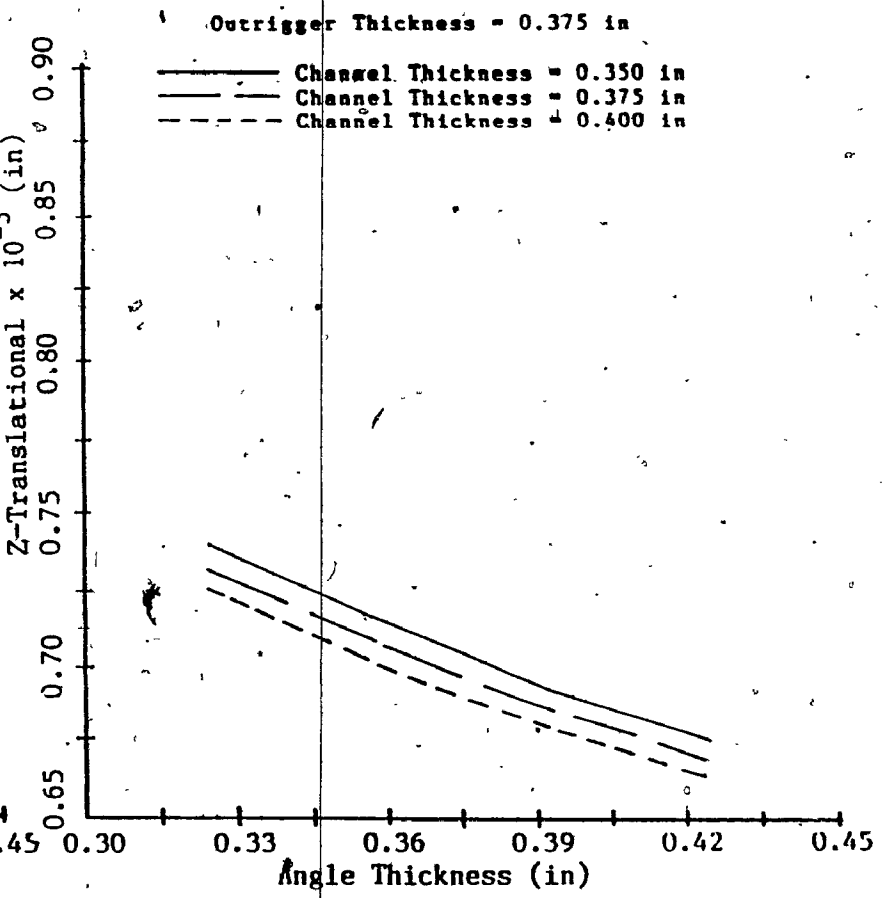

Figure 5.20b: Ansys Complete Model Analysis (Case 16-30) - Maximum Z-Translational Displacement for Support Structure of Tanker C

(For conversion to SI Units: 1 in = 0.0254 m)

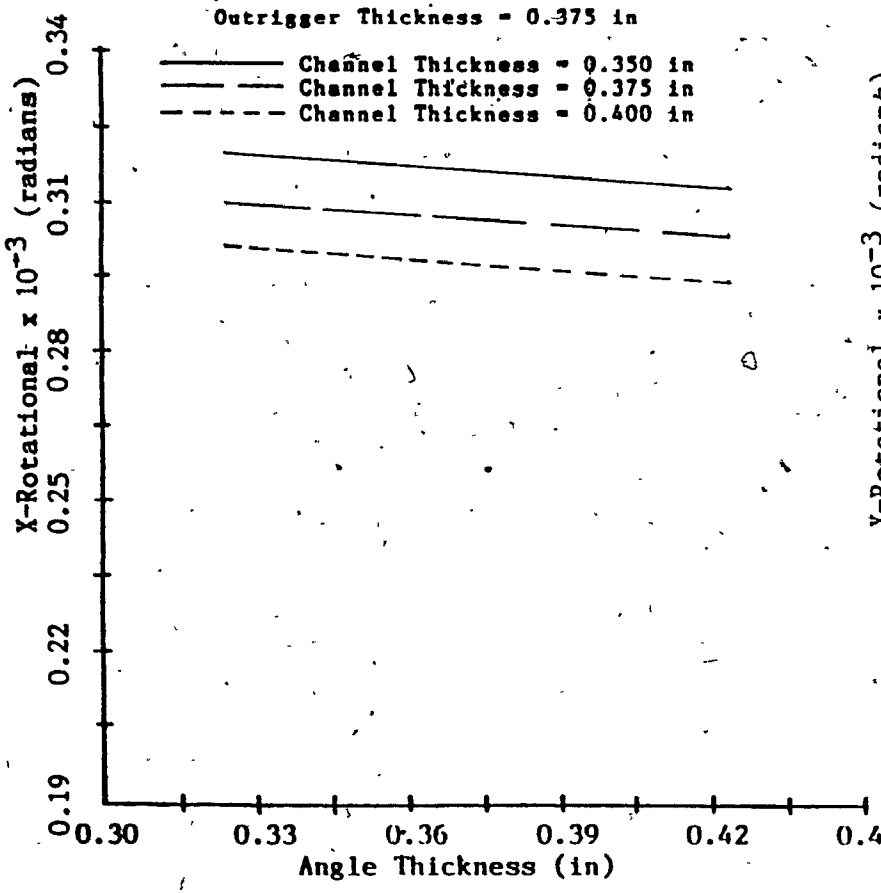

Figure 5.21b: Ansys Complete Model Analysis (Case 16-30) - Maximum X-Rotational Displacement for Support Structure of Tanker C

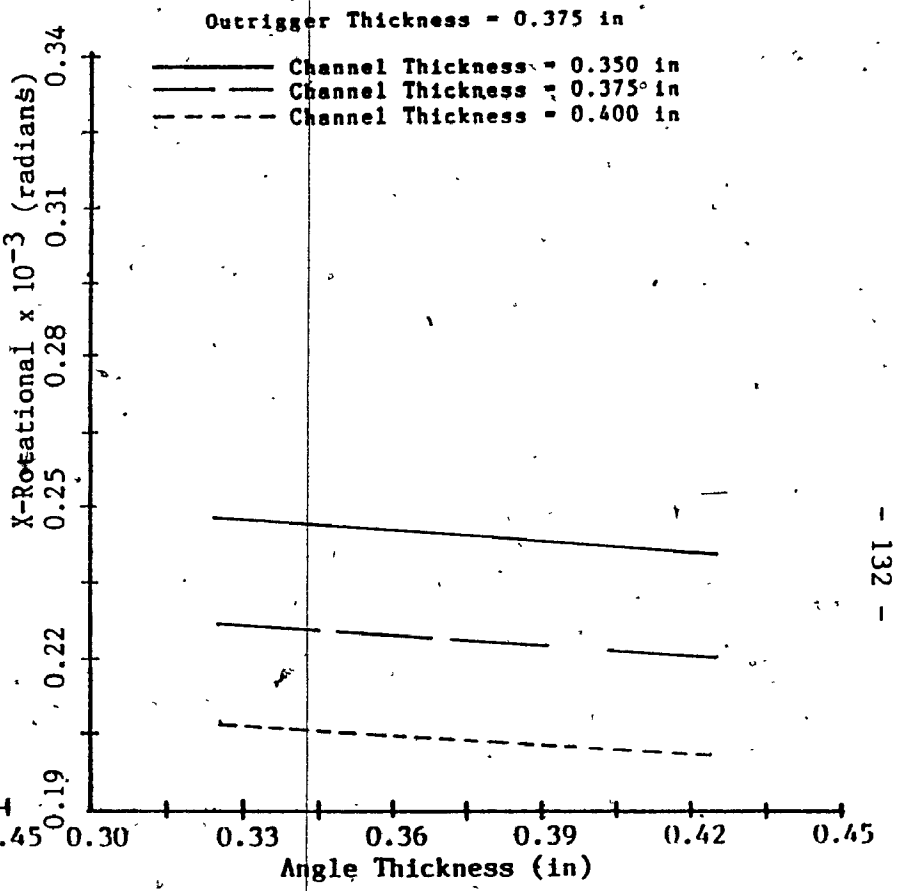

Figure 5.21a: Submodel Analysis (Case 16-30) - Maximum X-Rotational Displacement for Support Structure of Tanker C

(For conversion to SI Units: 1 in = 0.0254 m)

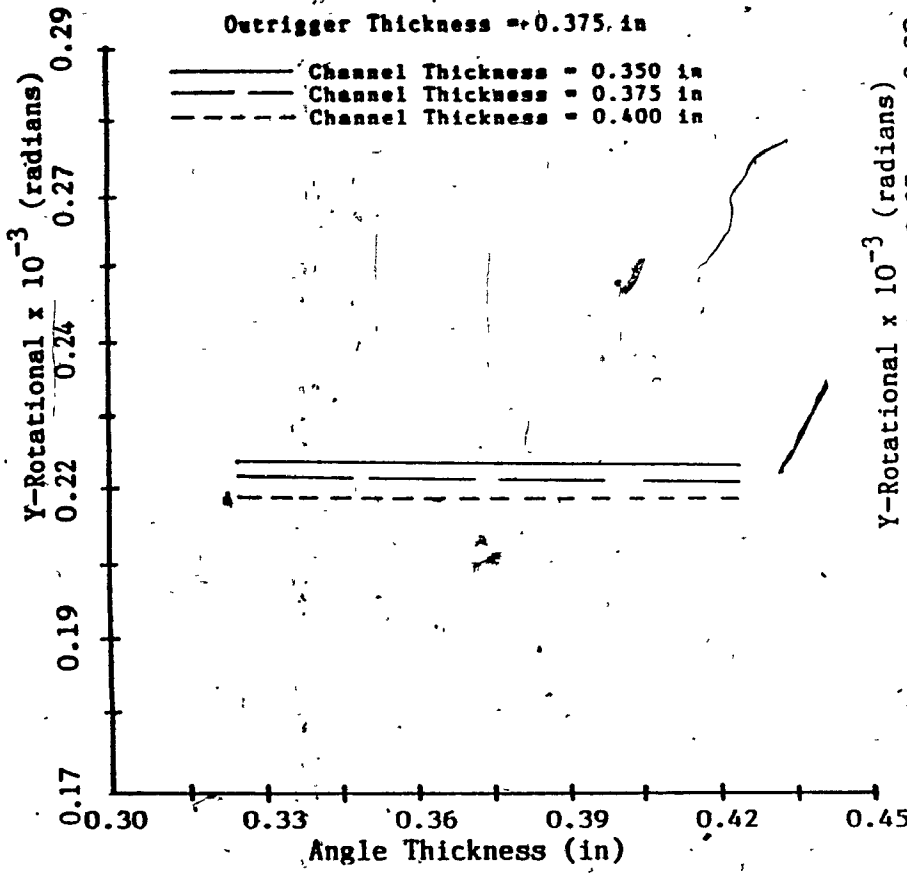

Figure 5.22a: Submodel Analysis (Case 16-30) - Maximum Y-Rotational Displacement for Support Structure of Tanker C

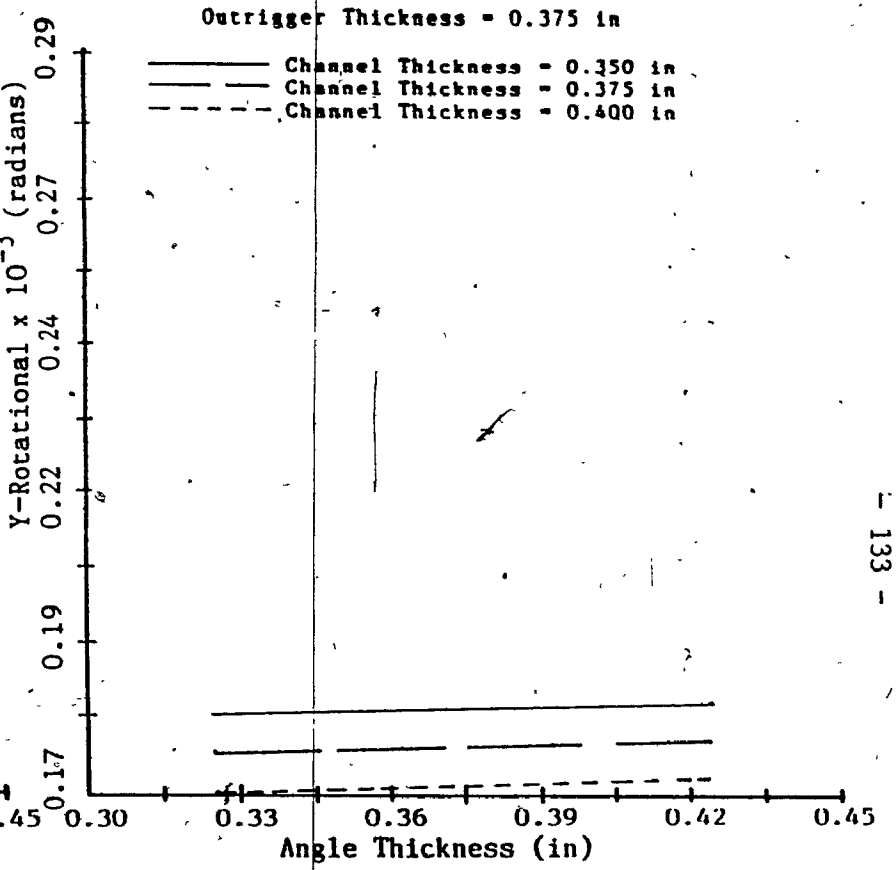

Figure 5.22b: Ansys Complete Model Analysis (Case 16-30) - Maximum Y-Rotational Displacement for Support Structure of Tanker C

(For conversion to SI Units: 1 in = 0.0254 m)

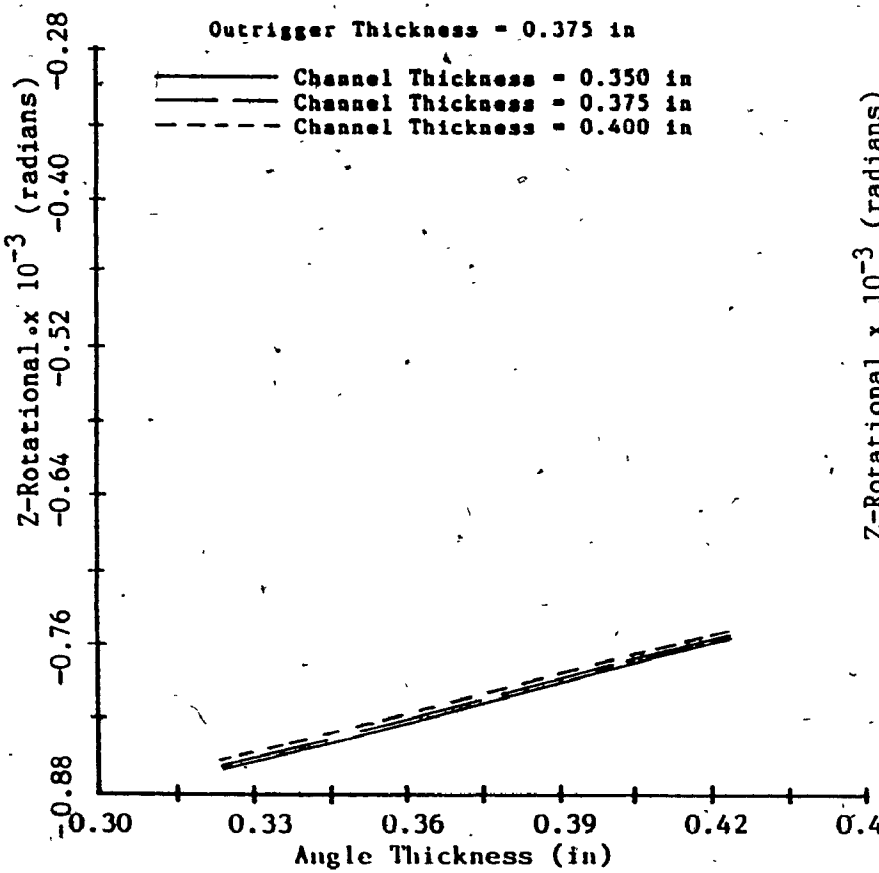

Figure 5.23a: Submodel Analysis (Case 16-30) - Maximum Z-Rotational Displacement for Support Structure of Tanker C

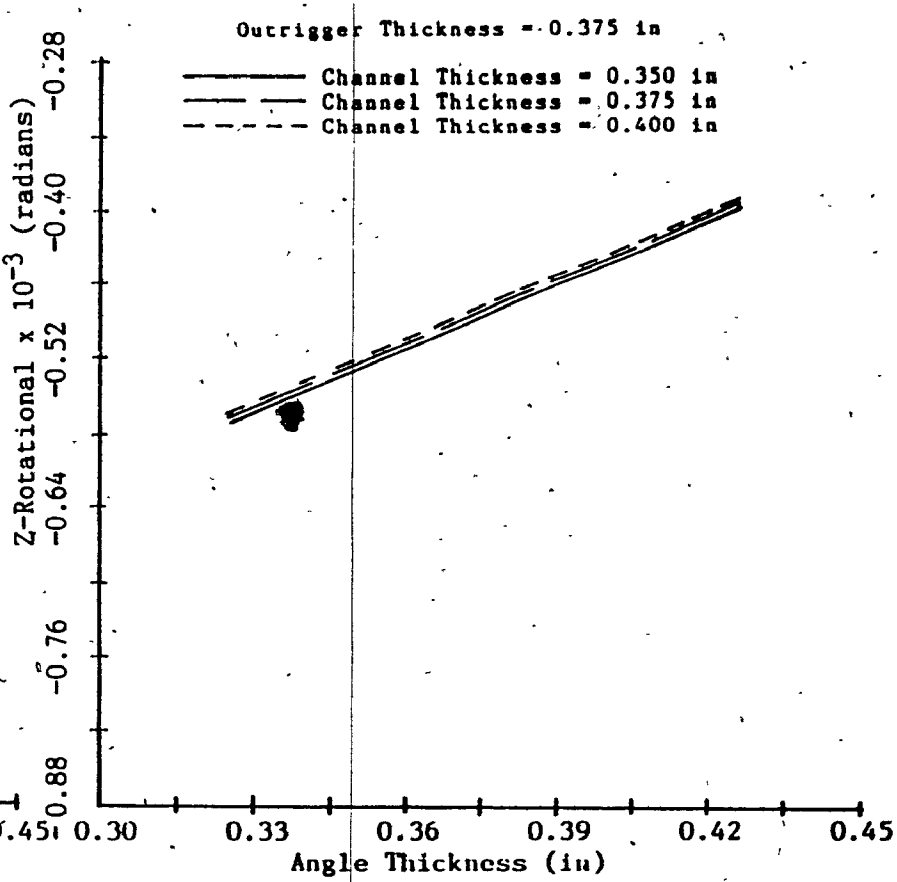

Figure 5.23b: Ansys Complete Model Analysis (Case 16-30) - Maximum Z-Rotational Displacement for Support Structure of Tanker C

(For conversion to SI Units: 1 in = 0.0254 m)

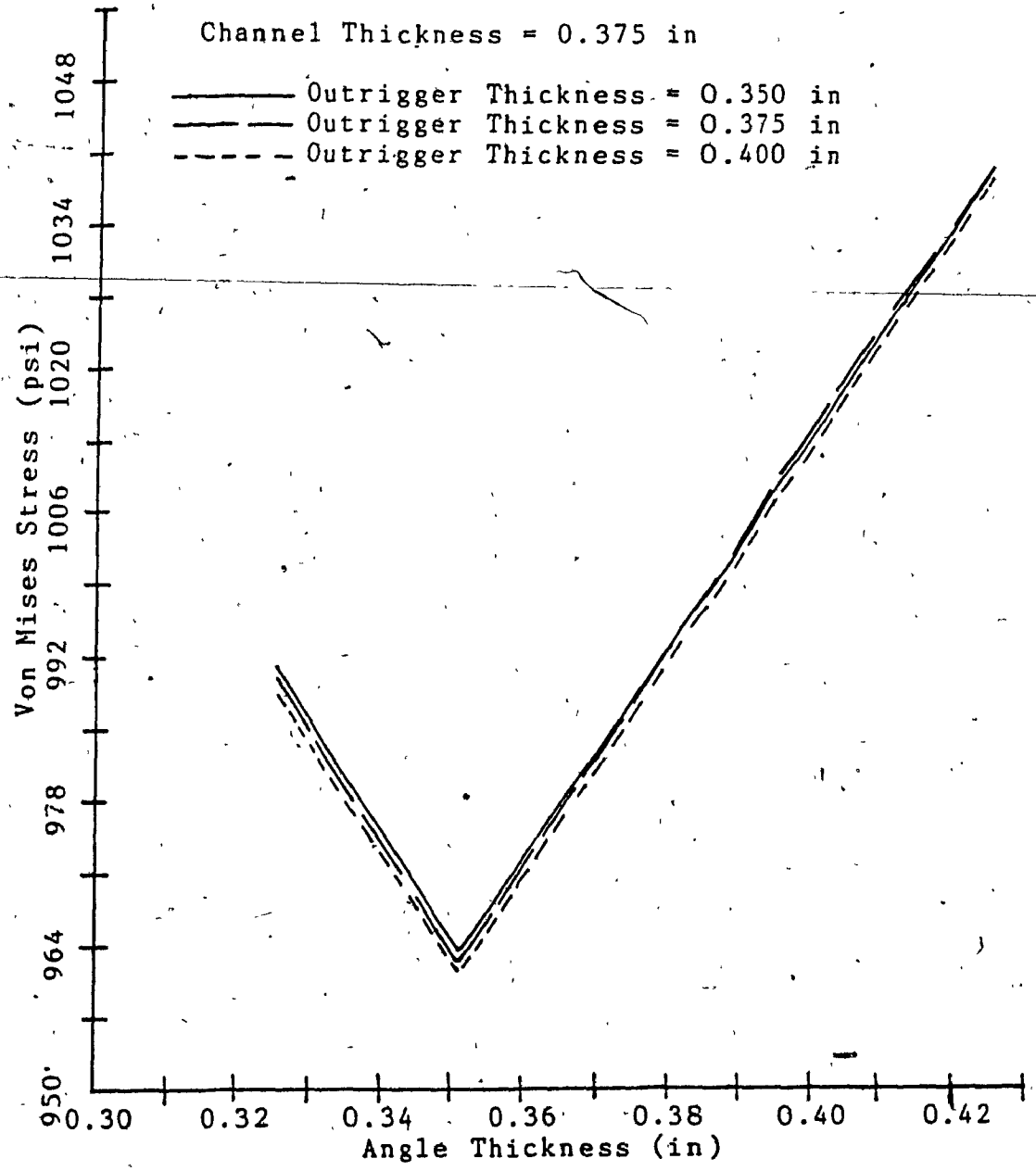

Figure 5.24: Submodel Analysis (Case 1-15) - Maximum Von Mises Stress for Support Structure of Tanker C

(For conversion to SI Units: 1 psi = 0.00689 MPa)

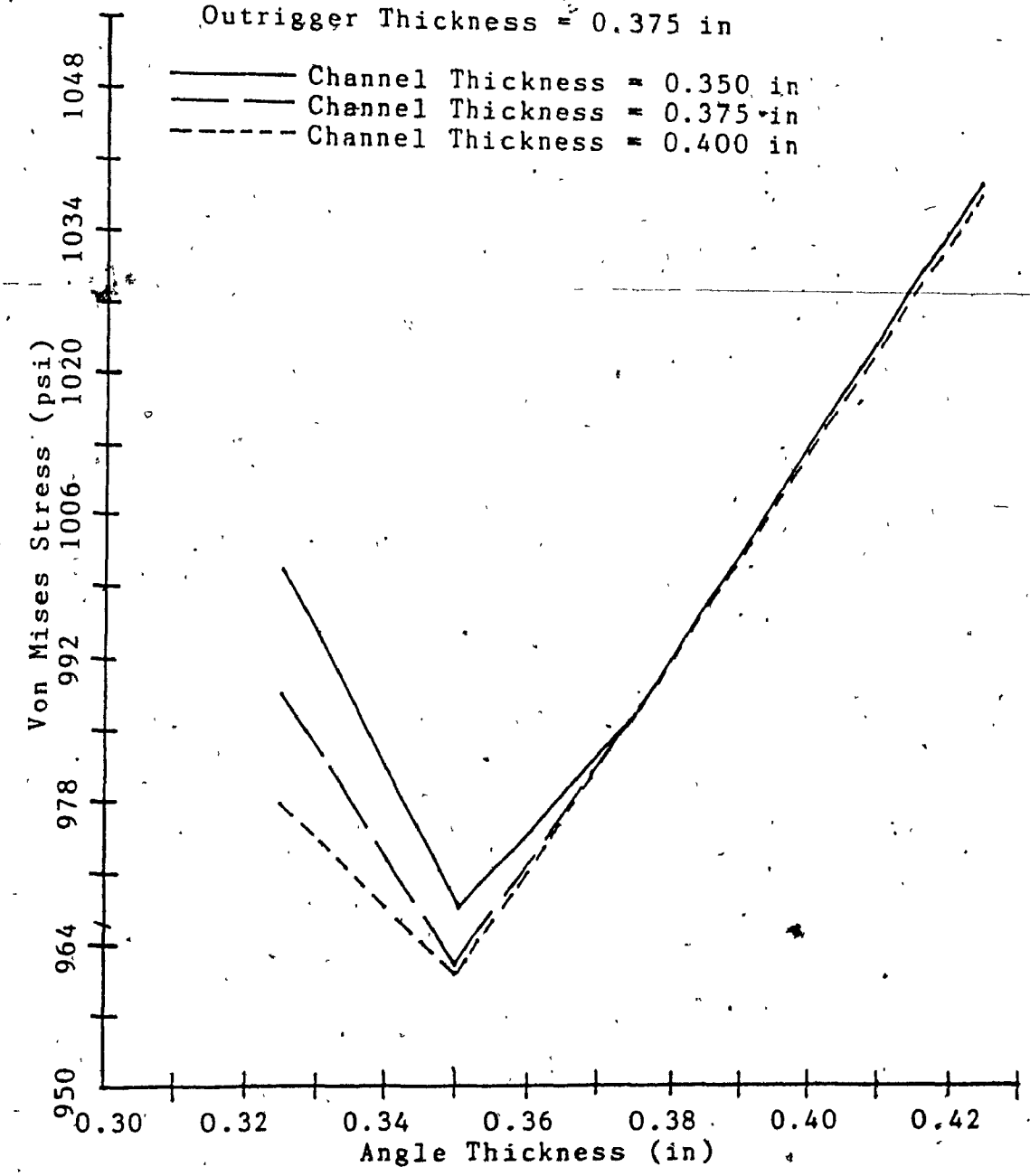

Figure 5.25: Submodel Analysis (Case 16-30) – Maximum Von Mises Stress for Support Structure of Tanker C

(For conversion to SI Units: 1 psi = 0.00689 MPa)

submodel reanalysis is shown in Figure 5.26 . The maximum stress value is 961 psi (6.62 MPa). A complete model analysis via an Ansys run for the same support parameters (component thicknesses) is shown in Figure 5.27. As in the base model comparison, the location of the maximum stress point has shifted, the magnitude of the maximum stress values in the two runs are close with an error of 5.2%.

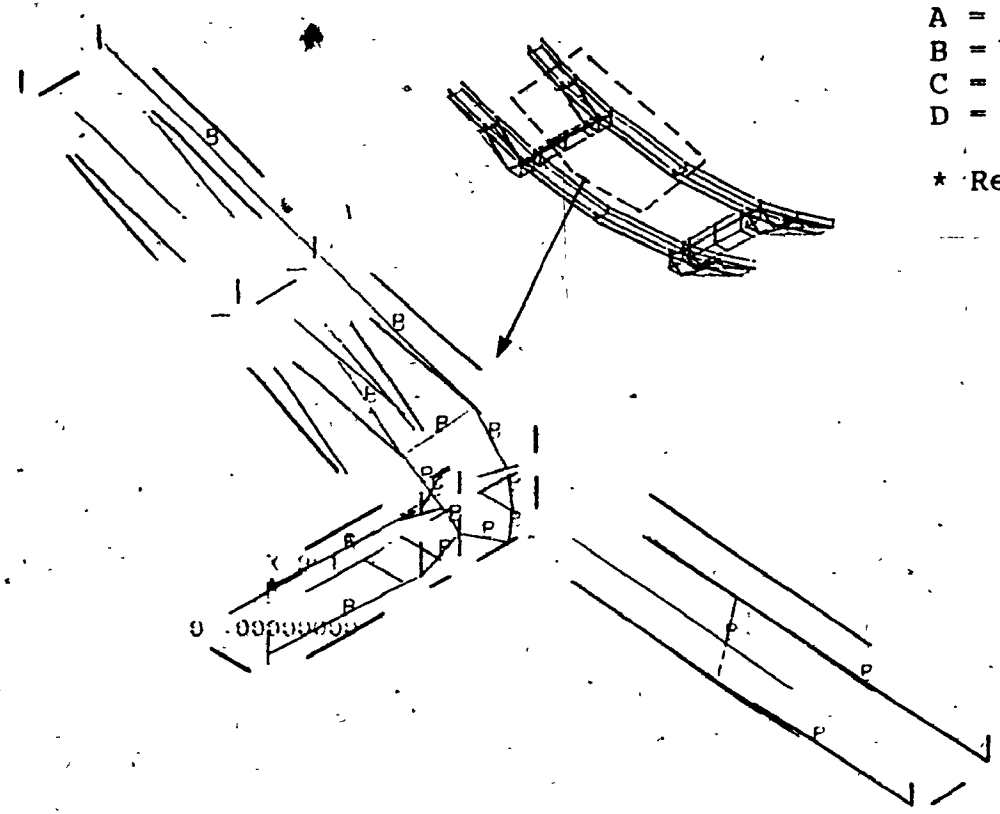

Figure 5.26: Stress Contours for the Support Structure of Tanker C - Submodel Analysis for Torsion Load
(Channel Thickness = 0.375 in, Angle Thickness = 0.350 in, Outrigger Thickness = 0.400 in)
(For conversion to SI Units: 1 in = 0.0254 m; 1 psi = 0.00689 MPa)

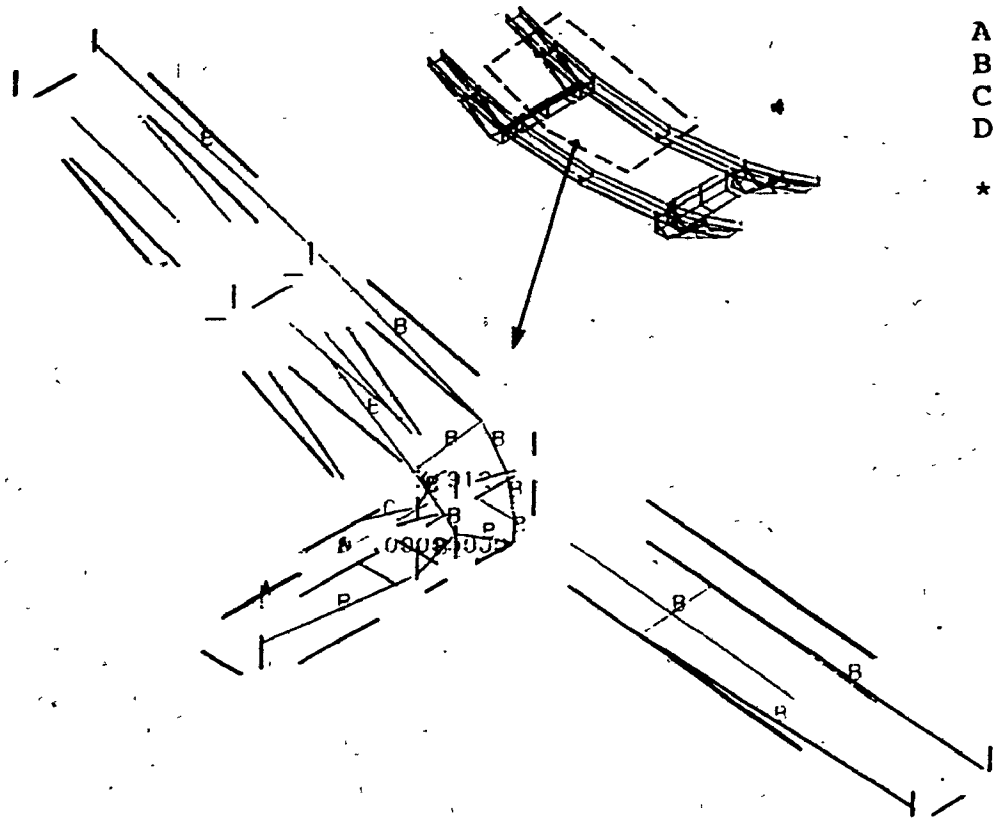

A = 0*
B = 400
C = 800
D = 1200

* Refers to stress value in psi.

Figure 5.27: Stress Contours for the Support Structure of Tanker C
- Complete Ansys Model Analysis for Torsion Load
(Channel Thickness = 0.375 in, Angle Thickness = 0.350 in,
Outrigger Thickness = 0.400 in)
(For conversion to SI Units: 1 in = 0.0254 m; 1 psi = 0.00689 MPa)

5.4 Summary

In this chapter, two case studies are presented on the effect of minor structural changes to single or multiple components within a submodel. The subcomponent reanalysis software described in the previous chapter was used for these case studies. Results of these case studies were validated with Ansys results for the same variation. The results were found to be quite close in the comparison.

CHAPTER 6

CONCLUSIONS AND RECOMMENDATIONS FOR FUTURE WORK

CHAPTER 6

CONCLUSIONS AND RECOMMENDATIONS FOR FUTURE WORK

6.1 Conclusions and Highlights of the Present Work

Due to the complexity of the shape and the design of liquid tankers, it is often necessary to carry out stress analysis on the complete model to determine their acceptability for a specific application. Often different parametric variations (on different parts of their body) have to be investigated to determine an optimum design for a particular application. These parametric studies are often performed by reanalyzing the complete model after incorporating the minor design variations. In this thesis, a technique which only requires a reanalysis of the section of interest in the complete model is presented. This technique significantly reduces the computational effort required in estimating stress values on the submodel of interest using the Finite Element method.

As a first step in illustrating the methodology of the new reanalysis technique, three types of liquid tankers were analyzed using Ansys finite element software. An Autotrol CAD workstation was used for creating the geometry model and the finite element modeling , while the Ansys software was used for the analysis and post-processing of the results. All models were analyzed using the static analysis option in Ansys software. The post-processing was

carried out utilizing the Ansys Post 25 post-processor to plot the data in the form of stress contours. Two types of loading: dead weight and torsion were considered. A parametric study involving thickness variation for the tanker body, and geometry and shape variation of the baffle was carried out for the three tankers.

In the second part of the thesis, a new technique for reanalysis of a submodel of interest via the Finite Element technique for design parametric variations is presented. This technique significantly reduces the computational efforts and eliminates analysis of complete model for design variations. In this technique, a submodel of the area of interest was first extracted from the complete model. The components of interest were then modified according to the parametric variations required in the new design. The submodel was then analyzed using a matrix partitioning technique. The complete software was developed to demonstrate this new technique. The ability to carry out a design sensitivity analysis with minimum of computational effort was incorporated into this software. Two case studies: baffle geometry and shape variation, and support component thickness variation, were studied. The results were validated using finite element analyses of the complete model with these parametric design changes.

6.2 Recommendations for Future Work

Recommendations for future work based on this thesis falls into two categories. The first is a more complete investigation for the optimum design of the liquid tankers within the given specifications. The second category is for improving the usage of the presented technique for the reanalysis of modified components in a finite element model.

Recommendations for a more complete analysis are given below:

1) Carry out a more detailed parametric study for different thickness variation of top and bottom of the tanker body.

2) Investigate more detailed baffle design variation.

3) Study fatigue analysis of tanker structure.

4) Conduct a detailed laboratory testing to validate results of the reanalysis technique.

The reanalysis software may be improved by the following recommendations.

1) Develop an interface routine to different finite element packages for automated stress evaluation and stress contour plotting of the components of interest.

2) Interface the reanalysis software with an optimization

package to get the optimum design solution for a component reanalysis.

3) Develop an interface package to other finite element softwares such as Nastran, etc.

4) Develop user friendly interactive graphic routines for the selection and integration of the new components in the submodel analysis.

5) Extend this technique for obtaining global mass matrices of submodels for subcomponent variations to carry out dynamic analysis.

REFERENCES

REFERENCES

1. Johannson, S.E., " What is a Tank Trailer ? ", Motor Truck, September 1965.
2. Johannson, S.E., " Selecting a General Purpose Chemical Tank ", Motor Truck, October 1965.
3. Thevendran, V. and Thambiratnam, David P., " Minimum Weight Design of Cylindrical Water Tanks ", International Journal for Numerical Methods in Engineering, Vol.23, 1986.
4. " Unigraphics Users Manual ", Mcdonnel Douglas Corporation, 1985.
5. " Euclid Users Manual ", Matra Datavision Inc., 1983.
6. " PDGS " - Information Pamphlets.
7. " Series 7000 - Advanced Graphics Software ", Auto-trol Technology Corporation, 1986.
8. McCormick, C. W., " Nastran User's Manual", May 1978, M.S.C. Corporation, Los Angeles.
9. DeSalvo, Gabriel J. and Swanson, John A., " ANSYS Engineering Analysis System User's Manual ", November 1981, Swanson Analysis Systems Inc., Pennsylvania.
10. " Patran-G User's Manual ", 1985, P.D.A. Engineering, Los Angeles.
11. " Stardyne User's Manual ", Control Data Corporation, Minneapolis, 1975

12. Wheatstone, W.D., " SPAR Structural Analysis Reference Manual ", NASA CR-158970-1, 1978

13. Klosterman, A.L. and Ard, R.H., " A Geometric Modelling Program for the System Designer ", Conference on CAD/CAM Technology in Mechanical Engineering, March 24-26, 1982, Massachusetts Institute of Technology.

14. Baer, A., Eastman, C. and Hension, M.," Geometric Modelling: A Survey ", Computer Aided Design, Vol. II, Sept. 5, 1979.

15. Krouse, J.K., " Geometric Models for CAD/CAM ", Machine Design, July 24, 1980.

16. Krouse, J.K., " Automated Drafting: The First Step to CAD/CAM ", Machine Design, May 21, 1981.

17. Krouse, J.K., " Computer Aided Design for Every Pocketbook ", Machine Design, November 20, 1980.

18. Kamal, M. and Wolf, J.A., " Finite Element Models for Automotive Vehicle Vibrations", ASME, 1977.

19. Kamal, M. and Wolf, J.A., " Modern Automotive Structural Analysis, " Van Nostrand Reinhold Co., 1982.

20. Waldleigh, K.H., " Applications of Finite Element Methodsto Complete Automobile Structural Design Evaluation ", SAE_740322.

21. Przemieniecki, J.S., " Matrix Structural Analysis of Substructures ", AIAA Journal, Vol 1, 1963.

22. Dodds, Robert H. and Lopez, L.A., " Substructuring in Linear and Nonlinear Analysis ", International Journal for Numerical Methods in Engineering, Vol 15, 1980.

23. Taig, I.C., " Automated Stress Analysis Using Substructures ", Matrix Methods in Structural Mechanics, November 1966.

24. Basas, Jesus E. and D'Souza, Valerian J., " Automatic Finite Element Model Generation of Automotive Components Using Ansys ", Ansys Conference Proceedings, April 1983.

25. Arora, J.S., " Survey of Structural Reanalysis Techniques", Journal of the Structural Division ASCE, April 1976.

26. Noor, Ahmed K. and Lowder, Harold E., " Approximate Techniques od Structural Reanalysis ", Computers and Structures, Vol 4, 1974.

27. Fox, Richard L., " Optimization Methods for Engineering Design ", Addison-Wesley Publishing Company, 1971.

28. George, Alan and Liu, Joseph W., " Computer Solutions of Large Sparse Positive Definate Systems ", Prentice Hall Inc., 1981.

29. Tewarson, Reginald P., " Sparse Matrices ", Academic Press, 1973.

30. Bathe, Klaus Jurgen and Wilson, Edward L., " Numerical Methods in Finite Element Analysis", Prentice Hall Inc., 1976.

31. Giles, Gary L., " Procedure for Automating Aircraft Wing Structural Design ", Journal of the Structural Division, ASCE, Vol 97, 1971.

32. Shanley, F.R., " Strength of Materials ", McGraw Hill Book Co., 1957.

33. Phansalkar, Suresh R., " Matrix Methods for Structural Reanalysis ", Journal of the Structural Division of ASCE, 1972.

APPENDIX I

BANDWIDTH OPTIMIZATION ALGORITHM

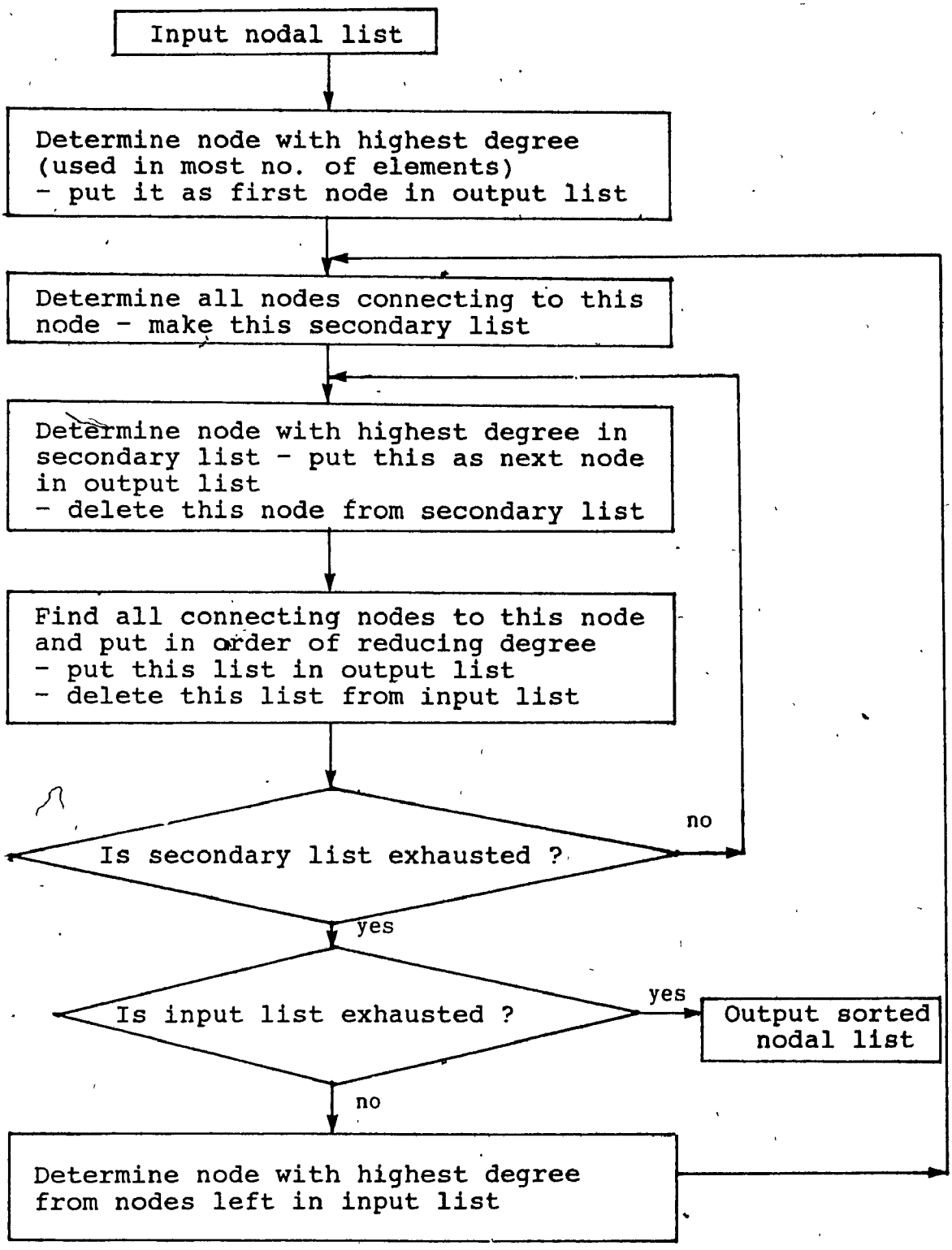

Figure AI.1: Bandwidth Optimization Algorithm Flowchart

APPENDIX II

PARTITIONED GLOBAL MATRIX ASSEMBLY PROCEDURE

APPENDIX II

Partitioned Global Matrix Assembly Procedure

The following lists a procedure for partitioned global matrix assembly from individual stiffness matrices (in global coordinates) of all the elements to be assembled and the nodal connectivity of the elements. A nodal listing of all the elements as well as the partitioning point in this list is also required.

1) Assign a double subscript (k_{ij}) to each element stiffness coefficient in all element stiffness matrices.

   The first subscript i, corresponds to the force in the global model for which the equation is written, while the second subscript j, designates the associated degree-of-freedom in the global model.

2) Create a two-dimensional array for a square matrix [K] whose size is equal to the number of degrees-of-freedom in the complete system.

3) Partition the [K] matrix into four matrices [K11], [K12], [K21], and [K22].

   The partition is determined by the inputted partitioned point in the nodal listing. Thus, the size of [K11] which is a square matrix corresponds to the number of degrees of freedom in the left side of the

partitioning point in the nodal listing. The size of [K22] which is also a square matrix is equal to the number of degrees of freedom to the right of the partitioning point in the nodal listing.

[K12] and [K21] correspond to the matrices on the right of [K11] and the left of [K22] in the original complete global matrix (Figure AIII.1a).

4) Access and place each element stiffness coefficient in the appropriate position corresponding to its subscripts in one of the four matrices [K11], [K12], [K21], or [K22]. If more than one coefficients are to be placed at the same position in any of the four partitioned global matrices, they are added to each other before the placement.

5) Repeat this procedure until the list of elements is exhausted resulting in the four assembled and partitioned matrices [K11], [K12], [K21], and [K22].

APPENDIX III

MATRIX INVERSION BY CHOLESKY'S TRANSFORMATION TECHNIQUE

APPENDIX III

Matrix Inversion by Chôlesky's Tranformation Technique

Cholesky's transformation technique for solving a set of linear simultaneous equations has been derived by Bathe and Wilson [30]. A modified method utilized in the matrix inversion routine in the reanalysis software is given below.

Let [K] be an n x n symmetric matrix to be inverted. Thus:

$$[K][K]^{-1} = [I] \qquad \text{(AIII-1)}$$

where $[K]^{-1}$ is the inverse of [K]

and [I] is an identity matrix of order n.

Let the matrix [K] be written as:

$$[K] = [L]\,[D]\,[L]^T \qquad \text{(AIII-2)}$$

where [L] is a lower triangular matrix,

[D] is a diagonal matrix,

and $[L]^T$ is the transpose of [L].

Thus if:

$$[L] = \begin{bmatrix} 1 & 0 & 0 & 0 & 0 & 0 \ldots\ldots 0 \\ L_{21} & 1 & 0 & 0 & 0 & 0 \ldots\ldots 0 \\ L_{31} & L_{32} & 1 & 0 & 0 & 0 \ldots\ldots 0 \\ \cdot & \cdot & \cdot & \cdot & \cdot & \cdot\cdot\cdot\cdot\cdot\cdot\cdot\cdot \\ \cdot & \cdot & \cdot & \cdot & \cdot & \cdot\cdot\cdot\cdot\cdot\cdot\cdot\cdot \\ L_{n1} & L_{n2} & L_{n3} & L_{n4} & L_{n5} & \cdot\cdot\cdot\cdot\cdot\cdot\cdot 1 \end{bmatrix}$$

and

$$[D] = \begin{bmatrix} D_{11} & 0 & 0 & 0 & 0 & 0 \ldots\ldots 0 \\ 0 & D_{22} & 0 & 0 & 0 & 0 \ldots\ldots 0 \\ 0 & 0 & D_{33} & 0 & 0 & 0 \ldots\ldots 0 \\ . & . & . & . & . & \ldots\ldots\ldots \\ . & . & . & . & . & \ldots\ldots\ldots \\ 0 & 0 & 0 & 0 & 0 & 0 \ldots\ldots D_{nn} \end{bmatrix}$$

and

$$[L]^T = \begin{bmatrix} 1 & L_{21} & L_{31} & \ldots\ldots\ldots\ldots\ldots & L_{n1} \\ 0 & 1 & L_{32} & \ldots\ldots\ldots\ldots & L_{n2} \\ 0 & 0 & 1 & L_{43} \ldots\ldots\ldots & L_{n3} \\ . & . & . & . & \ldots\ldots\ldots\ldots \\ . & . & . & . & \ldots\ldots\ldots\ldots \\ 0 & 0 & 0 & 0 & \ldots\ldots\ldots 1 \end{bmatrix}$$

The terms in the three matrices [L], [D], and $[L]^T$ can be determined by expanding Equation (AIII-2). This Equation can now be written as:

$$\begin{bmatrix} K_{11} & K_{12} & & .. K_{1n} \\ K_{21} & K_{22} & & .. K_{2n} \\ K_{31} & K_{32} & K_{33} & .. K_{3n} \\ . & . & & \ldots \\ . & . & & \ldots \\ K_{n1} & & & .. K_{nn} \end{bmatrix} = \begin{bmatrix} D_{11} & L_{21}D_{11} & L_{31}D_{11} & & L_{n1}D_{11} \\ L_{21}D_{11} & L_{21}^2D_{11}+D_{22} & L_{21}L_{31}D_{11}+L_{32}D_{22} & .. & \\ . & . & . & .. & \\ . & . & . & .. & \\ . & . & . & .. & \\ . & . & . & .. & \end{bmatrix} \quad \text{(AIII-3)}$$

Thus from the above Equation:

$$D_{11} = K_{11},\ L_{21} = \frac{K_{12}}{D_{11}},\ L_{31} = \frac{K_{13}}{D_{11}} \ldots\ldots\ldots, \text{etc.}$$

In general:

Let $m_j = m_k - j$ (m_k = half bandwidth of [K])

for $j = 2, \ldots\ldots, m_k$, and $i = m_j+1, \ldots\ldots, j-1$,

$$\begin{cases} G_{mj,j} = K_{mj,j} \\ G_{ij} = K_{ij} - \sum_{r=m_j}^{i-1} L_{ri} G_{rj} \end{cases} \qquad \text{(AIII-4)}$$

where the elements G_{ij} are defined as intermediate quantities and the calculation is completed using:

$$L_{ij} = \frac{G_{ij}}{D_{ij}} \qquad \text{(AIII-5)}$$

and

$$D_{jj} = K_{jj} - \sum_{r=m_j}^{j-1} L_r G_{rj} \qquad \text{(AIII-6)}$$

Thus once the matrices [L], [D], and $[L]^T$ have been determined, Equation (AIII-1) can be written as:

$$[L]\,[D]\,[L]^T\,[K]^{-1} = [I] \qquad \text{(AIII-7)}$$

Multiplying both sides of Equation (AIII-7) by $[L]^{-1}$ and simplifying:

$$[D]\,[L]^T[K]^{-1} = [L]^{-1}[I] \qquad \text{(AIII-8)}$$

Let $[L]^{-1}[I] = [W]$. [W] can be evaluated bu using forward substitution. Substituting the above and multiplying both sides of Equation (AIII-8) by $[D]^{-1}$:

$$[L]^T[K]^{-1} = [D]^{-1}[W] \qquad \text{(AIII-9)}$$

Let $[D]^{-1}[W] = [V]$. [V] can also be easilly evaluated as [D] is only a diagonal matrix. Substituting and multiplying both sides of Equation (AIII-9) by $[L]^{T^{-1}}$:

$$[K]^{-1} = [L]^{T^{-1}}[V] \qquad \text{(AIII-10)}$$

Equation (AIII-10) can be easilly solved by using backward substitution.